Published for SISSA by Springer

Received: *March 23, 2026*
Revised: *May 27, 2026*
Accepted: *June 7, 2026*
Published: *July 27, 2026*

Search for Higgs boson production at high transverse momentum in the WW decay channel in proton-proton collisions at $\sqrt{s} = 13$ TeV

The CMS collaboration

Full author list at the end of the paper

E-mail: cms-publication-committee-chair@cern.ch

Abstract: A search for Higgs boson (H) production at high transverse momentum (p_T) in the WW decay channel is presented. The analysis uses proton-proton collisions at $\sqrt{s} = 13\,\text{TeV}$ recorded by the CMS experiment in 2016–2018, corresponding to an integrated luminosity of $138\,\text{fb}^{-1}$. The visible decay products of the Higgs boson are reconstructed as a single large-radius jet with one isolated lepton or none (1ℓ and 0ℓ, respectively; $\ell = \text{e}, \mu$). The H-candidate jets are identified using an advanced transformer-based algorithm and are calibrated with the Lund jet plane reweighting technique. The 1ℓ channel is further split into gluon fusion, vector boson fusion, and associated production with hadronically decaying vector boson categories, while the 0ℓ channel considers all production processes inclusively. The measured cross section times the $\text{H} \to \text{WW}$ branching fraction relative to the standard model expectation is $\mu = -0.19^{+0.48}_{-0.46}$, indicating no evidence of a signal above the background. This measurement represents the first dedicated study of highly Lorentz-boosted $\text{H} \to \text{WW}$ decays, complementing earlier searches for high-p_T Higgs boson in other decay channels.

Keywords: Hadron-Hadron Scattering, Higgs Physics, Vector Boson Production

ArXiv ePrint: 2603.22233

https://doi.org/10.1007/JHEP07(2026)248

JHEP07(2026)248

Contents

1 Introduction

Since the discovery of a 125 GeV Higgs boson (H) by the ATLAS [1] and CMS [2, 3] Collaborations, extensive effort has been devoted to precision measurements of its properties and couplings [4, 5]. Measuring Higgs boson production at high transverse momentum, p_{T}, is a core component of this program at the CERN LHC. The high-p_{T} regime is especially important because theoretical predictions feature large logarithmic corrections and substantial higher-order effects [6], making measurements in this regime a powerful test of standard model (SM) calculations. Additionally, it serves as a sensitive probe for new phenomena, as deviations from the SM predictions could indicate the presence of effects beyond the SM at energy scales not directly accessible by the LHC [7–12].

The ATLAS and CMS Collaborations have reported measurements of the differential production cross section of the Higgs boson as a function of its transverse momentum, $p_{\mathrm{T}}^{\mathrm{H}}$, in a number of decay channels: $\mathrm{H} \to \mathrm{bb}$, $\mathrm{H} \to \gamma\gamma$, $\mathrm{H} \to \mathrm{WW} \to \mathrm{e}\nu\mu\nu$, $\mathrm{H} \to \tau\tau$, and $\mathrm{H} \to \mathrm{ZZ} \to 4\ell$ ($\ell = \mathrm{e}, \mu$), [13–17]. Among those, the sensitivity at the highest $p_{\mathrm{T}}^{\mathrm{H}}$ values probed so far is dominated by the $\mathrm{H} \to \mathrm{bb}$ [18–23] and $\mathrm{H} \to \tau\tau$ decay channels [24], which benefit from large branching fractions. These studies have enabled differential cross section measurements up to $p_T^H \approx 1\,\text{TeV}$ [21], thereby placing constraints on potential deviations from the SM in Lorentz-boosted topologies.

This paper presents the first search for highly Lorentz-boosted Higgs boson production decaying into a pair of W bosons, where at least one W boson decays into a pair of quarks, $\text{H} \to \text{WW} \to \ell\nu\text{qq}/\text{qqqq}$. The analysis is performed using proton-proton (pp) collision data at a center-of-mass energy of $\sqrt{s} = 13\,\text{TeV}$, collected with the CMS detector at the LHC in 2016–2018, corresponding to an integrated luminosity of $138\,\text{fb}^{-1}$ [25–27].

The W bosons originating from a Higgs boson with $p_T^H \gtrsim 250\,\text{GeV}$ are separated by a small angular distance $\Delta R = \sqrt{(\Delta\eta)^2 + (\Delta\phi)^2} < 0.8$, with $\Delta\eta$ and $\Delta\phi$ denoting pseudorapidity and azimuthal angle difference of the two W bosons, respectively. As a result, their final-state products are merged into a single large-radius jet. For leptonically decaying W bosons, leptons within the jet can still be identified as relatively isolated using a custom isolation variable that depends on the lepton p_T.

In the analysis, we categorize events into two channels based on whether they have one isolated lepton (1ℓ) or none (0ℓ), as illustrated in figure 1. Two different and complementary approaches are employed for these channels. The 0ℓ channel considers fully-hadronic WW decays as well as semileptonic WW decays with nonisolated leptons, while the 1ℓ channel exclusively targets 1ℓ+jets decays with an isolated lepton. The two channels feature similar baseline event selection, but adopt different Higgs boson identification and background estimation techniques tailored to their distinct background compositions.

While the overall measurement considers all Higgs boson production processes inclusively, the most sensitive channel, 1ℓ, further categorizes events into the three Higgs boson production processes with the largest cross section at the LHC: gluon fusion (ggF), vector boson fusion (VBF), and associated production with a vector boson (VH), where the vector boson, V (W or Z), decays hadronically. This allows for better modeling of the signal, as the relative contributions of these processes to the cumulative Higgs boson production cross section are expected to vary with p_T^H [6]. The associated production with a top quark-antiquark pair, $\text{t}\bar{\text{t}}\text{H}$, is not explicitly targeted with a dedicated region, although it still contributes as a minor signal component.

The H-candidate jet is identified using a jet tagging algorithm known as the particle transformer (ParT) [28]. This algorithm uses a self-attention neural network architecture [29] that dynamically weights jet constituent importance, trained on various large-radius jet topologies with excellent performance for identifying boosted Higgs boson decays to vector bosons, with performance and calibration for $\text{H} \to \text{WW}$ decays documented in ref. [30]. The Higgs boson four-momentum is reconstructed from the H-candidate jet and the missing p_T vector, $\vec{p}_T^{\,\text{miss}}$, for events containing a neutrino in the final state. In the VH category, the V candidate jet is identified with the ParticleNet algorithm [31, 32], while the VBF category requires the presence of two additional well-separated jets. The signal extraction is performed by fitting the invariant mass distribution of the reconstructed H or V boson candidates. Results are also presented as simplified template cross sections (STXS) [33] following the stage-1.2 binning scheme [34], which partitions the production phase space by Higgs boson kinematics.

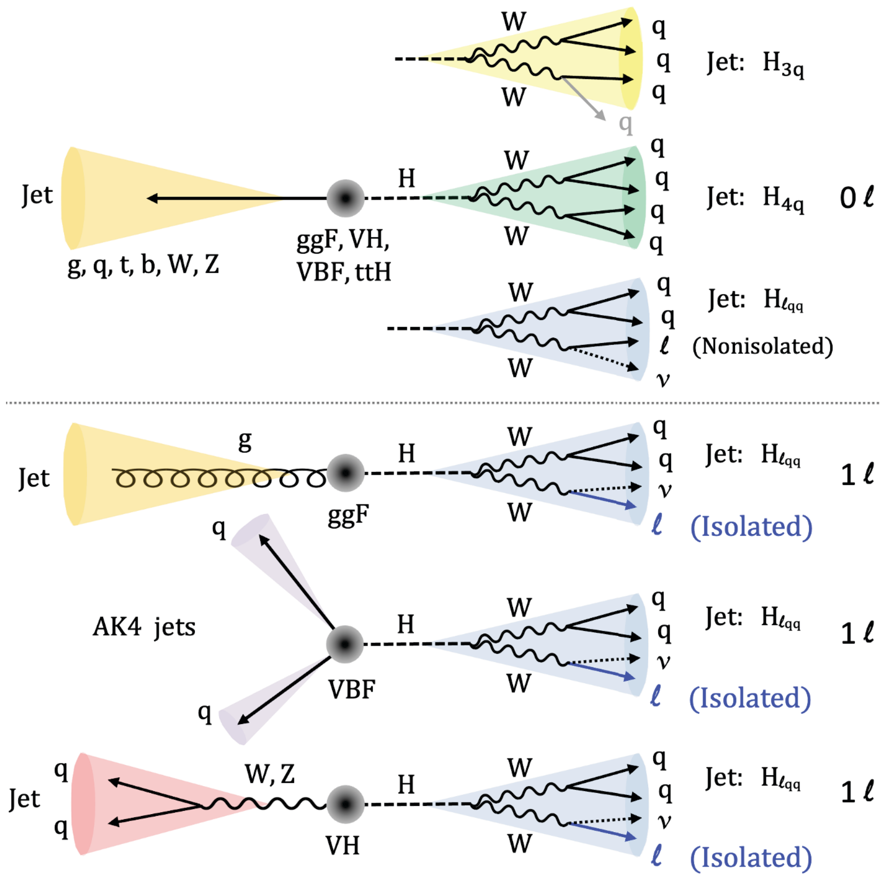

Figure 1. Illustration of the event topologies analyzed. Right: boosted Higgs boson final states from the $H \rightarrow WW \rightarrow \ell\nu qq/qqqq$ decay. Left: associated jets corresponding to the different production processes. From upper to lower: 0ℓ inclusive (all production and decay modes), and the 1ℓ ggF, VBF, and VH production processes.

The paper is organized as follows. The CMS detector is briefly described in section 2, followed by details of the event simulation in section 3 and event reconstruction in section 4. Section 5 presents the Higgs boson identification using the ParT algorithm and its calibration. The 0ℓ and 1ℓ channel analyses are described in sections 6 and 7, respectively, including event selections and background estimation methods. Systematic uncertainties are discussed in section 8 and results are presented in section 9, followed by a summary in section 10. Tabulated results for this analysis are provided in the HEPData record [35].

2 The CMS detector

The CMS apparatus [36, 37] is a multipurpose, nearly hermetic detector, designed to trigger on [38–40] and identify electrons (e), muons (μ), photons, and (charged and neutral) hadrons [41–43]. Its central feature is a superconducting solenoid of 6 m internal diameter, providing a magnetic field of 3.8 T. Within the solenoid volume are a silicon pixel and strip tracker, a lead tungstate crystal electromagnetic calorimeter (ECAL), and a brass and scintillator hadron calorimeter, each composed of a barrel and two endcap sections.

Forward calorimeters extend the pseudorapidity coverage provided by the barrel and endcap detectors. Muons are reconstructed using gas-ionization detectors embedded in the steel flux-return yoke outside the solenoid.

Events of interest are selected using a two-tiered trigger system. The first level, composed of custom hardware processors, uses information from the calorimeters and muon detectors to select events at a rate of around 100 kHz within a fixed latency of 4 μs [38]. The second level, known as the high-level trigger, consists of a farm of processors running a version of the full event reconstruction software optimized for fast processing, and reduces the event rate to a few kHz before data storage [39, 40].

More detailed descriptions of the CMS detector, together with a definition of the coordinate system used and the relevant kinematic variables, can be found in refs. [36, 37].

3 Event simulation

The ggF Higgs boson production process is simulated at next-to-leading order (NLO) accuracy in quantum chromodynamics (QCD) using the HJ-MiNLO event generator [44]. Finite top quark mass effects [45] are included following the recommendation of ref. [6]. The generated Higgs boson is required to have $p_T > 200$ GeV. The POWHEG generator 2.2 [46–48] is used to simulate Higgs boson production via VBF, VH, and associated production with a top quark-antiquark pair, $t\bar{t}H$, at NLO accuracy in QCD. The loop-induced $gg \to ZH$ process is generated separately at leading order (LO) with POWHEG [49]. In all signal simulations, the Higgs boson mass is set to 125 GeV. The inclusive cross sections for the ggF, VBF, VH, and $t\bar{t}H$ samples are taken from ref. [33]. The decay to a pair of W bosons is performed using JHUGEN v7.2.7 [50] for VBF, WH, and quark-induced ZH samples to properly account for spin correlations and angular distributions in these EW production processes, while PYTHIA 8.240 [51] is used for the remaining signal samples where such effects are less critical; all W boson decays are considered. The analysis includes events with $H \to ZZ$ decays from ggF production, simulated with the HJ-MiNLO generator, and $H \to \tau\tau$ decays, both of which are treated as background processes with nearly negligible contributions.

Background from jets produced via the strong interaction, commonly referred to as QCD multijet events, is modeled at LO accuracy using the MADGRAPH5_aMC@NLO 2.6.5 generator [52], including up to four final-state partons in the matrix element calculations. The $W(\ell\nu)$+jets process for the 1ℓ channel is modeled using the SHERPA Monte Carlo generator [53, 54]. In this setup, NLO matrix elements with up to two extra jets and LO matrix elements with up to four extra jets are calculated with COMIX 2.2.15 package [55]. For the 0ℓ channel, the $W(\ell\nu)$+jets process is simulated at LO accuracy using MADGRAPH5_aMC@NLO, in exclusive H_T ranges, where H_T is defined as the scalar sum of the transverse momenta of all generated jets, providing an adequately large event sample. The same H_T-binning procedure is applied to the $V(qq)$+jets process for both the 0ℓ and 1ℓ channels. Jets from the matrix element calculations and parton shower description are matched via the MLM scheme [56] for the LO MADGRAPH5_aMC@NLO samples, while SHERPA uses CKKW-based merging for $W(\ell\nu)$+jets, combining NLO (0–2 jets) and LO (3–4 jets) matrix elements [57]. The cross section of the $V(qq)$+jets process is corrected as a function of the boson p_T for higher-order QCD and electroweak (EW) effects. The QCD NLO corrections are derived

JHEP07(2026)248

using MADGRAPH5_aMC@NLO, simulating W and Z boson production with up to two additional partons and FxFx jet matching [58]. The EW NLO corrections are taken from theoretical calculations in refs. [59–62].

The production of top quark-antiquark pairs ($\mathrm{t\bar{t}}$) and single top quarks (single t), including tW and t-channel contributions, are modeled at NLO accuracy using the POWHEG generator [49, 63–67]. Single top quark production in the s-channel is simulated with MADGRAPH5_aMC@NLO at LO accuracy with the MLM jet matching scheme. The Drell-Yan production of lepton pairs through Z/γ^* is simulated at NLO accuracy with MADGRAPH5_aMC@NLO with up to two additional partons, using the FxFx jet matching scheme. The EW production of W and Z bosons with exactly two additional partons is modeled using MADGRAPH5_aMC@NLO at LO accuracy, corresponding to $\mathcal{O}(\alpha_S^4)$, where α_S denotes the strong coupling constant. Diboson processes are modeled at LO accuracy with PYTHIA 8.226, and the total cross sections are corrected to next-to-NLO accuracy with the MCFM 7.0 program [68]. Contributions from other processes are found to be negligible. Parton showering, fragmentation, and hadronization are modeled with PYTHIA 8.230 using the underlying event tune CP5 [69], with the exception of the samples produced with SHERPA. The parton distribution function (PDF) set NNPDF3.1 [70] at next-to-NLO accuracy is used for all processes.

For all simulated samples, the CMS detector response is modeled by GEANT4 [71, 72]. Independent samples are generated for each data-taking period using identical generator configurations, but accounting for changes in the accelerator and detector running conditions. The recorded data samples include additional pp interaction vertices from the same or nearby bunch crossings (pileup), generated with PYTHIA and added to all simulated events based on the expected pileup distribution. Corrections are applied to the simulated samples to match the pileup multiplicity distribution measured in the recorded data by era. Parton showering, fragmentation, and hadronization are modeled with PYTHIA 8.230 using the CP5 underlying event tune [69], with the exception of the samples produced with SHERPA.

4 Event reconstruction

The physics objects (e, μ, γ, charged and neutral hadrons) are reconstructed using the particle-flow (PF) algorithm [73], which uses an optimized combination of information from the various elements of the CMS detector to reconstruct individual particles (PF candidates). The primary vertex is taken to be the vertex corresponding to the hardest scattering in the event, evaluated using tracking information alone, as described in ref. [74].

The PF candidates are clustered into jets using the anti-k_T algorithm [75, 76]. The clustering algorithm, as implemented by the FASTJET package [76], is applied twice over the same inputs with distance parameter of 0.4 or 0.8, producing the AK4 or AK8 jet collections, respectively. The larger radius of the AK8 jet effectively captures the decay products of high-p_T Higgs bosons. For AK4 jets, the pileup effect is mitigated by excluding tracks that originate from pileup vertices and applying an offset correction to account for remaining contributions. For AK8 jets, the pileup-per-particle identification algorithm [77, 78] weights each PF candidate, prior to jet clustering, based on the likelihood of the particle to originate from the hard-scattering vertex. Jet energy corrections are derived to match the detector response to particle-level jets [79], and additional selection criteria remove jets dominated by anomalous contributions from instrumental effects or reconstruction failures [80]. The $\vec{p}_{\mathrm{T}}^{\text{miss}}$ is computed as the negative vector sum of the transverse momenta of all the PF candidates in an event, and its magnitude is denoted as $p_{\mathrm{T}}^{\text{miss}}$ [81]. The $\vec{p}_{\mathrm{T}}^{\text{miss}}$ is modified to account for corrections to the energy scale of the reconstructed jets in the event.

The AK8 jets must satisfy $p_{\mathrm{T}} > 200\,\text{GeV}$ and $|\eta| < 2.4$ to be considered in this analysis. The soft-drop algorithm [82], with parameters $\beta = 0$ and $z_{\text{cut}} = 0.1$, is applied to mitigate contamination from underlying event and pileup by removing PF candidates consistent with soft and wide-angle radiation from the jet. For jets originating from the fully hadronic decay of a massive boson, the soft-drop mass (m_{j}) distribution peaks near the boson mass, while for quark- and gluon-initiated jets, m_{j} has a smoothly falling spectrum. Each jet is assigned a discriminant score quantifying its compatibility with an H or V boson origin, as described in section 5.

Events with AK8 jets compatible with a hadronically decaying V boson from the V(qq)H production in the 1ℓ channel are identified using the ParticleNet algorithm [31, 32] which is based on a graph neural network trained to distinguish large-radius jets originating from scalar particles with two-pronged $\mathrm{X} \to \mathrm{qq}$ decays from QCD jets. Each prong corresponds to the fragmentation and hadronization of a colored parton from the X decay. To achieve decorrelation from the jet mass, signal resonances between 15 and 250 GeV are used, and jets from signal and background are reweighted to obtain flat m_{j} and p_{T} distributions. Merged $\mathrm{V} \to \mathrm{qq}$ decays are identified using a probability score defined as the sum of three tagger output scores for $\mathrm{X} \to \mathrm{bb}$, cc, and qq decays, where $\mathrm{q} \in \{\mathrm{u}, \mathrm{d}, \mathrm{s}\}$.

The $\mathrm{V} \to \mathrm{qq}$ jet tagging efficiency is calibrated in semileptonic $\mathrm{t\bar{t}}$ events with quarks using a tag-and-probe method [83]. For the $\mathrm{Z} \to \mathrm{bb}$ tagging, the efficiency is calibrated with the QCD proxy-jet method [84], where a boosted decision tree identifies suitable gluon-splitting, $\mathrm{g} \to \mathrm{bb}$, jets as proxies for the signal.

The AK4 jets must satisfy $p_{\mathrm{T}} > 30\,\text{GeV}$. Jets originating from a bottom quark, denoted as b jets, satisfy $|\eta| < 2.5$ and are identified with the DeepJet algorithm [85, 86]. The b jet identification requirements in this search use two working points (WPs), "medium" and "tight," corresponding to tagging efficiencies of about 75% and 60%, and probabilities of misidentifying a light-flavor quark or gluon jet as a b jet of 1% and 0.1%, respectively, as determined in a sample of simulated $\mathrm{t\bar{t}}$ events. The data-to-simulation differences in b-tagging efficiency are corrected via scale factors (SFs) applied to the simulation [86].

Muons are identified as tracks in the central tracker consistent with either a track or several hits in the muon system, and associated with calorimeter deposits compatible with the muon hypothesis [42]. Electrons are identified as a primary charged-particle track and potentially many ECAL energy clusters corresponding to this track extrapolation to the ECAL and to possible bremsstrahlung photons emitted along the way through the tracker material. They are identified with a multivariate discriminant described in ref. [87]. Isolation algorithms are designed to measure the amount of energy deposited near an object, such as a lepton. The relative isolation, I_{rel}, of μ (e) is calculated by summing the p_{T} of PF candidates in a cone of size $\Delta R < 0.4$ (0.3) centered on the lepton, corrected for neutral pileup contributions, and divided by the p_{T} of the lepton [42, 87]. Leptons emerging from the decay chain $\mathrm{H} \to \mathrm{WW} \to \ell\nu\mathrm{qq}$ of high-p_{T} Higgs bosons may fail I_{rel} requirements if they are produced inside or close to the jet from the hadronic W boson decay. However, they can still be identified using an optimized version of the isolation variable, referred to as "mini-isolation," I_{mini} [88]. The I_{mini} is defined identically to I_{rel}, but with a p_{T}-dependent cone size $\Delta R^{\text{mini-iso}}$ of 0.2, $10\,\mathrm{GeV}/p_{\mathrm{T}}^{\ell}$, and 0.05 for leptons with $p_{\mathrm{T}}^{\ell} < 50\,\mathrm{GeV}$, $50 < p_{\mathrm{T}}^{\ell} < 200\,\mathrm{GeV}$, and $p_{\mathrm{T}}^{\ell} > 200\,\mathrm{GeV}$, respectively.

5 Higgs boson identification and reconstruction

Higgs boson identification is performed using the ParT algorithm, a machine-learning model based on self-attention mechanisms and the transformer architecture [28]. The ParT algorithm extends the capabilities of ParticleNet [31], originally developed for distinguishing QCD jets from hadronically decaying resonances into two quarks ("two-pronged" jets) to a broader range of jet topologies, including those originating from $\mathrm{H} \to \mathrm{WW} \to \ell\nu\mathrm{qq}/\mathrm{qqqq}$ decays. Tagging these jets is particularly challenging due to the asymmetric kinematics of the intermediate W bosons.

For each jet, the ParT algorithm outputs 37 classification scores, each representing the probability that the jet belongs to a specific category. These categories distinguish jets by flavor — charm (c), b, light quarks, and hadronically decayed tau (τ_{h}) leptons — as well as by the number of the constituents (quarks or leptons), before parton shower and hadronization. In particular, $\mathrm{H} \to \mathrm{WW} \to \mathrm{qqqq}$ jets are subdivided into four-pronged ($\mathrm{H}_{4\mathrm{q}}$) and three-pronged ($\mathrm{H}_{3\mathrm{q}}$) classes to account for cases where not all decay products fall within the jet cone. The complete list of jet classes considered by ParT is shown in table 1.

The ParT model is trained on a sample of simulated jets in a kinematic range that satisfies $200 < p_{\mathrm{T}} < 2500\,\mathrm{GeV}$, $|\eta| < 2.4$, and $20 < m_{\mathrm{j}} < 260\,\mathrm{GeV}$. The training set includes jets from scalar resonances decaying into two-quark and WW channels, and top-like resonances decaying into bW channels, as well as jets produced in QCD multijet events. The generator-level resonance masses range from 15 to 250 GeV. The training employs mass decorrelation via sample reweighting to achieve uniform p_{T} and m_{j} distributions, preventing the tagger from using jet mass as a discriminant and avoiding background mass sculpting effects, following the ParticleNet strategy. Additionally, in the training samples, the H and W boson masses are varied together in order to maintain the W-to-H mass ratio fixed to the SM value of 0.64. This ensures that one W boson remains off-shell throughout the mass range and that the tagger is decorrelated from both the H and W boson masses simultaneously. Additional details on the model architecture and the ParT training are documented in ref. [30].

The 0ℓ channel defines a discriminant, $P(\mathrm{H}_{0\ell})$, from the sum of all 16 ParT $\mathrm{H} \to \mathrm{WW}$ scores, including both semileptonic and fully hadronic WW signal classes, as denoted in the upper part of table 1. Two exclusive selections based on $P(\mathrm{H}_{0\ell})$ are used: $P(\mathrm{H}_{0\ell}) > 0.99$ and $0.92 < P(\mathrm{H}_{0\ell}) < 0.99$, defining regions of high and moderate probability of containing $\mathrm{H}_{0\ell}$ signal events, respectively. These boundaries were chosen to maximize $S/\sqrt{B}$ (where S and B denote expected signal and background yields), yielding signal (background) efficiencies of 4.5% (0.02%) and 13.4% (0.35%) for the high and moderate probability regions, respectively.

The 1ℓ channel targets semileptonic WW decays, $\mathrm{H}_{\ell\mathrm{qq}}$, by identifying one isolated lepton *inside* the AK8 jet. This lepton-in-jet topology for background processes constitutes only a small fraction of the ParT training sample, as lepton-jet overlap is rare in boosted topologies,

	Category and decay mode	Final state class and substructure
Signal	$\mathrm{H} \to \mathrm{WW}$ fully hadronic	3q(0c), 3q(1c), 3q(2c), 4q(0c), 4q(1c), 4q(2c)
	$\mathrm{H} \to \mathrm{WW}$ semileptonic	eνqq(0c), eνqq(1c), $\mu\nu$qq(0c), $\mu\nu$qq(1c) $\tau_{\mathrm{e}}\nu$qq(0c), $\tau_{\mathrm{e}}\nu$qq(1c), $\tau_{\mu}\nu$qq(0c), $\tau_{\mu}\nu$qq(1c), $\tau_{\mathrm{h}}\nu$qq(0c), $\tau_{\mathrm{h}}\nu$qq(1c)
Background	$\mathrm{t} \to \mathrm{bW}$ hadronic	bq(0c), bq(1c), bqq(0c), bqq(1c)
	$\mathrm{t} \to \mathrm{bW}$ leptonic	beν, b$\mu\nu$, b$\tau_{\mathrm{h}}\nu$, b$\tau_{\mathrm{e}}\nu$, b$\tau_{\mu}\nu$
	$\mathrm{H, Z, W} \to \mathrm{qq}$	bb, cc, ss, qq ($\mathrm{q} = \mathrm{u/d}$)
	$\mathrm{H, Z} \to \tau\tau$	$\tau_{\mathrm{h}}\tau_{\mathrm{h}}$, $\tau_{\mathrm{h}}\tau_{\mathrm{e}}$, $\tau_{\mathrm{h}}\tau_{\mu}$
	QCD	b, bb, c, cc, others (light q and gluon)

Table 1. The 37 ParT jet classification categories. The categories are based on the decay modes of H and V bosons, top quarks, and on QCD processes. All listed decay products are assumed to be contained within the jet cone, except for neutrinos. Numbers like 4q indicate the multiplicity of the adjacent quark, while those in parentheses indicate the number of c quarks in the preceding quark sequence. Classes such as 3q or bq imply that one quark escapes the jet cone in $\mathrm{H} \to 4\mathrm{q}$ or $\mathrm{t} \to \mathrm{bqq}$ decays, respectively. Subscripts on τ indicate hadronic (h) or leptonic (e, μ) decays.

limiting the tagger's ability to reject $\mathrm{W}(\ell\nu)$+jets and similar backgrounds in this channel. To enhance the signal sensitivity and suppress the $\mathrm{W}(\ell\nu)$+jets background, a dedicated fine-tuning strategy is therefore developed. Specifically, the activations of the final hidden layer of ParT are used as input to a shallow neural network (multilayer perceptron) that categorizes jets into four classes: Higgs boson signal, QCD multijet, $\mathrm{t\bar{t}}$, and $\mathrm{W}(\ell\nu)$+jets, following the transfer learning approach introduced in ref. [89]. Fine-tuning is performed using a dedicated simulated data set of AK8 jets originating from these processes, selected such that the jets overlap with the leading lepton within a cone of radius 0.8, reflecting the topology of the single-lepton signal region (SR).

A separate sample of simulated Higgs boson signal events is used to prevent training data leakage into the validation set during the fine-tuning. The resulting discriminant, $P(\mathrm{H}_{1\ell})$, is defined from the Higgs boson probability output of the fine-tuned model, denoted as ParT-Finetuned.

Compared to the original ParT, the ParT-Finetuned tagger achieves nearly 60% higher signal efficiency at a background efficiency of 1% for $\mathrm{H} \to \mathrm{WW} \to \ell\nu\mathrm{qq}$ decays. This demonstrates the value of transfer learning: training large models on a broad set of classes and datasets, followed by targeted fine-tuning on a smaller subset specific to the topology of interest, as the 1ℓ final state here. A comparison was also made directly using the CMS statistical analysis tool Combine [90], observing similar increase in expected significance. Tagger performance curves (background vs. signal efficiency) for simulated jets are shown in figure 2, using a selection similar to the 0ℓ channel: $p_{\mathrm{T}}^{\mathrm{j}} > 400\,\mathrm{GeV}$, $m_{\mathrm{j}} > 50\,\mathrm{GeV}$, and $|\eta^{\mathrm{j}}| < 2.4$.

JHEP07(2026)248

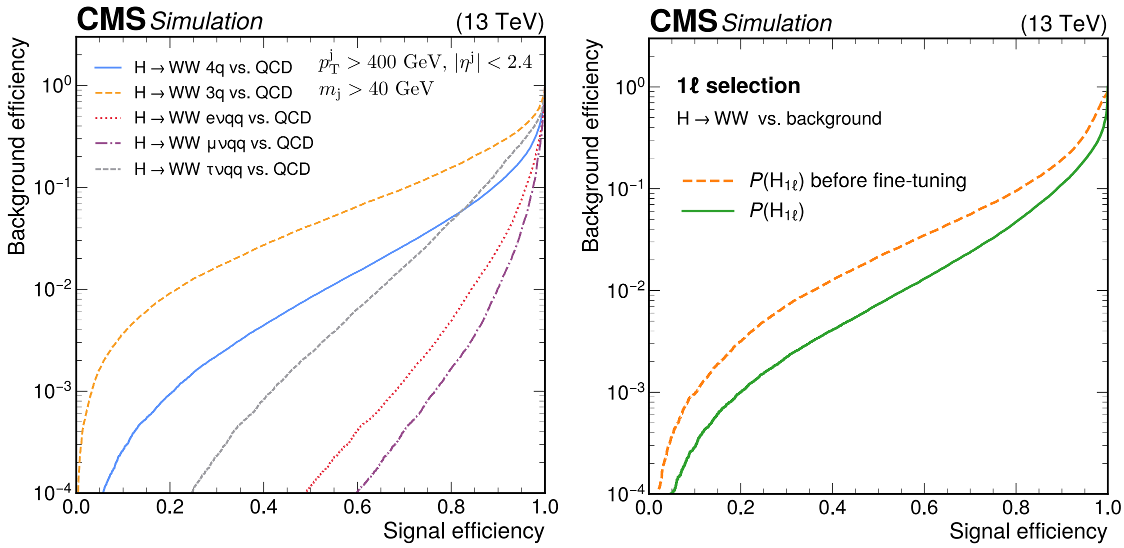

Figure 2. Performance curves showing the identification probability of background jets versus $\mathrm{H} \to \mathrm{WW}$ signal jets for PART and PART-FINETUNED. Left: discrimination performance of the PART model for various $\mathrm{H} \to \mathrm{WW}$ decays against the dominant QCD multijet background. Right: comparison of $P(\mathrm{H}_{1\ell})$ before and after fine-tuning, following the event selection in the 1ℓ channel. The background includes jets originating from QCD multijet events, $\mathrm{W}(\ell\nu)$+jets, and top quark processes.

The $\mathrm{H}_{\ell\mathrm{qq}}$, $\mathrm{H}_{4\mathrm{q}}$, and $\mathrm{H}_{3\mathrm{q}}$ simulated signal jets lack a suitable SM counterpart jet for calibration. Therefore, to calibrate the $P(\mathrm{H}_{0\ell})$ and $P(\mathrm{H}_{1\ell})$ discriminants, the Lund jet plane (LJP) reweighting technique [91] is applied to simulated jets with a fixed number of quark-initiated prongs. The method reclusters each jet into subjets, each representing the radiation pattern of an individual quark from the hard interaction. Corrections for each subjet are derived based on data-to-simulation ratios of LJP densities [92], which provide representations that capture the phase space density of different types of splittings in the two-dimensional space of momentum transfer and angular separation. These per-splitting corrections, measured in data using subjets from $\mathrm{W} \to \mathrm{qq}$ decays [91], are combined into a total correction for the simulated jet. In this analysis, the LJP reweighting is used to correct the signal selection efficiency in the $P(\mathrm{H}_{0\ell})$ and $P(\mathrm{H}_{1\ell})$ discriminants and to estimate the associated uncertainties. The corresponding SFs are defined as the ratio of efficiencies after the LJP reweighting to those from the uncorrected simulation, and are validated in $\mathrm{t\bar{t}}$-enriched control regions as described below.

The simulation is calibrated separately for each dominant signal component: $\mathrm{H}_{4\mathrm{q}}$, $\mathrm{H}_{3\mathrm{q}}$, and $\mathrm{H}_{\ell\mathrm{qq}}$, corresponding to jets containing four, three, and two quark-originated subjets, respectively. Jets are matched to their generator-level category and reclustered into the appropriate number of subjets based on their quark content, using the exclusive k_T algorithm [93, 94]. The splitting pattern is extracted using the clustering history of each subjet. For $\mathrm{H}_{\ell\mathrm{qq}}$ jets, reconstructed lepton and photon PF candidates within $\Delta R = 0.2$ of the generator-level lepton are removed before reclustering, to isolate the hadronic component from the leptonic one.

Individual SFs derived for each signal component are then combined to produce a global SF applicable to all signal jets in each analysis category. The resulting SFs range from 0.84 to 0.98, with total uncertainties of 9–27%, as described in section 8.

The procedure is validated in regions enriched in $\mathrm{t\bar{t}}$ events, which closely resemble the signal topology in the 0ℓ and 1ℓ channels and require at least one b-tagged jet. Generator-level information from the top quark decay is used to classify top quark jets as "matched" or "unmatched," with the reweighting applied only to the matched jets using the LJP ratios. For hadronic top quark decays (which serve as a proxy for jets with four or three quark-originated subjets), the matched component corresponds to $\mathrm{t} \to \mathrm{bqq}$ decays, where all the W boson daughter quarks and the b quark are within the jet radius. For jets with two quark-originated subjets and one lepton, the matched component comes from $\mathrm{t\bar{t}}$ events where both top quark decays are separated by small angular distances and the visible products from a leptonic W boson and a hadronic W boson decays are contained within the jet radius; this selection results in a $\mathrm{t} \to \ell\mathrm{qq}$ topology. The LJP-reweighted simulation is found to agree well with the data in the $P(\mathrm{H}_{0\ell})$ and $P(\mathrm{H}_{1\ell})$ distributions in a $\mathrm{t\bar{t}}$-dominated validation sample, confirming the validity of the SF corrections applied to top quark jets.

In this analysis, the Higgs boson is reconstructed as a single large-radius jet corrected for the potential presence of a neutrino. For signal jets, the m_j distribution exhibits a sharp peak near the nominal Higgs boson mass for $\mathrm{H_{4q}}$ jets and a broader peak for the $\mathrm{H_{3q}}$ and $\mathrm{H}_{\ell\mathrm{qq}}$ components, due to the partial reconstruction of the WW system. To improve the mass resolution for the $\mathrm{H}_{\ell\mathrm{qq}}$ signal, the reconstructed Higgs boson four-momentum is calculated as the sum of the jet four-momentum and the estimated four-momentum of the neutrino. The four-momentum of any lepton within the AK8 jet cone is included in the H-candidate jet momentum, since leptons within the jet cone are treated as PF constituents at jet reconstruction. The $\vec{p}_\mathrm{T}^\mathrm{miss}$ is attributed solely to the neutrino, with $\vec{p}_\mathrm{T}^{\,\nu} = \vec{p}_\mathrm{T}^\mathrm{miss}$. Since the H-candidate jet is highly boosted, the neutrino is expected to be collinear with the jet axis, thus we assume $\eta^\nu = \eta^\mathrm{j}$, enabling full four-momentum reconstruction for the neutrino. Then, the corrected mass of the H-candidate jet, referred to as m_j^*, is evaluated as the invariant mass of the reconstructed Higgs boson system. This definition aligns the peak position of the m_j^* distribution for $\mathrm{H}_{\ell\mathrm{qq}}$ signal jets to 125 GeV.

The correction to the jet mass is applied only to events with significant $p_\mathrm{T}^\mathrm{miss}$ aligned with the candidate jet. In the 0ℓ channel, this is quantified by requiring the ratio $p_\mathrm{T}^\mathrm{miss}/p_\mathrm{T}^\mathrm{j}$ to be greater than 0.1 and the azimuthal angle between $\vec{p}_\mathrm{T}^\mathrm{miss}$ and the jet, $|\Delta\phi(\mathrm{j}, \vec{p}_\mathrm{T}^\mathrm{miss})|$, to be less than 0.8. For events that do not meet these conditions, the mass of the H-candidate jet is taken as m_j. For all 1ℓ channels, the correction to the jet mass is always applied.

6 Analysis of the 0ℓ channel

The analysis in the 0ℓ channel considers all major Higgs boson production processes (ggF, VBF, VH, and $\mathrm{t\bar{t}H}$) decaying into final states without a lepton ($\mathrm{H_{4q}}$, $\mathrm{H_{3q}}$) or with a lepton that fails the isolation requirements ($\mathrm{H}_{\ell\mathrm{qq}}$). Four orthogonal SRs are defined, with background predictions derived from a combination of control regions (CRs) in data and simulation.

JHEP07(2026)248

6.1 Event selection

Events in the 0ℓ channel are selected using a combination of hadronic triggers. The hadronic triggers impose a minimum threshold on either the p_{T} of an AK8 jet or the event H_{T}, defined here as the scalar p_{T} sum of all AK4 jets in the event with $p_{\mathrm{T}} > 30\,\mathrm{GeV}$ and $|\eta| < 2.4$. For AK8 jets used in the trigger selection, a minimum trimmed jet mass of 30 or 50 GeV is also required [95]. The combined hadronic trigger efficiency is 75–80% for $200 < p_{\mathrm{T}} < 400\,\mathrm{GeV}$, 80–95% for $400 < p_{\mathrm{T}} < 450\,\mathrm{GeV}$, and nearly 100% for $p_{\mathrm{T}} > 450\,\mathrm{GeV}$. The efficiency is measured using AK8 jets in an independent sample of μ+jets $\mathrm{t\bar{t}}$ events collected with a single-muon trigger.

Offline, events are selected with two or three large-radius jets. To ensure high trigger efficiency, the highest p_{T} jet and the highest mass jet are required to satisfy $p_{\mathrm{T}} > 400\,\mathrm{GeV}$ and $m_{\mathrm{j}} > 50\,\mathrm{GeV}$, respectively. The jet with the highest $P(\mathrm{H}_{0\ell})$ discriminant value is identified as the H-candidate jet and must also satisfy $m_{\mathrm{j}} > 40\,\mathrm{GeV}$. Events with isolated leptons, as defined in section 4, are vetoed in the 0ℓ channel, but events with nonisolated leptons are included and contribute significantly to the sensitivity of this channel. No b-tagged jet veto is applied in the 0ℓ channel, as $\mathrm{t\bar{t}H}$ production is part of the signal considered. The 0ℓ channel contributes significantly less than the 1ℓ due to (a) the overwhelming QCD multijet background, (b) the ℓ isolation requirements, and (c) reduced trigger efficiency for $p_{\mathrm{T}}^{\mathrm{H}} < 400\,\mathrm{GeV}$.

In signal events, the dominant contribution originates from $\mathrm{H_{4q}}$ jets (≈28%), followed by $\mathrm{H_{3q}}$ (≈14%) and $\mathrm{H_{\ell qq}}$ (≈13%) jets, accounting for ≈55% of signal events in total. The remaining ≈45%, designated as "Other," arises because the H-candidate jet p_{T} threshold of 200 GeV allows for partially boosted topologies, where resolved W bosons from H decays or jets from associated production processes are misidentified as the H-candidate. This category includes jets matched to a V boson (≈18%), a gluon or light-flavor quark (≈10%), a top quark from $\mathrm{t\bar{t}H}$ production (≈5%), rare H decay topologies (≈3%), and jets unmatched to any of the above objects (≈9%).

Figure 3 shows the distributions of the H-candidate jet mass m_{j}, $P(\mathrm{H}_{0\ell})$ discriminant, $p_{\mathrm{T}}^{\mathrm{miss}}/p_{\mathrm{T}}^{\mathrm{j}}$, and $|\Delta\phi(\mathrm{j}, p_{\mathrm{T}}^{\mathrm{miss}})|$, in simulated background and signal events, where j corresponds to the H-candidate jet. The $\mathrm{H_{\ell qq}}$ signal, which is associated with energetic neutrinos aligned with the jet axis, can be isolated from the other signal components and the multijet background by selecting on $p_{\mathrm{T}}^{\mathrm{miss}}/p_{\mathrm{T}}^{\mathrm{j}}$ and $|\Delta\phi(\mathrm{j}, p_{\mathrm{T}}^{\mathrm{miss}})|$.

The SR is defined by $P(\mathrm{H}_{0\ell}) > 0.92$. It is first divided into two main categories based on the ratio of $p_{\mathrm{T}}^{\mathrm{miss}}$ to the H-candidate jet p_{T}: $\mathrm{SR_1}$ with $p_{\mathrm{T}}^{\mathrm{miss}}/p_{\mathrm{T}}^{\mathrm{j}} < 0.25$, which includes contributions from all three major signal components, and $\mathrm{SR_2}$ with $p_{\mathrm{T}}^{\mathrm{miss}}/p_{\mathrm{T}}^{\mathrm{j}} > 0.25$, where an additional requirement of $|\Delta\phi(\mathrm{j}, \vec{p}_{\mathrm{T}}^{\mathrm{miss}})| < 0.8$ ensures alignment between the reconstructed neutrino and the H-candidate jet in the transverse plane. Each category is further divided by signal purity into $\mathrm{SR_a}$ ($P(\mathrm{H}_{0\ell}) > 0.99$) for high purity and $\mathrm{SR_b}$ ($0.92 < P(\mathrm{H}_{0\ell}) < 0.99$) for medium purity, resulting in four statistically independent signal regions labeled $\mathrm{SR_{1a}}$, $\mathrm{SR_{1b}}$, $\mathrm{SR_{2a}}$, and $\mathrm{SR_{2b}}$.

Because of the high-$p_{\mathrm{T}}^{\mathrm{miss}}$ requirement, $\mathrm{SR_{2a}}$ and $\mathrm{SR_{2b}}$ are dominated by the $\mathrm{H_{\ell qq}}$ component, accounting for 75 and 93% of the total signal events, respectively. Despite the low-$p_{\mathrm{T}}^{\mathrm{miss}}$ selection, the composition of signal events in $\mathrm{SR_{1a}}$ is also dominated by $\mathrm{H_{\ell qq}}$

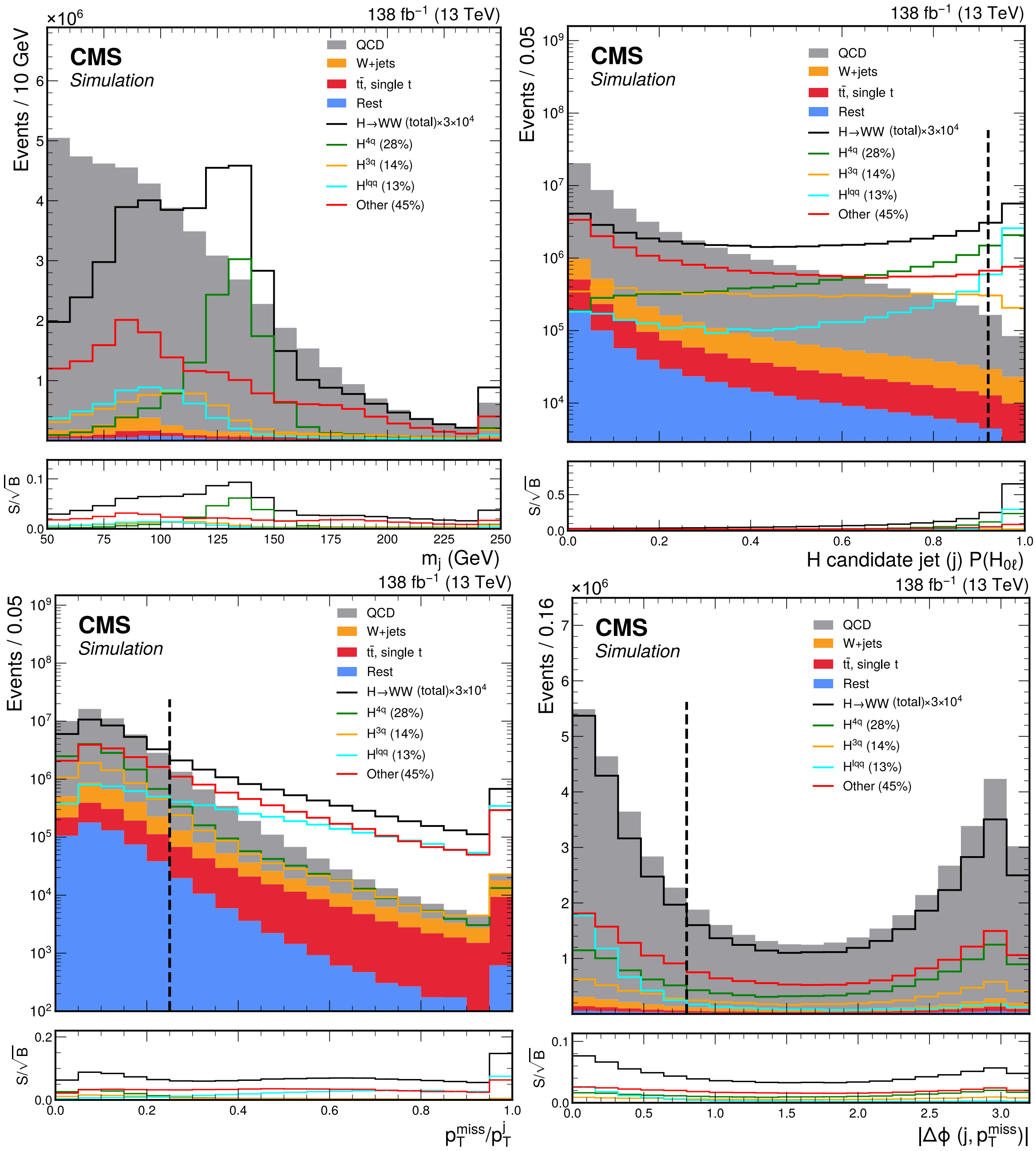

Figure 3. Distributions of the total simulated background and total signal (scaled by a factor of 3×10^4 for visibility) passing event selection in the 0ℓ channel, prior to the requirements on $P(\mathrm{H}_{0\ell})$, $p_{\mathrm{T}}^{\mathrm{miss}}/p_{\mathrm{T}}^{\mathrm{j}}$, and $|\Delta\phi(\mathrm{j}, \vec{p}_{\mathrm{T}}^{\,\mathrm{miss}})|$ used to define the SR. The signal is split into classes as defined in the text. The upper left and upper right panels show the soft-drop mass and PART score distributions for the H-candidate jet (j) $P(\mathrm{H}_{0\ell})$, respectively. The lower left and lower right panels display the $p_{\mathrm{T}}^{\mathrm{miss}}/p_{\mathrm{T}}^{\mathrm{j}}$ ratio and the angle $|\Delta\phi(\mathrm{j}, \vec{p}_{\mathrm{T}}^{\,\mathrm{miss}})|$, respectively. Vertical lines indicate the selection conditions imposed to define the SRs.

JHEP07(2026)248

Region	$p_{\mathrm{T}}^{\mathrm{miss}}/p_{\mathrm{T}}^{\mathrm{j}}$	$P(\mathrm{H}_{0\ell})$	$\lvert\Delta\phi(\mathrm{j},\vec{p}_{\mathrm{T}}^{\mathrm{miss}})\rvert$	Apply $p_{\mathrm{T}}^{\mathrm{miss}}$ correction if
SR_{1a}	<0.25	>0.99	any	$\lvert\Delta\phi\rvert < 0.8$, $p_{\mathrm{T}}^{\mathrm{miss}}/p_{\mathrm{T}}^{\mathrm{j}} > 0.1$
SR_{1b}	<0.25	0.92–0.99	any	$\lvert\Delta\phi\rvert < 0.8$, $p_{\mathrm{T}}^{\mathrm{miss}}/p_{\mathrm{T}}^{\mathrm{j}} > 0.1$
SR_{2a}	>0.25	>0.99	$\lvert\Delta\phi\rvert < 0.8$	always
SR_{2b}	>0.25	0.92–0.99	$\lvert\Delta\phi\rvert < 0.8$	always
CR_{1}	<0.25	<0.92	any	$\lvert\Delta\phi\rvert < 0.8$, $p_{\mathrm{T}}^{\mathrm{miss}}/p_{\mathrm{T}}^{\mathrm{j}} > 0.1$
CR_{2}	>0.25	<0.92	$\lvert\Delta\phi\rvert < 0.8$	always

Table 2. Kinematic requirements used to define the SRs and CRs in the 0ℓ channel. The rightmost columns list the conditions, combined with logical "AND", under which m_{j} is replaced by the corrected m_{j}^{*} mass. The $\lvert\Delta\phi\rvert$ denotes the azimuthal angle difference between $\vec{p}_{\mathrm{T}}^{\mathrm{miss}}$ and the Higgs boson candidate p_{T} vector.

at 63% because of the greater efficiency at high $P(\mathrm{H}_{0\ell})$ (figure 2, left; figure 3, upper right) compared to H_{4q}, which follows at 27%. The SR_{1b} is populated by H_{4q} at 57%, followed by $\mathrm{H}_{\ell qq}$ at 19%. The H_{3q} contribution ranges from 1 to 8%. Therefore, the sensitivity to Higgs boson production in the 0ℓ channel is driven by the semileptonic WW decays with a nonisolated lepton. The presence of $\mathrm{H}_{\ell qq}$ across all SRs necessitates a specialized Higgs boson mass reconstruction, incorporating information about the neutrino via $p_{\mathrm{T}}^{\mathrm{miss}}$ and $\lvert\Delta\phi(\mathrm{j},\vec{p}_{\mathrm{T}}^{\mathrm{miss}})\rvert$ even in the low-$p_{\mathrm{T}}^{\mathrm{miss}}$ regions SR_{1a} and SR_{1b}, as described at the end of section 5. All kinematic requirements defining the four SRs and two CRs (described in section 6.2) are summarized in table 2. All conditions and selection boundaries in table 2 were chosen to maximize $S/\sqrt{B}$.

The dominant $\mathrm{H}_{\ell qq}$ signal exhibits a broad m_{j} distribution peaking at masses lower than the Higgs boson mass due to the missing neutrino. The rightmost column of table 2 specifies conditions defining the phase space where m_{j} is corrected for neutrino reconstruction and replaced by m_{j}^{*}; elsewhere, $m_{\mathrm{j}}^{*} = m_{\mathrm{j}}$. These conditions are designed to shift the mean of the $\mathrm{H}_{\ell qq}$ mass distribution toward the Higgs boson mass and to minimize its width. This replacement shifts the mass distributions for all events in the affected regions to higher values.

6.2 Background estimation

The statistical analysis is performed over the m_{j}^{*} spectra in the four SRs, with background predictions derived separately for QCD multijet and other processes. The QCD multijet production dominates SR_{1a}, SR_{1b}, and SR_{2b} (>90%) and contributes subdominantly to SR_{2a} (30%); it is estimated using a data-driven method. The $\mathrm{W}(\ell\nu)$+jets and top quark backgrounds, which contribute significantly to SR_{2a}, as well as diboson processes, are estimated from simulation and validated in data.

6.2.1 The QCD multijet background

The QCD multijet process is the dominant background in all the SRs, except for SR_{2a}. We estimate this background using a data-driven method implementing two CRs, the CR_1 and CR_2, defined by requiring $P(\mathrm{H}_{0\ell}) < 0.92$, but still fulfilling the $p_{\mathrm{T}}^{\mathrm{miss}}/p_{\mathrm{T}}^{\mathrm{j}}$ condition of SR_1 and SR_2, respectively.

The QCD multijet background in each SR_{ir} ($i = 1, 2$; $r = \mathrm{a}, \mathrm{b}$) is estimated from the data distribution in the corresponding CR, multiplied by a polynomial transfer function (TF_{ir}) to account for the shape differences between the SR and CR. These differences arise from the kinematic correlation between m_j^* and the variables defining the SR, as well as residual differences in PART efficiency between data and simulation for background processes.

The prediction of the QCD background yield in SR_{ir} takes the form

$$N_{\mathrm{SR}_{ir}}^{\mathrm{QCD},k} = N_{\mathrm{CR}_i}^{\mathrm{QCD},k}\ \mathrm{TF}_{ir}(m_\mathrm{j}^{*k}), \tag{6.1}$$

where m_j^{*k} is the center of the k^th m_j^* bin, $N_{\mathrm{SR}_i}^{\mathrm{QCD},k}$ is the estimated number of QCD background events in bin k of SR_{ir}, and $N_{\mathrm{CR}_i}^{\mathrm{QCD},k}$ is the number of data events minus the number of predicted non-QCD background events in bin k of CR_i.

The QCD background in $\mathrm{SR}_{1\mathrm{a}}$ and $\mathrm{SR}_{2\mathrm{a}}$ is estimated from CR_1 and CR_2 using two transfer functions, $\mathrm{TF}_{1\mathrm{a}}$ and $\mathrm{TF}_{2\mathrm{a}}$, which share the same shape (determined by a simultaneous fit across all four regions) and have independent normalizations. For $\mathrm{SR}_{1\mathrm{b}}$ and $\mathrm{SR}_{2\mathrm{b}}$, the QCD background is estimated with two independent transfer functions, $\mathrm{TF}_{1\mathrm{b}}$ and $\mathrm{TF}_{2\mathrm{b}}$, each having its shape and normalization determined by a fit to its corresponding CR and SR pair. The resulting transfer functions are shown in figure 4 (right).

The polynomial transfer function, TF_{ir}, is defined using the Bernstein basis:

$$\mathrm{TF}_{ir}(m_\mathrm{j}^*) = \sum_{l=0}^{n} a_l b_{l,n}(m_\mathrm{j}^*) \tag{6.2}$$

where a_l are fitted coefficients, and $b_{l,n}$ are the m_j^*-dependent one-dimensional Bernstein basis polynomials of degree n, properly transformed to the m_j^* range probed. The optimal order of the transfer function, $\mathrm{TF}_{ir}(m_\mathrm{j}^*)$, is determined to be 3 for $\mathrm{TF}_{i\mathrm{a}}$ and 6 for $\mathrm{TF}_{i\mathrm{b}}$, based on the results of a Fisher F-test [96], performed independently for regions "a" and "b". These high-degree polynomials capture the smoothly varying kinematic differences between the SRs and CRs without introducing spurious structures.

The parameters of the polynomial function are treated as unconstrained in the fit to data. The post-fit results of the four TFs are shown in figure 4 (right). They demonstrate monotonic behavior and a smooth shape variation near the 125 GeV region, where the signal is most abundant. The predicted spectra for the QCD process are presented and discussed in section 9.

6.2.2 Other background processes

The background events from $\mathrm{W}(\ell\nu)$+jets and top quark production are predicted by simulation. Their normalization is validated in data in two background-enriched samples within a kinematic phase space consistent with $\mathrm{SR}_{2\mathrm{a}}$. The first sample is the subset of $\mathrm{SR}_{2\mathrm{a}}$ defined by requiring $m_\mathrm{j}^* > 160\,\mathrm{GeV}$, while the second sample is defined as the $\mathrm{SR}_{2\mathrm{a}}$ but inverting the angular requirement to $|\Delta\phi(\mathrm{j}, \vec{p}_\mathrm{T}^{\,\mathrm{miss}})| > 0.8$. These samples receive equal contributions from top quark and $\mathrm{W}(\ell\nu)$+jets production processes. The simulated events match the data m_j^* distribution at a 5% level in both normalization and shape within statistical uncertainties. Furthermore, this consistency has been verified under the following conditions: (a) applying a stricter than the SR $p_\mathrm{T}^\mathrm{miss}/p_\mathrm{T}^\mathrm{j} > 0.25$ requirement, which further suppresses QCD contributions,

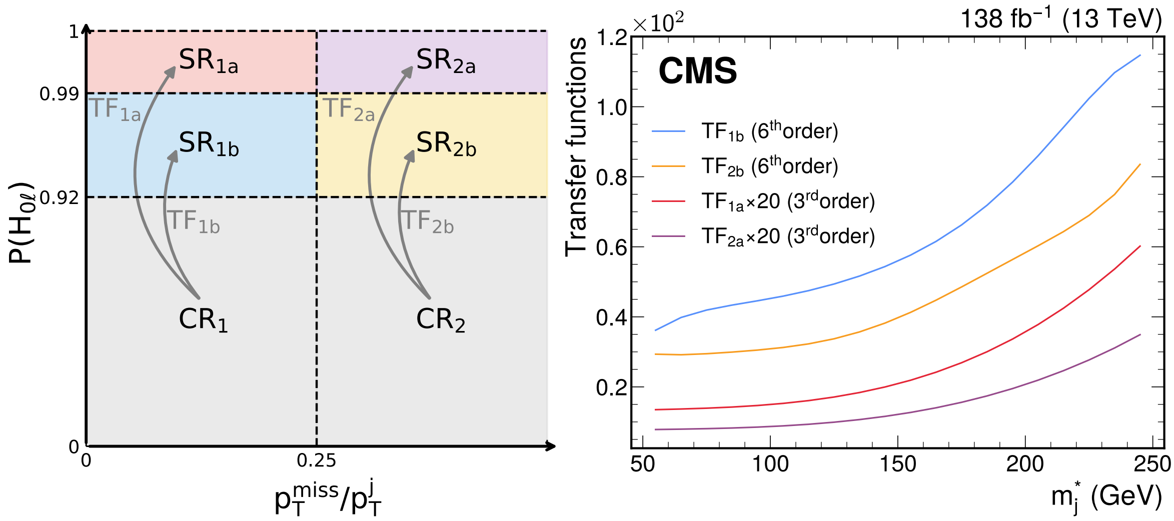

Figure 4. Illustration of the SRs and CRs, and the TFs used to relate the QCD background in the different regions (left). The TFs used to predict the QCD process in the four SRs as a function of the m_{j}^{*} (right).

(b) excluding narrow b-tagged jets, thereby enhancing W+jets fraction, and (c) requiring at least one b-tagged jet, increasing the presence of the top quark background.

Based on the observed data-to-simulation agreement in the aforementioned validation samples (all of which require a high PART score) and in relevant samples in the 1ℓ channel, a 5% rate uncertainty is assigned to each of the W+jets and top quark processes. This uncertainty collectively accounts for the limited simulation sample size, residual QCD contamination, and potential cross section mismodeling.

Events originating from the $\mathrm{H} \to \mathrm{ZZ} \to 4\mathrm{q}$ process are suppressed relative to $\mathrm{H} \to \mathrm{WW} \to 4\mathrm{q}$ decays because of the smaller branching fraction and reduced PART tagger efficiency, by factors of 10 and 3, respectively. This small fraction of background events entering SR_1 is estimated using simulation.

7 Analysis in the 1ℓ channel

The analysis in the 1ℓ channel focuses on events with one isolated lepton, targeting the $\mathrm{H}_{\ell\mathrm{qq}}$ final state. Events are partitioned into three mutually exclusive categories, targeting the ggF, VBF, and VH production processes.

7.1 Event selection

Online, events are collected using a combination of single-lepton (μ or e) triggers. For μ (e), these triggers require a p_{T} threshold of 50 (115) GeV and no isolation requirement, or a p_{T} above 24–27 (27–35) GeV and a I_{rel} requirement. The range indicates the difference in triggers across the different data-taking periods. At high p_{T}, single-electron triggers are complemented by a single photon trigger with thresholds of $p_{\mathrm{T}} > 175\,\mathrm{GeV}$ for the 2016 data-taking period and $p_{\mathrm{T}} > 200\,\mathrm{GeV}$ for the 2017 and 2018 periods. The isolated-lepton triggers allow for a lower p_{T}^{ℓ} threshold, even if they are less efficient for the signal. This motivates the

JHEP07(2026)248

following definition of an "isolated lepton" in the offline analysis. Muons are required to have $I_{\mathrm{mini}} < 0.2$ for $p_{\mathrm{T}} > 55\,\mathrm{GeV}$ and $I_{\mathrm{rel}} < 0.2$ for $30 < p_{\mathrm{T}} < 55\,\mathrm{GeV}$. Electrons are required to have $I_{\mathrm{rel}} < 0.15$ for $38 < p_{\mathrm{T}} < 120\,\mathrm{GeV}$, with no I_{mini} requirement for $p_{\mathrm{T}} > 120\,\mathrm{GeV}$.

Offline, events are required to contain at least one large-radius AK8 jet with $p_{\mathrm{T}} > 250\,\mathrm{GeV}$ and exactly one isolated μ or e. The H-candidate jet is defined as the AK8 jet satisfying $P(\mathrm{H}_{1\ell}) > 0.75$ and $m_{\mathrm{j}} > 40\,\mathrm{GeV}$, with an isolated lepton located in its vicinity, requiring the ΔR distance between the lepton and the jet axis to lie within $0.03 < \Delta R < 0.8$. Therefore, the lepton is one of the PF candidates of the jet, contributing to its mass and momentum.

The VBF category (1ℓ VBF) selects events with two additional AK4 jets accompanying the H-candidate jet, with the requirement that the jets be well separated and do not geometrically overlap. The two AK4 jets are required to have a pseudorapidity separation of $|\Delta\eta_{\mathrm{jj}}| > 3.5$ and an invariant mass of $m_{\mathrm{jj}} > 1\,\mathrm{TeV}$; the selection criteria were chosen to maximize the sensitivity to VBF production. If an event contains more than two AK4 jets, the two highest-p_{T} jets are used to compute $\Delta\eta_{\mathrm{jj}}$ and m_{jj}. Events containing fewer than two AK4 jets, or where $|\Delta\eta_{\mathrm{jj}}| < 3.5$ or $m_{\mathrm{jj}} < 1\,\mathrm{TeV}$, fall into the VH or ggF categories. Events with an additional AK8 jet tagged by the PARTICLENET algorithm as originating from a V boson ($P(\mathrm{V}) > 0.9$), satisfying $p_{\mathrm{T}} > 250\,\mathrm{GeV}$ and $m_{\mathrm{j}} > 40\,\mathrm{GeV}$, are assigned to the VH category. This V boson identification corresponds to selection efficiencies of approximately 33 and 0.5% for signal and background jets, respectively. Events without additional jets satisfying the above criteria are assigned to the ggF category. The H-candidate jet must also satisfy tagger requirements specific to each category: $P(\mathrm{H}_{1\ell}) > 0.93$ for the ggF category, and $P(\mathrm{H}_{1\ell}) > 0.905$ for the VBF and VH categories. This selection condition has been verified to preserve the background m_{j}^{*} peak location and shape, with no artificial enhancement observed near 125 GeV across different tagger score selections.

For the ggF and VBF categories, we require $p_{\mathrm{T}}^{\mathrm{miss}} > 20\,\mathrm{GeV}$ and, since signal events feature $\vec{p}_{\mathrm{T}}^{\mathrm{miss}}$ aligned with the H-candidate jet, we apply $|\Delta\phi(\mathrm{j}, \vec{p}_{\mathrm{T}}^{\mathrm{miss}})| < \pi/2$. To suppress $\mathrm{t\bar{t}}$ and single t backgrounds, events must not contain any b-tagged AK4 jets with the tight WP in the hemisphere opposite to the H-candidate jet. In the VH category, we reject events with a b-tagged AK4 jet that does not overlap with V- or H-tagged large-radius jet. Furthermore, events are required to have $p_{\mathrm{T}}^{\mathrm{miss}} > 30\,\mathrm{GeV}$, but there is no requirement on $|\Delta\phi(\mathrm{j}, \vec{p}_{\mathrm{T}}^{\mathrm{miss}})|$ in this category.

The ggF category is subdivided into three bins based on the p_{T} of the reconstructed H-candidate jet ($p_{\mathrm{T}}^{\mathrm{j}}$), with ranges of 250–350, 350–500, and >500 GeV. These bins are chosen to maximize the diagonal elements of the migration matrix (M_{mig}), which is formed using $p_{\mathrm{T}}^{\mathrm{j}}$ at the reconstructed level and the corresponding $p_{\mathrm{T}}^{\mathrm{H}}$ at the generator level. The corresponding $p_{\mathrm{T}}^{\mathrm{H}}$ bins are 200–300, 300–450, and >450 GeV, consistent with the recommendations of the simplified template cross section (STXS) framework version 1.2 [33, 34]. This choice facilitates future combined measurements of the differential Higgs boson production cross section as a function of $p_{\mathrm{T}}^{\mathrm{H}}$. The migration between generator-level STXS bins and the reconstruction-level

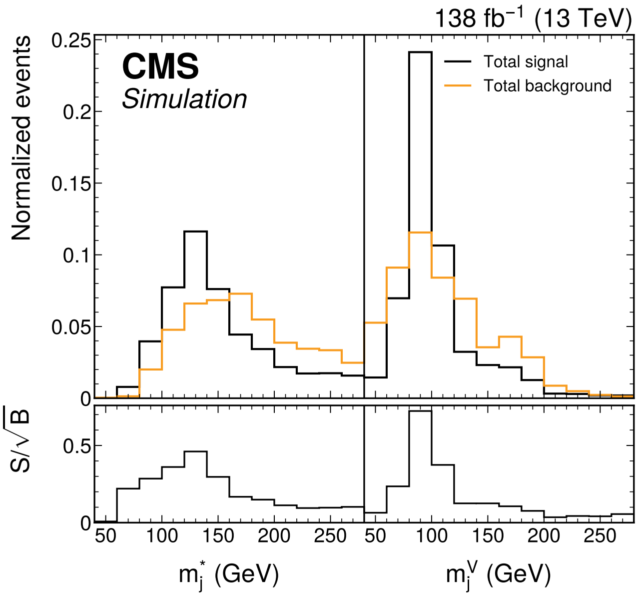

Figure 5. Distributions of m_{j}^* (left) and the $m_{\mathrm{j}}^{\mathrm{V}}$ (right) in the VH SR for simulated signal and background, normalized to unit area. The lower panels show the bin-by-bin $S/\sqrt{B}$. The superior signal-to-background separation of $m_{\mathrm{j}}^{\mathrm{V}}$, owing to its narrower resonant peak, motivates its use as the VH discriminant.

categories used in the 1ℓ channel is given by the matrix M_{mig}:

$$M_{\mathrm{mig}} = \begin{pmatrix} 0.72 & 0.05 & 0.14 & 0.09 \\ 0.02 & 0.78 & 0.18 & 0.02 \\ 0.05 & 0.20 & 0.70 & 0.05 \\ 0.05 & 0.04 & 0.26 & 0.65 \end{pmatrix},$$

where each row presents the fraction of generated signal events in the corresponding STXS bin reconstructed in each analysis category. The rows correspond to the VBF ($m_{\mathrm{jj}}^{\mathrm{gen}} > 1\,\mathrm{TeV}$, where $m_{\mathrm{jj}}^{\mathrm{gen}}$ is the generator-level dijet invariant mass) and ggF ($p_{\mathrm{T}}^{\mathrm{H}} \in [200, 300]$, $[300, 450]$, $> 450\,\mathrm{GeV}$) STXS bins, and the columns correspond to the VBF and ggF analysis categories at reconstruction level ($p_{\mathrm{T}}^{\mathrm{j}} \in [250, 350]$, $[350, 500]$, $> 500\,\mathrm{GeV}$). The dominant diagonal indicates good correspondence between the generator and the reconstruction binning.

The signal extraction is performed with a binned maximum likelihood fit, using the m_{j}^* in the ggF and VBF channels, and the V-candidate jet soft-drop mass, $m_{\mathrm{j}}^{\mathrm{V}}$, in the VH channel. The m_{j}^* distribution exhibits a broad peak, with the resolution limited by the presence of one or more neutrinos from decays of W bosons or τ leptons. For the VH channel, the $m_{\mathrm{j}}^{\mathrm{V}}$ distribution exhibits a sharper peak and more distinct shape differences from key backgrounds than m_{j}^*, as shown in figure 5, making it the preferred discriminant for this channel. A coarse binning is applied to the $m_{\mathrm{j}}^{\mathrm{V}}$ distribution, concentrating most signal events in a single bin ($70 < m_{\mathrm{j}}^{\mathrm{V}} < 110\,\mathrm{GeV}$) that captures events from both WH and ZH production processes. Limited event yields prevent a two-dimensional fit using both resonance masses.

7.2 Background estimation

The dominant sources of background are the W($\ell\nu$)+jets and $t\bar{t}$ processes, where a high-p_T lepton from a W boson decay is merged within a jet. Both contributions are estimated from simulation with corrections derived from data CRs. The background from events with misidentified leptons or leptons from heavy-flavor hadron decays (nonprompt leptons) is suppressed by the identification and isolation requirements imposed on the μ and e candidates, as well as the PART tagger selection, while the remaining contribution is estimated directly from data. Other subdominant sources of background originate from the Z+jets and diboson processes, and are estimated from simulation.

7.2.1 Nonprompt-lepton background

Background events containing nonprompt leptons misidentified as prompt, isolated leptons could be selected for the SR. This background includes the QCD multijet process. Using the data-driven method described below, its contribution to the total background yield in the signal and control regions is estimated to be less than 2%. The contribution of this background is obtained by reweighting events from a control sample containing lepton candidates that pass looser selection criteria than those of the SR, but fail the SR requirements. This sample has a minor contribution from EW processes containing genuine prompt leptons, which is subtracted from data using the simulation-based estimate. The weights, called misidentified-lepton factors, are measured in QCD-enriched samples, as $\epsilon_{\text{misID}}/(1-\epsilon_{\text{misID}})$, where ϵ_{misID} is the probability of a nonprompt lepton satisfying the less stringent criteria to also pass the SR criteria. The QCD-enriched samples follow the SR selection, except for requiring exactly one loose (rather than tight and isolated) lepton, no b-tagged AK4 jets at the loose DEEPJET WP, and $p_T^{\text{miss}} < 20\,\text{GeV}$ to suppress prompt-lepton contamination from W+jets and ensure orthogonality to the SR.

The misidentified-lepton factors are parameterized as a function of the p_T and η of the leptons. The uncertainty relative to the subtraction of the prompt-lepton background is also propagated into the misidentified-lepton factors. This method is described in detail in ref. [97].

7.2.2 The W + *jets* and top quark backgrounds

The background contributions from W($\ell\nu$)+jets and $t\bar{t}$ processes are estimated from simulation, with their rates constrained using data from CRs enriched in these processes. The CRs are defined by minimally modifying the selections of each SR to ensure orthogonality while preserving the same kinematic features.

To estimate the W($\ell\nu$)+jets contribution, a single "W+jets CR" is defined as a sideband in the PART discriminant, $P(\text{H}_{1\ell}) \in [0.75, 0.90]$. In the combined fit, this CR simultaneously constrains the W($\ell\nu$)+jets background in the ggF, VBF, and VH SRs, yielding a normalization SF of $0.89^{+0.13}_{-0.12}$. The correlated treatment is motivated by the kinematic similarity between the CR and SRs. Fitting each SR independently yields stable SFs and negligible impact on the result, indicating that acceptance differences among these regions are negligible. In addition, theoretical uncertainties on the W+jets process are treated as uncorrelated across the three SRs, as described in section 8, providing further freedom to absorb residual per-SR effects.

The $t\bar{t}$ contribution rate is estimated using two CRs: the "ggF/VBF Top CR" for the ggF and VBF categories collectively, and the "VH Top CR" specific to the VH category. These two CRs select distinct regions of phase space to account for possible mismodeling of the selection efficiency $P(\mathrm{V})$, which is applied only in the VH category, allowing independent normalization in the fit. The ggF/VBF Top CR requires $P(\mathrm{H}_{1\ell}) > 0.90$ and at least one b-tagged jet at the tight WP. The VH Top CR requires $P(\mathrm{H}_{1\ell}) > 0.75$, at least one b-tagged jet at the medium WP, and a V-tagged AK8 jet. In the combined fit of all channels, the $t\bar{t}$ normalization scale factors are $0.97^{+0.17}_{-0.14}$ for the ggF and VBF categories, and $2.01^{+0.38}_{-0.31}$ for the VH category. It has been verified that the larger SF arises from mismodeled selection efficiency specific to the requirement of two jets tagged for a signature that includes a hadronic V boson decay, which is common to the ParticleNet and ParT tagging requirements. In the $t\bar{t}$ events passing the 1ℓ selection, there is only one hadronic W boson decay. Therefore, passing all tagging requirements relies on another jet in the event, with extra radiation mimicking a two-prong structure; a topology not captured by the tagging efficiency scale factors. This situation is common to VH top CR and SR for $t\bar{t}$ events, but does not affect the signal, which has two genuine hadronic V boson decays.

We studied the potential mismodeling of the $t\bar{t}$ acceptance between the inclusive ggF/VBF Top CR and the VBF SR, where the latter probes a different kinematic phase space requiring two forward AK4 jets. Comparing the data-to-simulation agreement in the Top CR under its nominal selection and with additional VBF-like forward-jet requirements, accounting for the statistical limitations of the VBF category, yields a rate difference of 20%. Assigning this as an additional rate uncertainty exclusively to the $t\bar{t}$ normalization in the VBF SR was found to have a negligible impact on the result.

8 Systematic uncertainties

We consider several sources of systematic uncertainties of experimental and theoretical nature, which are summarized in table 3. They are included as nuisance parameters in the signal extraction procedure treated according to the frequentist paradigm [98].

Common experimental uncertainties between channels, affecting all simulation samples (both signal and background), include the uncertainty in the integrated luminosity, which varies between 1.2 and 2.5% for individual data-taking periods and amounts to 1.6% overall [25–27], and the uncertainty in the modeling of pileup interactions, evaluated by varying the total pp inelastic cross section by $\pm 4.5\%$ [99]. The jet energy scale and resolution corrections, as well as those of unclustered particles, are varied within their uncertainty as a function of jet p_{T} and η, and are propagated to the acceptance and mass observables of SRs. These uncertainties range from 0.5 to 8.0%.

Uncertainties in the trigger efficiency for the combination of single-lepton triggers, and the efficiencies for lepton reconstruction, identification, and isolation are evaluated as functions of lepton p_{T} and η. The overall magnitude of these uncertainties is 0.5% for the trigger efficiency uncertainty and 3–5% for uncertainties in the reconstruction and identification efficiency for μ and e.

The jet mass scale and resolution are corrected using data-to-simulation SFs close to unity (0.98–1.00 and 0.80–1.20, respectively), indicating good agreement between data and

		Channel	Effect		Corr.	
	Source of uncertainty		S and/or B	s or r	P	Y
Experimental	Integrated luminosity	0ℓ & 1ℓ	S & B	r	✓	✓
	Pileup	0ℓ & 1ℓ	S & B	s	✓	u
	Trigger	0ℓ & 1ℓ	S & B	r	✓	✓
	Jet energy scale	0ℓ & 1ℓ	S & B	s	✓	✓
	Jet energy resolution	0ℓ & 1ℓ	S & B	s	✓	u
	Jet mass scale & resolution	0ℓ & 1ℓ	S & B	s	✓	u
	Prefiring	0ℓ & 1ℓ	S & B	s	✓	u
	Unclustered energy	0ℓ & 1ℓ	S & B	s	✓	✓
	Simulated sample size	0ℓ & 1ℓ	S & B	s	u	u
	PART tagging efficiency	0ℓ & 1ℓ	S	r	u	✓
	μ/e rejection	0ℓ	S	s	—	✓
	QCD background estimate TFs	0ℓ	B	s	—	✓
	QCD estimate statistical uncertainty	0ℓ	B	s	—	u
	Top quark & W+jets bkg. normalization	0ℓ	B	r	—	✓
	PARTICLENET tagging efficiency	1ℓ	S	r	u	✓
	b tagging efficiency	1ℓ	S & B	r	✓	✓
	μ/e reconstruction, & isolation	1ℓ	S & B	r	✓	✓
	$t\bar{t}$ & single t floating normalization	1ℓ	B	r	✓	✓
	W+jets floating normalization	1ℓ	B	r	✓	✓
	Misid. ℓ rate, stat. uncertainty	1ℓ	B	s	—	u
	Misid. ℓ rate, EW SF stat. uncertainty	1ℓ	B	s	✓	✓
	Misid. ℓ rate, SF flavor & normalization	1ℓ	B	r	✓	✓
Theoretical	Branching fraction $\mathcal{B}(\mathrm{H} \to \mathrm{WW})$	0ℓ & 1ℓ	S	r	✓	✓
	α_S	0ℓ & 1ℓ	S & B	r	✓	✓
	Parton shower model	0ℓ & 1ℓ	S & B	s	u	✓
	Ren. & fact. scales, rate & acceptance	0ℓ & 1ℓ	S & B	s	u	✓
	PDF	0ℓ & 1ℓ	S & B	s	u	✓
	PDF acceptance	0ℓ & 1ℓ	S & B	s	u	✓
	QCD LO/NLO correction V+jets	1ℓ	B	s	u	✓
	EW NLO correction V+jets	1ℓ	B	r	u	✓

Table 3. Systematic uncertainty sources considered in the analysis. Left to right columns: the sources, the channels, whether the uncertainty affects signal (S) or background (B), its influence on shape (s) or rate (r), and whether the nuisances are (un)correlated (u or ✓) among different process models (P) or among the data-taking years (Y).

simulation [84]. The corresponding uncertainties are propagated to the analysis observables, m_{j}^{*} and $m_{\mathrm{j}}^{\mathrm{V}}$, for signal processes and background W boson matched jets, ranging from 0.5 to 7.0%.

During 2016–2017, mistiming in the ECAL endcaps ($2.5 < |\eta| < 3.0$) caused partial trigger efficiency loss ("prefiring") [38], corrected in simulation using control samples in data. The associated shape and rate uncertainties were found to have a minor impact but are included for all simulation-based samples.

The $\mathrm{H} \to \mathrm{WW}$ efficiency corrections for $P(\mathrm{H}_{0\ell})$ and $P(\mathrm{H}_{1\ell})$ are applied exclusively to signal processes, as only these processes contain such a genuine H-candidate jet. Uncertainties from the LJP reweighting method are propagated to these corrections and have a relative impact ranging from 5 to 15%. Three main sources of uncertainty are considered: (1) statistical, due to the limited event count used to derive the data-to-simulation ratio of LJP densities; (2) systematic, from modeling effects impacting the simulation in the ratio's denominator; and (3) extrapolation, related to applying the correction to subjets with higher p_{T} than those used in the control sample. The dominant uncertainty stems from the LJP method's assumption that jets can be reclustered into a prescribed number of subjets, each matching a quark. This uncertainty is decomposed into three components: (3a) "number of prongs," corresponding to the ambiguity in choosing the number of subjets and assessed by varying the number of subjets used in reclustering; (3b) "unclustered," corresponding to the presence of a generator-level quark failing to match any subjet even after varying the number of subjets, evaluated by scaling the weights for such events by factors of 5 and 1/5; and (3c) "distortion," arising from limitations in the reclustering procedure, such as misassignment of PF candidates to subjets, which can distort the reconstructed splitting tree. The latter component, which is the dominant one, is estimated by comparing LJP densities from the original W+jets sample and simulated signal, with their ratio providing the corresponding uncertainty. Details are given in ref. [91].

The LJP-based correction to the signal efficiency for the $P(\mathrm{H}_{0\ell})$ discriminant, combining $\mathrm{H}_{\ell\mathrm{qq}}$, $\mathrm{H}_{3\mathrm{q}}$, and $\mathrm{H}_{4\mathrm{q}}$ final states, is $0.84^{+0.14}_{-0.22}$ for $P(\mathrm{H}_{0\ell}) > 0.99$ and $0.95^{+0.13}_{-0.15}$ for $0.92 < P(\mathrm{H}_{0\ell}) < 0.99$. For the $P(\mathrm{H}_{1\ell})$ discriminant, considering the $\mathrm{H}_{\ell\mathrm{qq}}$ final state, the correction is $0.98^{+0.10}_{-0.24}$ for $P(\mathrm{H}_{1\ell}) > 0.905$ and $0.95^{+0.10}_{-0.28}$ for $P(\mathrm{H}_{1\ell}) > 0.93$. Unclustered quarks dominate the uncertainty, with rate effects ranging from 11 to 16% for $P(\mathrm{H}_{0\ell})$ and from 9 to 27% for $P(\mathrm{H}_{1\ell})$.

In the VH regions, the signal and top quark processes are assigned V-candidate jet tagging efficiency uncertainties of 3–7%, determined from calibration in semileptonic $\mathrm{t\bar{t}}$ events for W boson decays [83] and from the QCD proxy method for Z boson decays [84], respectively.

There are also experimental uncertainties in the estimation of the nonprompt-lepton background in the 1ℓ channel. This background is affected by the statistical uncertainty in the data sample used to derive the misidentified-lepton factors and by the uncertainty in the estimate of the prompt lepton contamination from EW processes that is subtracted from that sample. An overall 25% normalization uncertainty is assigned to the nonprompt-lepton background template based on a closure test in a QCD multijet-enriched sample, accounting for systematic uncertainties in the $\epsilon_{\mathrm{misID}}$ determination.

The $W(\ell\nu)$+jets and $t\bar{t}$ background yields are determined by floating normalization parameters constrained by the corresponding CRs as detailed in section 7.2.2. The resulting uncertainties in the fitted normalizations, corresponding to the statistical uncertainties, are about 15% for $W(\ell\nu)$+jets and 20% for $t\bar{t}$.

In addition to experimental uncertainties, theoretical uncertainties are included in the final fit to account for inaccuracies in the modeling of SM processes. Uncertainties in the V(qq)+jets processes account for missing higher-order QCD and mixed QCD-EW effects beyond those described in section 3, following the prescription of ref. [62]. The QCD NLO correction is implemented as a shape nuisance, propagating to the fit observables through the boson p_T dependence, while the mixed QCD-EW correction is implemented as a rate nuisance. The uncertainties due to the renormalization and factorization scales chosen for the simulated Higgs boson samples are propagated to the total expected yield of the Higgs boson signal according to the prescription recommended in ref. [6].

Uncertainties in the event yields due to initial- and final-state radiation are also calculated for all Higgs boson production processes by varying the renormalization scale and non-singular term using the PYTHIA 8 showering algorithm [51]. The PDFs and α_S uncertainties are further split between the cross section normalization uncertainties computed in ref. [33] for the Higgs boson signal and their effect on the acceptance. These uncertainties are neglected for other processes estimated from data.

Finally, the uncertainties due to the limited number of events in the simulated samples are included independently for each mass distribution bin in each category. These uncertainties are modeled with a single nuisance parameter per bin, following the Barlow-Beeston procedure [100] using the simplifying approximation from ref. [101].

The dominant systematic uncertainty in the 0ℓ channel arises from the modeling of the QCD multijet background through the fitted coefficients of the transfer function. In the 1ℓ channel, the dominant uncertainty arises from the asymmetric uncertainty in the PART tagger efficiency and the size of simulated signal samples in the VBF category.

9 Results

The signal is extracted from a binned maximum likelihood fit to the m_j^* (or m_j^V) distribution using the sum of the signal and background contributions. In the 0ℓ channel, the m_j^* distribution spans the 50–250 GeV range with 10 GeV binning. In the 1ℓ channel, it covers the 75–235 GeV range with 20 GeV binning. In the VH channel, the V-candidate jet soft-drop mass covers 40–180 GeV with a variable bin width. The test statistic chosen to determine the signal yield and the associated confidence intervals is based on the profile likelihood ratio [98],

$$t_\mu = -2\ln\left(\frac{\mathcal{L}(\mu, \hat{\hat{\vec{\nu}}}(\mu))}{\mathcal{L}(\hat{\mu}, \hat{\vec{\nu}})}\right), \tag{9.1}$$

where $\mathcal{L}$ denotes the combined likelihood function, and μ is the signal strength, defined as the ratio of the measured cross section to the SM expectation, taken as the parameter of interest. The $\hat{\mu}$ is its best fit value, while $\hat{\hat{\vec{\nu}}}(\mu)$ and $\hat{\vec{\nu}}$ represent the conditional and global maximum likelihood estimators of the nuisance parameters, respectively. The following results have been determined using COMBINE tool [90], which is based on the ROOFIT [102] and ROOSTATS [103] frameworks.

Separate fits are first performed for each production process and final state: the six regions of the 0ℓ channel (two CRs and four SRs) and the eight regions in the 1ℓ channel (three CRs and five SRs), to extract individual results. A simultaneous fit of all the regions is then performed to obtain the combined result. The observed data, post-fit background, and pre-fit signal distributions are shown in figures 6, 7, and 8. These correspond, respectively, to the 0ℓ SRs, the 1ℓ (ggF and VBF) SRs and CRs, and the 1ℓ VH SR and Top CR. The lower panels display the pull distributions, defined as the difference between the observed and post-fit predicted background event yields divided by the statistical uncertainty in the data, σ_{stat}. The total fit uncertainty σ_{fit} (also normalized to σ_{stat}) is overlaid. The data and fitted distributions are summed for all data-taking periods. Each signal production process is shown together with its sum, using pre-fit predictions scaled to the signal strength indicated in the legend, to allow direct comparison with the background.

The best fit value of the signal strength μ, defined as the measured cross section times the $\mathrm{H} \to \mathrm{WW}$ branching fraction relative to the SM expectation, and a 68% confidence level (CL) interval are extracted as $\mu = -0.19^{+0.48}_{-0.46}$ following ref. [104]. Figure 9 shows the observed scan of the test statistic t_μ as a function of μ for the combination of all channels. The result is decomposed into statistical and systematic uncertainties, yielding $\mu = -0.19^{+0.48}_{-0.46} = -0.19^{+0.30}_{-0.32}\,(\text{syst})^{+0.37}_{-0.34}\,(\text{stat})$.

To estimate the signal significance, we use the test statistic q_0 for the discovery of a positive signal,

$$q_0 = \begin{cases} -2\ln\left(\frac{\mathcal{L}(0,\hat{\hat{\vec{\nu}}}(0))}{\mathcal{L}(\hat{\mu},\hat{\vec{\nu}})}\right) & \text{if } \hat{\mu} > 0 \\ 0 & \text{otherwise.} \end{cases} \tag{9.2}$$

The expected and observed significances of the signal are estimated using the asymptotic formulae, $Z_0 = \sqrt{q_0}$ [105]. The expected significance is 1.86σ, while the observed significance is found to be 0.0σ as the best fit value of the signal strength is negative. The observed result lies below the SM expectation, $\mu = 1$, by 2.1 standard deviations when allowing for negative signal strength based on the uncapped test statistic t_0 [105].

The results are summarized in table 4. The signal strength scales all the signal processes by the same factor.

Figure 10 shows the observed and expected signal strength (left) and significance (right) for $\mathrm{H} \to \mathrm{WW}$ in all the channels for the full data set. Combined results are shown alongside individual contributions from each channel. For the 1ℓ channel, results are also shown for an alternative measurement using four independent signal strengths for the ggF and VBF processes, corresponding to different STXS generator-level $p_{\mathrm{T}}^{\mathrm{H}}$ bins introduced in section 7.1. For the ggF process, a signal strength is assigned to each bin of $p_{\mathrm{T}}^{\mathrm{H}}$: $[200, 300)$, $[300, 450)$, and $[450, +\infty)$ GeV. For the VBF process, an additional signal strength is assigned to the contribution satisfying $m_{\mathrm{jj}} > 1\,\text{TeV}$ for two forward generator-level jets.

The unfolded fiducial cross sections for the alternative measurement in the 1ℓ channel are shown in figure 11, together with predictions from the signal event generators. The cross section is extracted simultaneously in generator-level ggF and VBF bins following

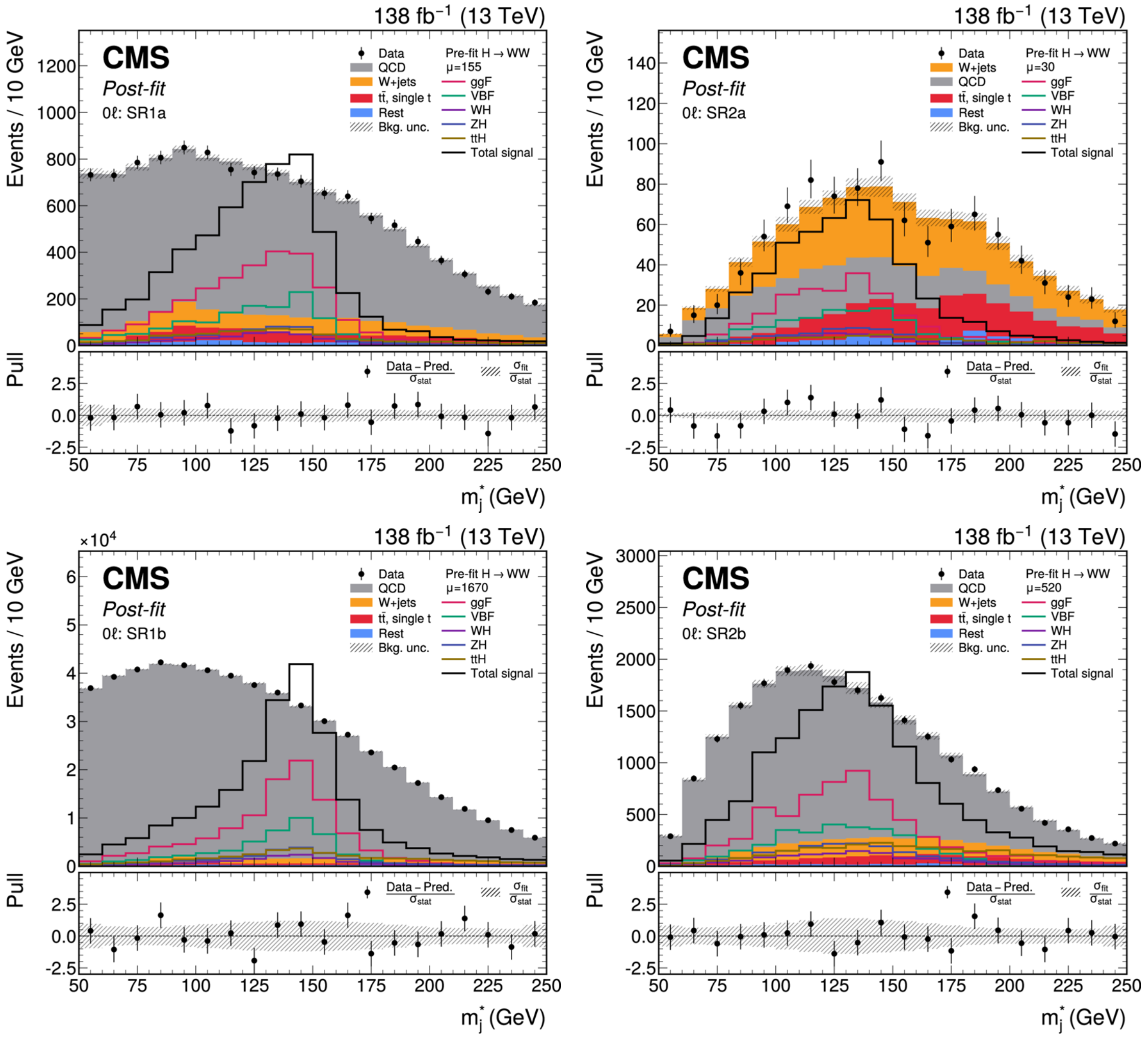

Figure 6. Post-fit m_j^* distributions in the 0ℓ channel, showing the predicted background with total uncertainty, observed data, and the expected pre-fit signal scaled by the labeled strength μ. From left to right, upper to lower, the plots correspond to $\mathrm{SR_{1a}}$, $\mathrm{SR_{2a}}$, $\mathrm{SR_{1b}}$, and $\mathrm{SR_{2b}}$. The lower panel of each plot presents the pull distribution, as well as the σ_fit normalized to the σ_stat.

	Signal strength μ		Significance σ	
Channel	Observed	Expected	Observed	Expected
0ℓ (Inclusive)	$+3.61^{+3.11}_{-2.73}$	$+1.00^{+2.86}_{-2.79}$	1.32	0.36
1ℓ (ggF + VBF)	$-0.30^{+0.49}_{-0.50}$	$+1.00^{+0.80}_{-0.62}$	0.00	1.68
1ℓ VH	$+0.03^{+1.92}_{-1.77}$	$+1.00^{+1.75}_{-1.52}$	0.01	0.65
Combination	$-0.19^{+0.48}_{-0.46}$	$+1.00^{+0.70}_{-0.56}$	0.00	1.86

Table 4. Observed and expected signal strength μ (second column) and significance σ (third column) for $\mathrm{H} \to \mathrm{WW}$ in the 0ℓ and 1ℓ channels, followed by the combined results.

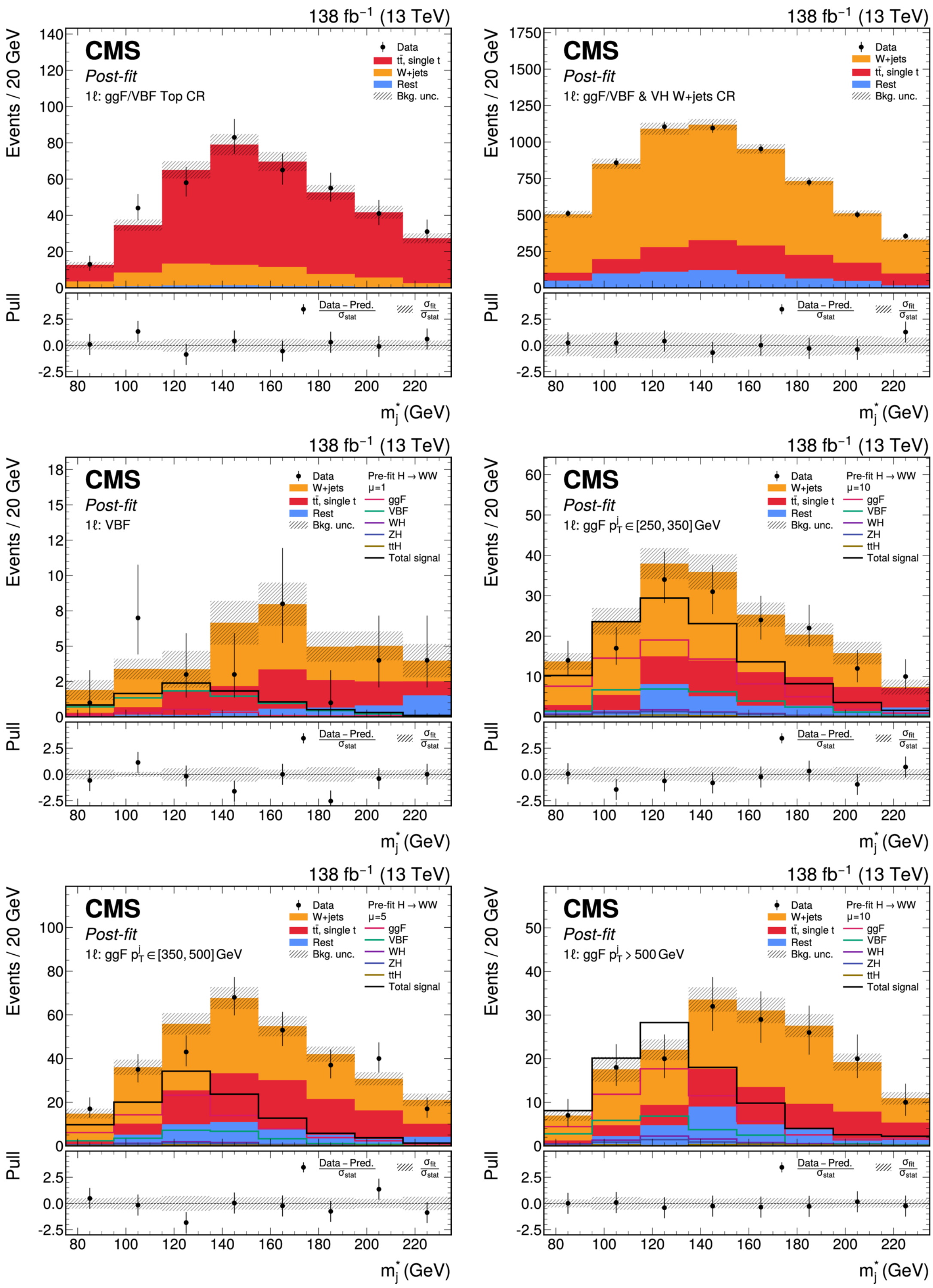

Figure 7. Post-fit m_{j}^* distributions in the 1ℓ channel, showing the predicted background with total uncertainty, observed data, and the expected pre-fit signal scaled by the labeled strength μ. Left to right and upper to lower: top CR, W+jets CR, VBF SR, and the ggF SRs binned in p_{T} as $[250, 350)$, $[350, 500)$, and $[500, +\infty)$ GeV, respectively. The lower panel of each plot presents the pull distribution, as well as σ_{fit} normalized to the σ_{stat}.

JHEP07(2026)248

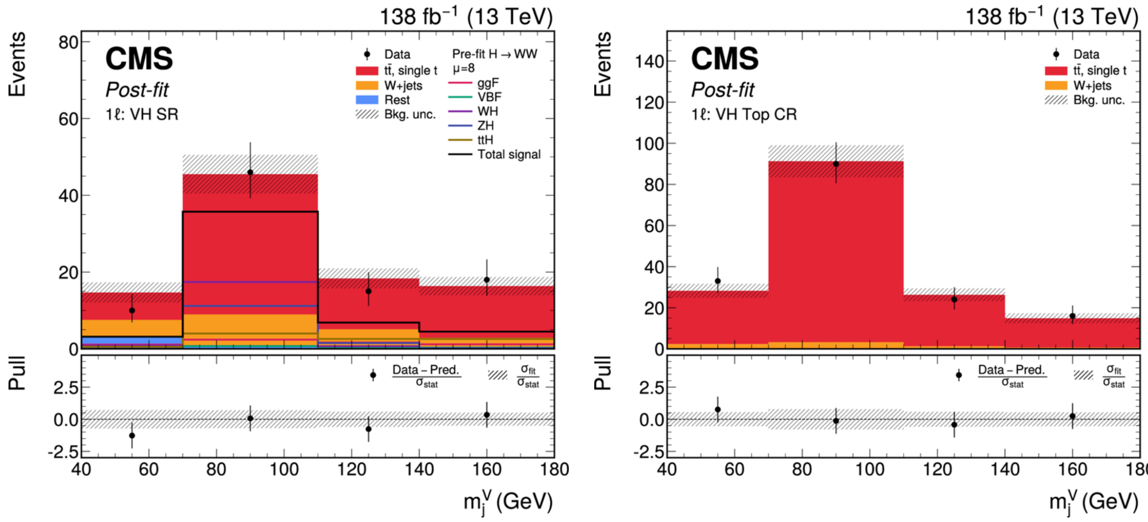

Figure 8. Post-fit $m_{\mathrm{j}}^{\mathrm{V}}$ distributions in the VH channel, showing the predicted background with total uncertainty, observed data, and expected signal, split by production process. Left to right: VH SR and VH Top CR. The lower panel of each plot presents the pull distribution, as well as σ_{fit} normalized to the σ_{stat}. The predicted pre-fit signal is scaled for visibility.

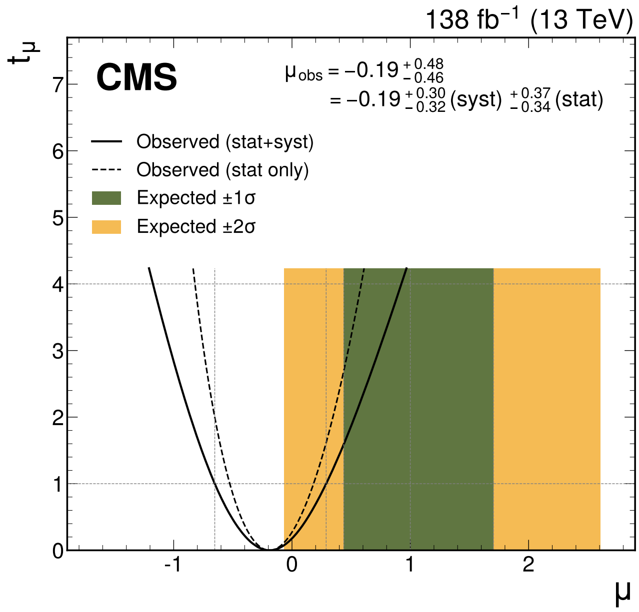

Figure 9. Observed scan of the profile likelihood test statistic t_μ as a function of the signal strength μ for the combination of all the channels. The solid lines correspond to profiling all statistical and systematic uncertainties, while the dashed lines correspond to profiling only the statistical uncertainties.

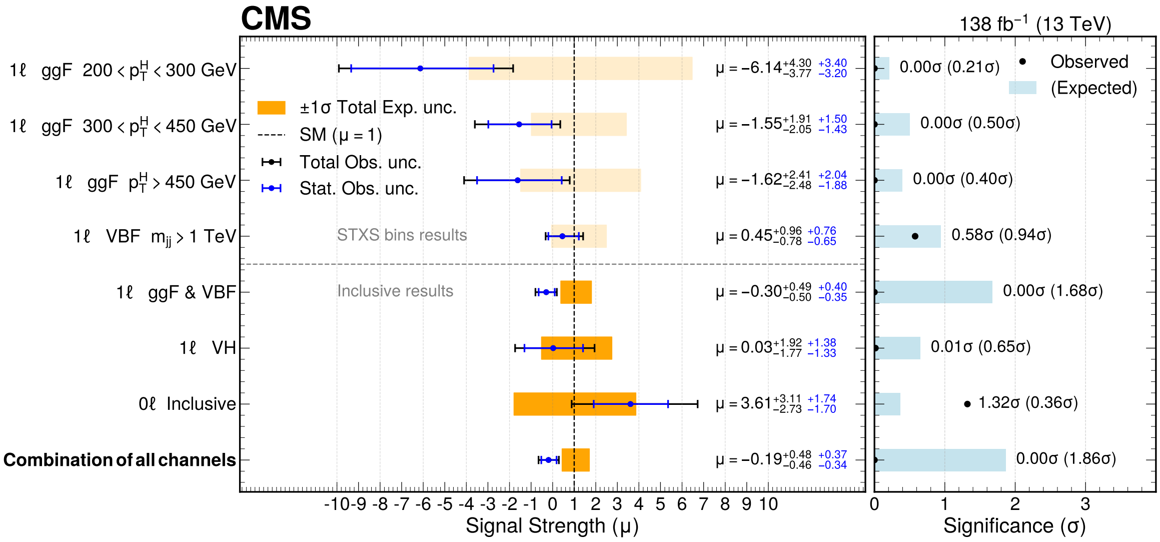

Figure 10. Observed and expected signal strength (left) and significance (right) for H $\rightarrow$ WW in all the channels using the full data set. Combined results are presented alongside individual contributions from each channel. Total expected uncertainties are indicated by yellow bands, while signal strength significances are shown with light blue bars. Blue and black lines represent statistical and total observed uncertainties, respectively.

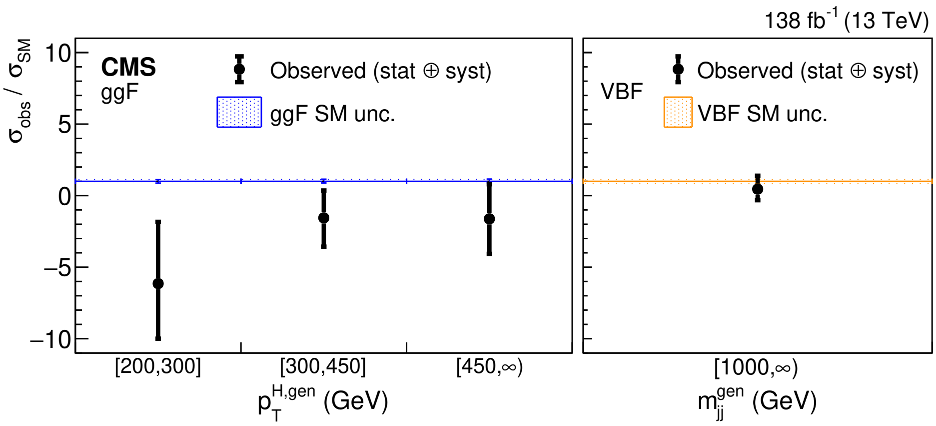

Figure 11. Unfolded measurement of the STXS cross sections in generator-level bins for three bins of Higgs boson p_T and one bin of m_{jj} in the 1ℓ channel. Measured cross sections are divided by standard-model expectations. Blue and orange uncertainty bands include theoretical uncertainties affecting the signal acceptance.

the STXS stage 1.2 scheme, similar to ref. [106], as described in section 7.1, to enable future combined differential cross section measurements in p_T^H bins. A maximum likelihood unfolding technique is employed to correct for detector acceptance and resolution effects in the measured production cross section. Each of the three cross section bins is modeled as a separate process with an independent signal strength parameter in the likelihood fit. Only theoretical uncertainties that impact the signal acceptance in the analysis selection are

Uncertainty source	Relative contribution to $\Delta\mu$
Total statistical uncertainty	75%
Total systematic uncertainty	66%
Simulated sample size	44%
PaRT tagging efficiency	35%
1ℓ background normalizations ($\mathrm{t\bar{t}}$, W+jets)	34%
0ℓ QCD background model (TFs & statistics)	28%
b tagging efficiency	26%
Background theory (NLO effects, parton shower, α_S)	21%
Other sources (pileup, prefiring, unclustered energy, misid. ℓ, ParticleNet tagger eff.)	17%
Signal theory (renormalization & factorization scales, PDF, parton shower, α_S, $\mathcal{B}$)	15%
Jet energy scale and resolution	13%
Triggers	11%
μ/e reconstruction, isolation & identification	9%
Jet mass scale & resolution	4%
Integrated luminosity	3%

Table 5. Relative contributions to $\Delta\mu$ from each uncertainty source, symmetrized as $(\Delta\mu_+ + \Delta\mu_-)/2$ and normalized to the total uncertainty. As nuisance-parameter groups are not statistically orthogonal, their sum may exceed 100%.

Decay	Production	Ref.	p_T^H [GeV] & bins	μ_{obs} total	μ_{obs} per p_T^H bin	Significance Obs.	Exp.
	Inclusive	[19]	> 450	$3.7^{+1.6}_{-1.5}$	—	2.5	0.7
$\mathrm{H \to bb}$	ggF	[106]	300–450–650–∞	$1.6^{+1.7}_{-1.5}$	$-2.1^{+4.8}_{-5.0}$ $1.9^{+1.8}_{-1.9}$ $2.0^{+3.0}_{-2.5}$	4.0	—
	VBF		> 200	$4.9^{+1.9}_{-1.6}$	$7.7^{+6.5}_{-6.1}$ $2.9^{+1.7}_{-1.5}$		
	V(qq)H	[20]	> 450	$0.72^{+0.75}_{-0.71}$	—	1.0	1.64
$\mathrm{H \to \tau\tau}$	Inclusive	[24]	> 250	$1.64^{+0.68}_{-0.54}$	—	3.5	2.2
$\mathrm{H \to WW}$	ggF+VBF	This analysis	200–300–450–∞	$-0.30^{+0.49}_{-0.50}$	$-6.15^{+4.32}_{-3.85}$ $-1.56^{+1.91}_{-2.01}$ $-1.62^{+2.42}_{-2.45}$	0.00	1.68
	VH		> 250	$0.03^{+1.92}_{-1.77}$	—	0.01	0.65
	Combination		> 250	$-0.19^{+0.48}_{-0.46}$	—	0.00	1.86

Table 6. Summary and comparison of the results with complementary CMS boosted H searches [19, 20, 24, 106]. For $\mathrm{H \to bb}$ ($\mathrm{H \to WW}$) VBF, the bins are on m_{jj}^{gen}: 1.0–1.5 and > 1.5 TeV (> 1 TeV).

considered. The best fit cross sections and their uncertainties are obtained by scaling each fitted signal strength and its uncertainty by the corresponding simulated SM cross section.

A breakdown of the uncertainty in μ, denoted $\Delta\mu$, is provided in table 5, obtained from profile-likelihood scans when each group of nuisance parameters is fixed to its post-fit value while the remaining parameters are profiled. Finally, the results of recent CMS searches for high-p_T H production are summarized in table 6.

JHEP07(2026)248

10 Summary

A search for Higgs boson (H) production at high transverse momentum is presented in the decay channel $\mathrm{H} \to \mathrm{WW}$. The analysis uses proton-proton collision data collected at $\sqrt{s} = 13\,\mathrm{TeV}$ with the CMS experiment, corresponding to an integrated luminosity of $138\,\mathrm{fb}^{-1}$, and focuses on WW decays with one or no isolated lepton (1ℓ and 0ℓ, respectively; $\ell = \mathrm{e}, \mu$) in the final state. The final states are characterized by a single large-radius jet containing the hadronic decay products of the W bosons, utilizing the jet substructure resulting from the Lorentz-boosted topology of the Higgs boson decay. The 1ℓ channel categorizes events by the dominant Higgs boson production mechanisms: gluon fusion, vector boson fusion, and vector boson associated production, while the 0ℓ channel remains inclusive across all production processes. The particle transformer algorithm leverages advanced machine-learning techniques to identify H-candidate jets with intricate substructure, missing transverse momentum aligned with the jet, or leptons inside the jet. It is calibrated with the Lund jet plane reweighting method and fine-tuned to optimize the expected signal significance in the 1ℓ channel, achieving 60% higher signal efficiency than the baseline tagger. The invariant mass of the candidate jet H or vector boson is used for signal extraction. The expected signal significance is 1.86 standard deviations, while the observed signal strength relative to the standard model expectation is $\mu = -0.19^{+0.48}_{-0.46}$, indicating no evidence of a signal above the background. These measurements represent the first dedicated study of highly Lorentz-boosted $\mathrm{H} \to \mathrm{WW}$ decays, complementing earlier searches for high transverse momentum Higgs boson production in other decay channels and production processes.

JHEP07(2026)248

Acknowledgments

We congratulate our colleagues in the CERN accelerator departments for the excellent performance of the LHC and thank the technical and administrative staffs at CERN and at other CMS institutes for their contributions to the success of the CMS effort. In addition, we gratefully acknowledge the computing centers and personnel of the Worldwide LHC Computing Grid and other centers for delivering so effectively the computing infrastructure essential to our analyses. Finally, we acknowledge the enduring support for the construction and operation of the LHC, the CMS detector, and the supporting computing infrastructure provided by the following funding agencies: SC (Armenia), BMBWF and FWF (Austria); FNRS and FWO (Belgium); CNPq, CAPES, FAPERJ, FAPERGS, and FAPESP (Brazil); MES and BNSF (Bulgaria); CERN; CAS, MoST, and NSFC (China); MINCIENCIAS (Colombia); MSES and CSF (Croatia); RIF (Cyprus); SENESCYT (Ecuador); ERC PRG and PSG, TARISTU24-TK10 and MoER TK202 (Estonia); Academy of Finland, MEC, and HIP (Finland); CEA and CNRS/IN2P3 (France); SRNSF (Georgia); BMFTR, DFG, and HGF (Germany); GSRI (Greece); NKFIH (Hungary); DAE and DST (India); IPM (Iran); SFI (Ireland); INFN (Italy); MSIT and NRF (Republic of Korea); MES (Latvia); LMTLT (Lithuania); MOE and UM (Malaysia); BUAP, CINVESTAV, CONACYT, LNS, SEP, and UASLP-FAI (Mexico); MOS (Montenegro); MBIE (New Zealand); PAEC (Pakistan); MES, NSC, and NAWA (Poland); FCT (Portugal); MESTD (Serbia); MICIU/AEI and PCTI (Spain); MOSTR (Sri Lanka); Swiss Funding Agencies (Switzerland); MST (Taipei); MHESI

(Thailand); TUBITAK and TENMAK (Türkiye); NASU (Ukraine); STFC (United Kingdom); DOE and NSF (U.S.A.).

Individuals have received support from the Marie-Curie program and the European Research Council and Horizon 2020 Grant, contract Nos. 675440, 724704, 752730, 758316, 765710, 824093, 101115353, 101002207, 101001205, and COST Action CA16108 (European Union); the Leventis Foundation; the Alfred P. Sloan Foundation; the Alexander von Humboldt Foundation; the Science Committee, project no. 22rl-037 (Armenia); the Fonds pour la Formation à la Recherche dans l'Industrie et dans l'Agriculture (FRIA) and Fonds voor Wetenschappelijk Onderzoek contract No. 1228724N (Belgium); the Beijing Municipal Science & Technology Commission, No. Z191100007219010, the Fundamental Research Funds for the Central Universities, the Ministry of Science and Technology of China under Grant No. 2023YFA1605804, the Natural Science Foundation of China under Grant No. 12535004, and USTC Research Funds of the Double First-Class Initiative No. YD2030002017 (China); the Ministry of Education, Youth and Sports (MEYS) of the Czech Republic; the Shota Rustaveli National Science Foundation, grant FR-22-985 (Georgia); the Deutsche Forschungsgemeinschaft (DFG), among others, under Germany's Excellence Strategy — EXC 2121 "Quantum Universe" — 390833306, and under project number 400140256 — GRK2497; the Hellenic Foundation for Research and Innovation (HFRI), Project Number 2288 (Greece); the Hungarian Academy of Sciences, the New National Excellence Program — ÚNKP, the NKFIH research grants K 131991, K 133046, K 138136, K 143460, K 143477, K 146913, K 146914, K 147048, 2020-2.2.1-ED-2021-00181, TKP2021-NKTA-64, and 2025-1.1.5-NEMZ_KI-2025-00004 (Hungary); the Council of Science and Industrial Research, India; ICSC — National Research Center for High Performance Computing, Big Data and Quantum Computing, FAIR — Future Artificial Intelligence Research, and CUP I53D23001070006 (Mission 4 Component 1), funded by the NextGenerationEU program, the Italian Ministry of University and Research (MUR) under Bando PRIN 2022 — CUP I53C24002390006, PRIN PRIMULA 2022RBYK7T (Italy); the Latvian Council of Science; the Ministry of Education and Science, project no. 2022/WK/14, and the National Science Center, contracts Opus 2021/41/B/ST2/01369, 2021/43/B/ST2/01552, 2023/49/B/ST2/03273, and the NAWA contract BPN/PPO/2021/1/00011 (Poland); the Fundação para a Ciência e a Tecnologia (Portugal); the National Priorities Research Program by Qatar National Research Fund; MICIU/AEI/10.13039/501100011033, ERDF/EU, "European Union NextGenerationEU/PRTR", projects PID2022-142604OB-C21, PID2022-139519OB-C21, PID2023-147706NB-I00, PID2023-148896NB-I00, PID2023-146983NB-I00, PID2023-147115NB-I00, PID2023-148418NB-C41, PID2023-148418NB-C42, PID2023-148418NB-C43, PID2023-148418NB-C44, PID2024-158190NB-C22, RYC2021-033305-I, RYC2024-048719-I, CNS2023-144781, CNS2024-154769 and Plan de Ciencia, Tecnología e Innovación de Asturias, Spain; the Chulalongkorn Academic into Its 2nd Century Project Advancement Project, the National Science, Research and Innovation Fund program IND_FF_68_369_2300_097, and the Program Management Unit for Human Resources & Institutional Development, Research and Innovation, grant B39G680009 (Thailand); the Eric & Wendy Schmidt Fund for Strategic Innovation through the CERN Next Generation Triggers project under grant agreement number SIF-2023-004; the Kavli Foundation; the Nvidia Corporation; the SuperMicro Corporation; the Welch Foundation, contract C-1845; and the Weston Havens Foundation (U.S.A.).

JHEP07(2026)248

Data Availability Statement. Release and preservation of data used by the CMS Collaboration as the basis for publications is guided by the CMS data preservation, re-use and open access policy.

Code Availability Statement. The CMS core software is publicly available on GitHub.

References

[1] ATLAS collaboration, *Observation of a new particle in the search for the Standard Model Higgs boson with the ATLAS detector at the LHC*, *Phys. Lett. B* **716** (2012) 1 [arXiv:1207.7214] [INSPIRE].

[2] CMS collaboration, *Observation of a new boson at a mass of 125 GeV with the CMS experiment at the LHC*, *Phys. Lett. B* **716** (2012) 30 [arXiv:1207.7235] [INSPIRE].

[3] CMS collaboration, *Observation of a new boson with mass near 125 GeV in pp collisions at* $\sqrt{s} = 7$ *and* 8 *TeV*, *JHEP* **06** (2013) 081 [arXiv:1303.4571] [INSPIRE].

[4] ATLAS collaboration, *A detailed map of Higgs boson interactions by the ATLAS experiment ten years after the discovery*, *Nature* **607** (2022) 52 [*Erratum ibid.* **612** (2022) E24] [arXiv:2207.00092] [INSPIRE].

[5] CMS collaboration, *A portrait of the Higgs boson by the CMS experiment ten years after the discovery*, *Nature* **607** (2022) 60 [arXiv:2207.00043] [INSPIRE].

[6] K. Becker et al., *Precise predictions for boosted Higgs production*, *SciPost Phys. Core* **7** (2024) 001 [arXiv:2005.07762] [INSPIRE].

[7] C. Grojean, E. Salvioni, M. Schlaffer and A. Weiler, *Very boosted Higgs in gluon fusion*, *JHEP* **05** (2014) 022 [arXiv:1312.3317] [INSPIRE].

[8] M. Schlaffer et al., *Boosted Higgs shapes*, *Eur. Phys. J. C* **74** (2014) 3120 [arXiv:1405.4295] [INSPIRE].

[9] S. Dawson, I.M. Lewis and M. Zeng, *Usefulness of effective field theory for boosted Higgs production*, *Phys. Rev. D* **91** (2015) 074012 [arXiv:1501.04103] [INSPIRE].

[10] M. Grazzini, A. Ilnicka, M. Spira and M. Wiesemann, *Modeling BSM effects on the Higgs transverse-momentum spectrum in an EFT approach*, *JHEP* **03** (2017) 115 [arXiv:1612.00283] [INSPIRE].

[11] F. Maltoni, K. Mawatari and M. Zaro, *Higgs characterisation via vector-boson fusion and associated production: NLO and parton-shower effects*, *Eur. Phys. J. C* **74** (2014) 2710 [arXiv:1311.1829] [INSPIRE].

[12] C. Degrande et al., *Electroweak Higgs boson production in the standard model effective field theory beyond leading order in QCD*, *Eur. Phys. J. C* **77** (2017) 262 [arXiv:1609.04833] [INSPIRE].

[13] CMS collaboration, *Measurement and interpretation of differential cross sections for Higgs boson production at* $\sqrt{s} = 13$ *TeV*, *Phys. Lett. B* **792** (2019) 369 [arXiv:1812.06504] [INSPIRE].

[14] CMS collaboration, *Measurement of the Higgs boson inclusive and differential fiducial production cross sections in the diphoton decay channel with pp collisions at* $\sqrt{s} = 13$ *TeV*, *JHEP* **07** (2023) 091 [arXiv:2208.12279] [INSPIRE].

[15] CMS collaboration, *Measurement of the inclusive and differential Higgs boson production cross sections in the leptonic WW decay mode at $\sqrt{s} = 13$ TeV*, *JHEP* **03** (2021) 003 [arXiv:2007.01984] [INSPIRE].

[16] CMS collaboration, *Measurement of the inclusive and differential Higgs boson production cross sections in the decay mode to a pair of τ leptons in pp collisions at $\sqrt{s} = 13$ TeV*, *Phys. Rev. Lett.* **128** (2022) 081805 [arXiv:2107.11486] [INSPIRE].

[17] CMS collaboration, *Measurements of inclusive and differential cross sections for the Higgs boson production and decay to four-leptons in proton-proton collisions at $\sqrt{s} = 13$ TeV*, *JHEP* **08** (2023) 040 [arXiv:2305.07532] [INSPIRE].

[18] CMS collaboration, *Inclusive search for a highly boosted Higgs boson decaying to a bottom quark-antiquark pair*, *Phys. Rev. Lett.* **120** (2018) 071802 [arXiv:1709.05543] [INSPIRE].

[19] CMS collaboration, *Inclusive search for highly boosted Higgs bosons decaying to bottom quark-antiquark pairs in proton-proton collisions at $\sqrt{s} = 13$ TeV*, *JHEP* **12** (2020) 085 [arXiv:2006.13251] [INSPIRE].

[20] CMS collaboration, *Search for a boosted Higgs boson decaying to bottom quark pairs in association with a W or Z boson in proton-proton collisions at $\sqrt{s} = 13$ TeV*, *Phys. Lett. B* **879** (2026) 140534 [arXiv:2601.05362] [INSPIRE].

[21] ATLAS collaboration, *Constraints on Higgs boson production with large transverse momentum using $H \to b\bar{b}$ decays in the ATLAS detector*, *Phys. Rev. D* **105** (2022) 092003 [arXiv:2111.08340] [INSPIRE].

[22] ATLAS collaboration, *Study of high-transverse-momentum Higgs boson production in association with a vector boson in the qqbb final state with the ATLAS detector*, *Phys. Rev. Lett.* **132** (2024) 131802 [arXiv:2312.07605] [INSPIRE].

[23] ATLAS collaboration, *Evidence of Higgs boson inclusive production at high transverse momentum decaying to a pair of b-quarks with the ATLAS detector*, arXiv:2603.19369 [INSPIRE].

[24] CMS collaboration, *Measurement of the production cross section of a Higgs boson with large transverse momentum in its decays to a pair of τ leptons in proton-proton collisions at $\sqrt{s} = 13$ TeV*, *Phys. Lett. B* **857** (2024) 138964 [arXiv:2403.20201] [INSPIRE].

[25] CMS collaboration, *Precision luminosity measurement in proton-proton collisions at $\sqrt{s} = 13$ TeV in 2015 and 2016 at CMS*, *Eur. Phys. J. C* **81** (2021) 800 [arXiv:2104.01927] [INSPIRE].

[26] CMS collaboration, *CMS luminosity measurement for the 2017 data-taking period at $\sqrt{s} = 13$ TeV*, CMS-PAS-LUM-17-004 (2018) [INSPIRE].

[27] CMS collaboration, *CMS luminosity measurement for the 2018 data-taking period at $\sqrt{s} = 13$ TeV*, CMS-PAS-LUM-18-002 (2019) [INSPIRE].

[28] H. Qu, C. Li and S. Qian, *Particle transformer for jet tagging*, arXiv:2202.03772 [INSPIRE].

[29] A. Vaswani et al., *Attention is all you need*, in the proceedings of the *31st International Conference on Neural Information Processing Systems*, Long Beach, U.S.A., December 04–09 (2017) [arXiv:1706.03762] [INSPIRE].

[30] CMS collaboration, *Particle transformers for identifying Lorentz-boosted Higgs bosons decaying to a pair of W bosons*, arXiv:2604.09809 [INSPIRE].

[31] H. Qu and L. Gouskos, *ParticleNet: jet tagging via particle clouds*, *Phys. Rev. D* **101** (2020) 056019 [arXiv:1902.08570] [INSPIRE].

[32] CMS collaboration, *Identification of heavy, energetic, hadronically decaying particles using machine-learning techniques*, 2020 *JINST* **15** P06005 [arXiv:2004.08262] [INSPIRE].

JHEP07(2026)248

[33] LHC Higgs Cross Section Working Group collaboration, *Handbook of LHC Higgs cross sections: 4. Deciphering the nature of the Higgs sector*, CERN Yellow Rep. Monogr. **2** (2017) 1 [arXiv:1610.07922] [INSPIRE].

[34] N. Berger et al., *Simplified template cross sections — stage 1.1 and 1.2*, arXiv:1906.02754 [DOI:10.21468/SciPostPhysCommRep.15] [INSPIRE].

[35] *HEPData record for this analysis*, https://doi.org/10.17182/hepdata.167419 (2026)

[36] CMS collaboration, *The CMS experiment at the CERN LHC*, 2008 *JINST* **3** S08004 [INSPIRE].

[37] CMS collaboration, *Development of the CMS detector for the CERN LHC run 3*, 2024 *JINST* **19** P05064 [arXiv:2309.05466] [INSPIRE].

[38] CMS collaboration, *Performance of the CMS level-1 trigger in proton-proton collisions at* $\sqrt{s} = 13$ *TeV*, 2020 *JINST* **15** P10017 [arXiv:2006.10165] [INSPIRE].

[39] CMS collaboration, *The CMS trigger system*, 2017 *JINST* **12** P01020 [arXiv:1609.02366] [INSPIRE].

[40] CMS collaboration, *Performance of the CMS high-level trigger during LHC run 2*, 2024 *JINST* **19** P11021 [arXiv:2410.17038] [INSPIRE].

[41] CMS collaboration, *Electron and photon reconstruction and identification with the CMS experiment at the CERN LHC*, 2021 *JINST* **16** P05014 [arXiv:2012.06888] [INSPIRE].

[42] CMS collaboration, *Performance of the CMS muon detector and muon reconstruction with proton-proton collisions at* $\sqrt{s} = 13$ *TeV*, 2018 *JINST* **13** P06015 [arXiv:1804.04528] [INSPIRE].

[43] CMS collaboration, *Description and performance of track and primary-vertex reconstruction with the CMS tracker*, 2014 *JINST* **9** P10009 [arXiv:1405.6569] [INSPIRE].

[44] K. Hamilton, P. Nason, C. Oleari and G. Zanderighi, *Merging* $H/W/Z + 0$ *and* 1 *jet at NLO with no merging scale: a path to parton shower + NNLO matching*, *JHEP* **05** (2013) 082 [arXiv:1212.4504] [INSPIRE].

[45] T. Neumann, *NLO Higgs+jet production at large transverse momenta including top quark mass effects*, *J. Phys. Comm.* **2** (2018) 095017 [arXiv:1802.02981] [INSPIRE].

[46] P. Nason and C. Oleari, *NLO Higgs boson production via vector-boson fusion matched with shower in POWHEG*, *JHEP* **02** (2010) 037 [arXiv:0911.5299] [INSPIRE].

[47] G. Luisoni, P. Nason, C. Oleari and F. Tramontano, $HW^{\pm}/HZ + 0$ *and* 1 *jet at NLO with the POWHEG BOX interfaced to GoSam and their merging within MiNLO*, *JHEP* **10** (2013) 083 [arXiv:1306.2542] [INSPIRE].

[48] H.B. Hartanto, B. Jager, L. Reina and D. Wackeroth, *Higgs boson production in association with top quarks in the POWHEG BOX*, *Phys. Rev. D* **91** (2015) 094003 [arXiv:1501.04498] [INSPIRE].

[49] S. Alioli, P. Nason, C. Oleari and E. Re, *A general framework for implementing NLO calculations in shower Monte Carlo programs: the POWHEG BOX*, *JHEP* **06** (2010) 043 [arXiv:1002.2581] [INSPIRE].

[50] S. Bolognesi et al., *On the spin and parity of a single-produced resonance at the LHC*, *Phys. Rev. D* **86** (2012) 095031 [arXiv:1208.4018] [INSPIRE].

[51] T. Sjöstrand et al., *An introduction to PYTHIA 8.2*, *Comput. Phys. Commun.* **191** (2015) 159 [arXiv:1410.3012] [INSPIRE].

[52] J. Alwall et al., *The automated computation of tree-level and next-to-leading order differential cross sections, and their matching to parton shower simulations*, *JHEP* **07** (2014) 079 [arXiv:1405.0301] [INSPIRE].

JHEP07(2026)248

[53] T. Gleisberg et al., *Event generation with SHERPA 1.1*, *JHEP* **02** (2009) 007 [arXiv:0811.4622] [INSPIRE].

[54] SHERPA collaboration, *Event generation with Sherpa 2.2*, *SciPost Phys.* **7** (2019) 034 [arXiv:1905.09127] [INSPIRE].

[55] T. Gleisberg and S. Hoeche, *Comix, a new matrix element generator*, *JHEP* **12** (2008) 039 [arXiv:0808.3674] [INSPIRE].

[56] J. Alwall et al., *Comparative study of various algorithms for the merging of parton showers and matrix elements in hadronic collisions*, *Eur. Phys. J. C* **53** (2008) 473 [arXiv:0706.2569] [INSPIRE].

[57] S. Hoeche, F. Krauss, M. Schonherr and F. Siegert, *QCD matrix elements + parton showers: the NLO case*, *JHEP* **04** (2013) 027 [arXiv:1207.5030] [INSPIRE].

[58] R. Frederix and S. Frixione, *Merging meets matching in MC@NLO*, *JHEP* **12** (2012) 061 [arXiv:1209.6215] [INSPIRE].

[59] S. Kallweit et al., *NLO electroweak automation and precise predictions for W+multijet production at the LHC*, *JHEP* **04** (2015) 012 [arXiv:1412.5157] [INSPIRE].

[60] S. Kallweit et al., *NLO QCD+EW predictions for V+jets including off-shell vector-boson decays and multijet merging*, *JHEP* **04** (2016) 021 [arXiv:1511.08692] [INSPIRE].

[61] S. Kallweit et al., *NLO QCD+EW automation and precise predictions for V+multijet production*, in the proceedings of the *50th Rencontres de Moriond on QCD and High Energy Interactions*, La Thuile, Italy, March 21–28 (2015) [arXiv:1505.05704] [INSPIRE].

[62] J.M. Lindert et al., *Precise predictions for V+jets dark matter backgrounds*, *Eur. Phys. J. C* **77** (2017) 829 [arXiv:1705.04664] [INSPIRE].

[63] P. Nason, *A new method for combining NLO QCD with shower Monte Carlo algorithms*, *JHEP* **11** (2004) 040 [hep-ph/0409146] [INSPIRE].

[64] S. Frixione, P. Nason and C. Oleari, *Matching NLO QCD computations with parton shower simulations: the POWHEG method*, *JHEP* **11** (2007) 070 [arXiv:0709.2092] [INSPIRE].

[65] S. Alioli, S.-O. Moch and P. Uwer, *Hadronic top-quark pair-production with one jet and parton showering*, *JHEP* **01** (2012) 137 [arXiv:1110.5251] [INSPIRE].

[66] S. Alioli, P. Nason, C. Oleari and E. Re, *NLO single-top production matched with shower in POWHEG: s- and t-channel contributions*, *JHEP* **09** (2009) 111 [*Erratum ibid.* **02** (2010) 011] [arXiv:0907.4076] [INSPIRE].

[67] R. Frederix, E. Re and P. Torrielli, *Single-top t-channel hadroproduction in the four-flavour scheme with POWHEG and aMC@NLO*, *JHEP* **09** (2012) 130 [arXiv:1207.5391] [INSPIRE].

[68] J.M. Campbell and R.K. Ellis, *MCFM for the Tevatron and the LHC*, *Nucl. Phys. B Proc. Suppl.* **205-206** (2010) 10 [arXiv:1007.3492] [INSPIRE].

[69] CMS collaboration, *Extraction and validation of a new set of CMS PYTHIA8 tunes from underlying-event measurements*, *Eur. Phys. J. C* **80** (2020) 4 [arXiv:1903.12179] [INSPIRE].

[70] NNPDF collaboration, *Parton distributions from high-precision collider data*, *Eur. Phys. J. C* **77** (2017) 663 [arXiv:1706.00428] [INSPIRE].

[71] GEANT4 collaboration, *GEANT4 — a simulation toolkit*, *Nucl. Instrum. Meth. A* **506** (2003) 250 [INSPIRE].

[72] J. Allison et al., *GEANT4 developments and applications*, *IEEE Trans. Nucl. Sci.* **53** (2006) 270 [INSPIRE].

[73] CMS collaboration, *Particle-flow reconstruction and global event description with the CMS detector*, 2017 *JINST* **12** P10003 [arXiv:1706.04965] [INSPIRE].

JHEP07(2026)248

[74] D. Contardo et al., *Technical proposal for the phase-II upgrade of the CMS detector*, CERN-LHCC-2015-010 (2015) [DOI:10.17181/CERN.VU8I.D59J] [INSPIRE].

[75] M. Cacciari, G.P. Salam and G. Soyez, *The anti-k_t jet clustering algorithm*, *JHEP* **04** (2008) 063 [arXiv:0802.1189] [INSPIRE].

[76] M. Cacciari, G.P. Salam and G. Soyez, *FastJet user manual*, *Eur. Phys. J. C* **72** (2012) 1896 [arXiv:1111.6097] [INSPIRE].

[77] CMS collaboration, *Pileup mitigation at CMS in 13 TeV data*, 2020 *JINST* **15** P09018 [arXiv:2003.00503] [INSPIRE].

[78] D. Bertolini, P. Harris, M. Low and N. Tran, *Pileup per particle identification*, *JHEP* **10** (2014) 059 [arXiv:1407.6013] [INSPIRE].

[79] CMS collaboration, *Jet energy scale and resolution in the CMS experiment in pp collisions at 8 TeV*, 2017 *JINST* **12** P02014 [arXiv:1607.03663] [INSPIRE].

[80] CMS collaboration, *Jet algorithms performance in 13 TeV data*, CMS-PAS-JME-16-003 (2017) [INSPIRE].

[81] CMS collaboration, *Performance of missing transverse momentum reconstruction in proton-proton collisions at $\sqrt{s} = 13$ TeV using the CMS detector*, 2019 *JINST* **14** P07004 [arXiv:1903.06078] [INSPIRE].

[82] A.J. Larkoski, S. Marzani, G. Soyez and J. Thaler, *Soft drop*, *JHEP* **05** (2014) 146 [arXiv:1402.2657] [INSPIRE].

[83] CMS collaboration, *Calibration of the top and W jet tagging efficiency in 13 TeV data collected by the CMS experiment in 2016–2018*, CMS-DP-2025-010, CERN, Geneva, Switzerland (2025).

[84] CMS collaboration, *Performance of heavy-flavour jet identification in Lorentz-boosted topologies in proton-proton collisions at $\sqrt{s} = 13$ TeV*, 2025 *JINST* **20** P11006 [arXiv:2510.10228] [INSPIRE].

[85] E. Bols et al., *Jet flavour classification using DeepJet*, 2020 *JINST* **15** P12012 [arXiv:2008.10519] [INSPIRE].

[86] CMS collaboration, *Performance of the DeepJet b tagging algorithm using 41.9 fb^{-1} of data from proton-proton collisions at 13 TeV with phase 1 CMS detector*, CMS-DP-2018-058, CERN, Geneva, Switzerland (2018).

[87] CMS collaboration, *Performance of electron reconstruction and selection with the CMS detector in proton-proton collisions at $\sqrt{s} = 8$ TeV*, 2015 *JINST* **10** P06005 [arXiv:1502.02701] [INSPIRE].

[88] K. Rehermann and B. Tweedie, *Efficient identification of boosted semileptonic top quarks at the LHC*, *JHEP* **03** (2011) 059 [arXiv:1007.2221] [INSPIRE].

[89] C. Li et al., *Accelerating resonance searches via signature-oriented pre-training*, arXiv:2405.12972 [INSPIRE].

[90] CMS collaboration, *The CMS statistical analysis and combination tool: Combine*, *Comput. Softw. Big Sci.* **8** (2024) 19 [arXiv:2404.06614] [INSPIRE].

[91] CMS collaboration, *A method for correcting the substructure of multiprong jets using the Lund jet plane*, *JHEP* **11** (2025) 038 [arXiv:2507.07775] [INSPIRE].

[92] F.A. Dreyer, G.P. Salam and G. Soyez, *The Lund jet plane*, *JHEP* **12** (2018) 064 [arXiv:1807.04758] [INSPIRE].

[93] S. Catani, Y.L. Dokshitzer, M.H. Seymour and B.R. Webber, *Longitudinally invariant K_t clustering algorithms for hadron hadron collisions*, *Nucl. Phys. B* **406** (1993) 187 [INSPIRE].

JHEP07(2026)248

[94] S.D. Ellis and D.E. Soper, *Successive combination jet algorithm for hadron collisions*, *Phys. Rev. D* **48** (1993) 3160 [hep-ph/9305266] [INSPIRE].

[95] D. Krohn, J. Thaler and L.-T. Wang, *Jet trimming*, *JHEP* **02** (2010) 084 [arXiv:0912.1342] [INSPIRE].

[96] R.A. Fisher, *On the interpretation of χ^2 from contingency tables, and the calculation of P*, *J. Roy. Statist. Soc.* **85** (1922) 87.

[97] CMS collaboration, *Measurements of properties of the Higgs boson decaying to a W boson pair in pp collisions at $\sqrt{s} = 13$ TeV*, *Phys. Lett. B* **791** (2019) 96 [arXiv:1806.05246] [INSPIRE].

[98] ATLAS et al. collaborations, *Procedure for the LHC Higgs boson search combination in Summer 2011*, CMS-NOTE-2011-005 (2011) [INSPIRE].

[99] CMS collaboration, *Measurement of the inelastic proton-proton cross section at $\sqrt{s} = 13$ TeV*, *JHEP* **07** (2018) 161 [arXiv:1802.02613] [INSPIRE].

[100] R.J. Barlow and C. Beeston, *Fitting using finite Monte Carlo samples*, *Comput. Phys. Commun.* **77** (1993) 219 [INSPIRE].

[101] J.S. Conway, *Incorporating nuisance parameters in likelihoods for multisource spectra*, in the proceedings of the *PHYSTAT 2011*, Geneva, Switzerland, January 17–20 (2011) [DOI:10.5170/CERN-2011-006.115] [arXiv:1103.0354] [INSPIRE].

[102] W. Verkerke and D.P. Kirkby, *The RooFit toolkit for data modeling*, *eConf C* **0303241** (2003) MOLT007 [physics/0306116] [INSPIRE].

[103] L. Moneta et al., *The RooStats project*, *PoS* **ACAT2010** (2010) 057 [arXiv:1009.1003] [INSPIRE].

[104] CMS collaboration, *Precise determination of the mass of the Higgs boson and tests of compatibility of its couplings with the standard model predictions using proton collisions at 7 and 8 TeV*, *Eur. Phys. J. C* **75** (2015) 212 [arXiv:1412.8662] [INSPIRE].

[105] G. Cowan, K. Cranmer, E. Gross and O. Vitells, *Asymptotic formulae for likelihood-based tests of new physics*, *Eur. Phys. J. C* **71** (2011) 1554 [*Erratum ibid.* **73** (2013) 2501] [arXiv:1007.1727] [INSPIRE].

[106] CMS collaboration, *Measurement of boosted Higgs bosons produced via vector boson fusion or gluon fusion in the $H \to b\bar{b}$ decay mode using LHC proton-proton collision data at $\sqrt{s} = 13$ TeV*, *JHEP* **12** (2024) 035 [arXiv:2407.08012] [INSPIRE].

The CMS collaboration

A. Hayrapetyan[1], V. Makarenko[1], A. Tumasyan[1,a], W. Adam[2], L. Benato[2], T. Bergauer[2], M. Dragicevic[2], P.S. Hussain[2], M. Jeitler[2,b], N. Krammer[2], A. Li[2], D. Liko[2], M. Matthewman[2], J. Schieck[2,b], R. Schöfbeck[2,b], M. Shooshtari[2], M. Sonawane[2], N. Van Den Bossche[2], W. Waltenberger[2], C.-E. Wulz[2,b], T. Janssen[3], H. Kwon[3], D. Ocampo Henao[3], T. Van Laer[3], P. Van Mechelen[3], D. Ahmadi[4], J. Bierkens[4], N. Breugelmans[4], J. D'Hondt[4], S. Dansana[4], A. De Moor[4], M. Delcourt[4], C. Gupta[4], F. Heyen[4], Y. Hong[4], P. Kashko[4], S. Lowette[4], I. Makarenko[4], S. Nandakumar[4], S. Tavernier[4], M. Tytgat[4,c], G.P. Van Onsem[4], S. Van Putte[4], D. Vannerom[4], T. Wybouw[4], A. Beshr[5], B. Bilin[5], F. Caviglia Roman[5], B. Clerbaux[5], A.K. Das[5], I. De Bruyn[5], G. De Lentdecker[5], E. Ducarme[5], H. Evard[5], L. Favart[5], A. Khalilzadeh[5], A. Malara[5], M.A. Shahzad[5], A. Sharma[5], L. Thomas[5], M. Vanden Bemden[5], C. Vander Velde[5], P. Vanlaer[5], F. Zhang[5], A. Cauwels[6], M. De Coen[6], D. Dobur[6], C. Giordano[6], G. Gokbulut[6], K. Kaspar[6], D. Kavtaradze[6], D. Marckx[6], K. Skovpen[6], A.M. Tomaru[6], J. van der Linden[6], J. Vandenbroeck[6], H. Aarup Petersen[7], S. Bein[7], A. Benecke[7], A. Bethani[7], G. Bruno[7], A. Cappati[7], J. De Favereau De Jeneret[7], C. Delaere[7], F. Gameiro Casalinho[7], A. Giammanco[7], A.O. Guzel[7], V. Lemaitre[7], J. Lidrych[7], P. Malek[7], S. Turkcapar[7], G.A. Alves[8], M. Barroso Ferreira Filho[8], E. Coelho[8], M.V. Gonçalves Sales[8], C. Hensel[8], D. Matos Figueiredo[8], T. Menezes De Oliveira[8], C. Mora Herrera[8], P. Rebello Teles[8], M. Soeiro[8], E.J. Tonelli Manganote[8,d], A. Vilela Pereira[8], W.L. Aldá Júnior[9], H. Brandao Malbouisson[9], W. Carvalho[9], J. Chinellato[9,e], M. Costa Reis[9], E.M. Da Costa[9], D. Da Silva Dalto[9], G.G. Da Silveira[9,f], D. De Jesus Damiao[9], S. Fonseca De Souza[9], R. Gomes De Souza[9], S. S. Jesus[9], T. Laux Kuhn[9,f], K. Maslova[9], K. Mota Amarilo[9], L. Mundim[9], H. Nogima[9], J.P. Pinheiro[9], A. Santoro[9], A. Sznajder[9], M. Thiel[9], F. Torres Da Silva De Araujo[9,g], C.A. Bernardes[10], L. Calligaris[10], J. Carvalho Leite[10], F. Damas[10], T.R. Fernandez Perez Tomei[10], E.M. Gregores[10], B. Lopes Da Costa[10], I. Maietto Silverio[10], P.G. Mercadante[10], S.F. Novaes[10], Sandra S. Padula[10], V. Scheurer[10], A. Aleksandrov[11], G. Antchev[11], P. Danev[11], R. Hadjiiska[11], P. Iaydjiev[11], M. Shopova[11], G. Sultanov[11], A. Dimitrov[12], L. Litov[12], B. Pavlov[12], P. Petkov[12], A. Petrov[12], S. Keshri[13], D. Laroze[13], M. Meena[13], S. Thakur[13], W. Brooks[14], T. Cheng[15], T. Javaid[15], L. Wang[15], L. Yuan[15], J. Gu[16], Z. Hu[16], Z. Liang[16], J. Liu[16], X. Wang[16], Y. Wang[16], H. Yang[16], S. Zhang[16], G.M. Chen[17,h], H.S. Chen[17,h], M. Chen[17,h], Y. Chen[17], Q. Hou[17], X. Hou[17], F. Iemmi[17], C.H. Jiang[17], H. Liao[17], G. Liu[17], Z.-A. Liu[17,i], S. Song[17], J. Tao[17], C. Wang[17,h], J. Wang[17], H. Zhang[17], J. Zhao[17], A. Agapitos[18], Y. Ban[18], A. Carvalho Antunes De Oliveira[18], S. Deng[18], X. Geng[18], B. Guo[18], Q. Guo[18], Z. He[18], C. Jiang[18], A. Levin[18], C. Li[18], Q. Li[18], Y. Mao[18], S. Qian[18], S.J. Qian[18], X. Qin[18], C. Quaranta[18], X. Sun[18], D. Wang[18], J. Wang[18], T. Yang[18], M. Zhang[18], Y. Zhao[18], C. Zhou[18], X. Hua[19], S. Yang[19], Z. You[20], N. Lu[21], G. Bauer[22,j,k], L. Chen[22], Z. Cui[22,k], B. Li[22,l], H. Wang[22], K. Yi[22,m], J. Zhang[22], C. Li[23], Y. Li[24], Y. Zhou[24,n], Z. Lin[25], C. Lu[25], M. Xiao[25,o], C. Avila[26], A. Cabrera[26], C. Florez[26], J.A. Reyes Vega[26], C. Rendón[27], M. Rodriguez[27], A.A. Ruales Barbosa[27], J.D. Ruiz Alvarez[27], N. Godinovic[28], D. Lelas[28], A. Sculac[28], M. Kovac[29], A. Petkovic[29],

T. Sculac[29], P. Bargassa[30], V. Brigljevic[30], D. Ferencek[30], K. Jakovcic[30], A. Starodumov[30], T. Susa[30], A. Attikis[31], K. Christoforou[31], S. Konstantinou[31], C. Leonidou[31], L. Paizanos[31], F. Ptochos[31], P.A. Razis[31], H. Rykaczewski[31], H. Saka[31], A. Stepennov[31], M. Finger[32,†], M. Finger Jr.[32], E. Acurio[33], E. Carrera Jarrin[34], H. Abdalla[35,p], Y. Assran[35,q,r], A. Hussein[36], H. Mohammed[36], K. Jaffel[37], M. Kadastik[37], T. Lange[37], C. Nielsen[37], J. Pata[37], M. Raidal[37], N. Seeba[37], L. Tani[37], E. Brücken[38], A. Milieva[38], K. Osterberg[38], M. Voutilainen[38], F. Garcia[39], T. Hilden[39], P. Inkaew[39], K.T.S. Kallonen[39], R. Kumar Verma[39], T. Lampén[39], K. Lassila-Perini[39], B. Lehtela[39], S. Lehti[39], T. Lindén[39], N.R. Mancilla Xinto[39], M. Myllymäki[39], M.m. Rantanen[39], S. Saariokari[39], N.T. Toikka[39], J. Tuominiemi[39], N. Bin Norjoharuddeen[40], H. Kirschenmann[40], P. Luukka[40], H. Petrow[40], M. Besancon[41], F. Couderc[41], M. Dejardin[41], D. Denegri[41], P. Devouge[41], J.L. Faure[41], F. Ferri[41], P. Gaigne[41], S. Ganjour[41], P. Gras[41], F. Guilloux[41], G. Hamel de Monchenault[41], M. Kumar[41], V. Lohezic[41], Y. Maidannyk[41], J. Malcles[41], F. Orlandi[41], L. Portales[41], S. Ronchi[41], M.Ö. Sahin[41], P. Simkina[41], M. Titov[41], M. Tornago[41], R. Amella Ranz[42], F. Beaudette[42], G. Boldrini[42], P. Busson[42], C. Charlot[42], M. Chiusi[42], T.D. Cuisset[42], O. Davignon[42], A. De Wit[42], T. Debnath[42], I.T. Ehle[42], S. Ghosh[42], A. Gilbert[42], R. Granier de Cassagnac[42], M. Manoni[42], M. Nguyen[42], S. Obraztsov[42], C. Ochando[42], R. Salerno[42], J.B. Sauvan[42], Y. Sirois[42], G. Sokmen[42], Y. Song[42], L. Urda Gómez[42], A. Zabi[42], A. Zghiche[42], J.-L. Agram[43,s], J. Andrea[43], D. Bloch[43], J.-M. Brom[43], E.C. Chabert[43], C. Collard[43], G. Coulon[43], S. Falke[43], U. Goerlach[43], A.-C. Le Bihan[43], G. Saha[43], A. Savoy-Navarro[43,t], P. Vaucelle[43], A. Di Florio[44], B. Orzari[44], D. Amram[45], S. Beauceron[45], B. Blancon[45], G. Boudoul[45], N. Chanon[45], D. Contardo[45], P. Depasse[45], H. El Mamouni[45], J. Fay[45], E. Fillaudeau[45], S. Gascon[45], M. Gouzevitch[45], C. Greenberg[45], G. Grenier[45], B. Ille[45], E. Jourd'Huy[45], M. Lethuillier[45], B. Massoteau[45], L. Mirabito[45], A. Purohit[45], M. Vander Donckt[45], C. Verollet[45], D. Chokheli[46], I. Lomidze[46], Z. Tsamalaidze[46,u], K.F. Adamowicz[47], V. Botta[47], S. Consuegra Rodríguez[47], L. Feld[47], K. Klein[47], M. Lipinski[47], P. Nattland[47], V. Oppenländer[47], A. Pauls[47], D. Pérez Adán[47], C. Daumann[48], S. Diekmann[48], N. Eich[48], D. Eliseev[48], F. Engelke[48], J. Erdmann[48], M. Erdmann[48], M.Z. Farkas[48], B. Fischer[48], T. Hebbeker[48], K. Hoepfner[48], A. Jung[48], N. Kumar[48], M.y. Lee[48], F. Mausolf[48], M. Merschmeyer[48], A. Meyer[48], A. Pozdnyakov[48], W. Redjeb[48], H. Reithler[48], U. Sarkar[48], V. Sarkisovi[48], A. Schmidt[48], C. Seth[48], A. Sharma[48], J.L. Spah[48], V. Vaulin[48], U. Willemsen[48], S. Zaleski[48], F.P. Zinn[48], M.R. Beckers[49], G. Flügge[49], N. Hoeflich[49], T. Kress[49], A. Nowack[49], O. Pooth[49], A. Stahl[49], A. Abel[50], M. Aldaya Martin[50], J. Alimena[50], Y. An[50], I. Andreev[50], J. Bach[50], S. Baxter[50], H. Becerril Gonzalez[50], O. Behnke[50], A. Belvedere[50], F. Blekman[50,v], K. Borras[50,w], A. Campbell[50], S. Chatterjee[50], L.X. Coll Saravia[50], G. Eckerlin[50], D. Eckstein[50], E. Gallo[50,v], A. Geiser[50], M. Guthoff[50], A. Hinzmann[50], M. Kasemann[50], C. Kleinwort[50], R. Kogler[50], M. Komm[50], D. Krücker[50], F. Labe[50], W. Lange[50], D. Leyva Pernia[50], J.h. Li[50], K.-Y. Lin[50], K. Lipka[50,x], W. Lohmann[50,y], J. Malvaso[50], R. Mankel[50], I.-A. Melzer-Pellmann[50], M. Mendizabal Morentin[50], A.B. Meyer[50], G. Milella[50], K. Moral Figueroa[50], A. Mussgiller[50], L.P. Nair[50], J. Niedziela[50], A. Nürnberg[50], J. Park[50], E. Ranken[50], A. Raspereza[50], D. Rastorguev[50],

L. Rygaard[50], M. Scham[50,z,aa], S. Schnake[50,w], P. Schütze[50], C. Schwanenberger[50,v], D. Schwarz[50], D. Selivanova[50], K. Sharko[50], M. Shchedrolosiev[50], D. Stafford[50], M. Torkian[50], S. Vashishtha[50], A. Ventura Barroso[50], R. Walsh[50], D. Wang[50], Q. Wang[50], K. Wichmann[50], L. Wiens[50,w], C. Wissing[50], Y. Yang[50], S. Zakharov[50], A. Zimermmane Castro Santos[50], A.R. Alves Andrade[51], M. Antonello[51], S. Bollweg[51], M. Bonanomi[51], L. Ebeling[51], K. El Morabit[51], Y. Fischer[51], M. Frahm[51], E. Garutti[51], A. Grohsjean[51], A.A. Guvenli[51], J. Haller[51], D. Hundhausen[51], M. Jalalvandi[51], G. Kasieczka[51], P. Keicher[51], R. Klanner[51], W. Korcari[51], T. Kramer[51], C.c. Kuo[51], J. Lange[51], A. Lobanov[51], J. Matthiesen[51], L. Moureaux[51], K. Nikolopoulos[51], K.J. Pena Rodriguez[51], N. Prouvost[51], B. Raciti[51], M. Rieger[51], D. Savoiu[51], P. Schleper[51], M. Schröder[51], J. Schwandt[51], M. Sommerhalder[51], H. Stadie[51], G. Steinbrück[51], T. Tore von Schwartz[51], R. Ward[51], B. Wiederspan[51], M. Wolf[51], C. Yede[51], A. Brusamolino[52], E. Butz[52], Y.M. Chen[52], T. Chwalek[52], A. Dierlamm[52], G.G. Dincer[52], D. Druzhkin[52], U. Elicabuk[52], N. Faltermann[52], M. Giffels[52], A. Gottmann[52], F. Hartmann[52,ab], F. Hummer[52], U. Husemann[52], J. Kieseler[52], M. Klute[52], J. Knolle[52], R. Kunnilan Muhammed Rafeek[52], O. Lavoryk[52], J.M. Lawhorn[52], S. Maier[52], T. Mehner[52], M. Molch[52], A.A. Monsch[52], M. Mormile[52], Th. Müller[52], E. Pfeffer[52], M. Presilla[52], G. Quast[52], K. Rabbertz[52], B. Regnery[52], R. Schmieder[52], T. Selezneva[52], N. Shadskiy[52], I. Shvetsov[52], H.J. Simonis[52], L. Sowa[52], L. Stockmeier[52], K. Tauqeer[52], M. Toms[52], B. Topko[52], N. Trevisani[52], C. Verstege[52], T. Voigtländer[52], R.F. Von Cube[52], J. Von Den Driesch[52], C. Winter[52], R. Wolf[52], W.D. Zeuner[52], X. Zuo[52], G. Anagnostou[53], G. Daskalakis[53], A. Kyriakis[53], G. Melachroinos[54], Z. Painesis[54], I. Paraskevas[54], N. Plastiras[54], N. Saoulidou[54], K. Theofilatos[54], E. Tziaferi[54], E. Tzovara[54], K. Vellidis[54], I. Zisopoulos[54], T. Chatzistavrou[55], G. Karapostoli[55], K. Kousouris[55], E. Siamarkou[55], G. Tsipolitis[55], I. Evangelou[56], C. Foudas[56], P. Katsoulis[56], P. Kokkas[56], P.G. Kosmoglou Kioseoglou[56], N. Manthos[56], I. Papadopoulos[56], J. Strologas[56], C. Hajdu[57], D. Horvath[57,ac,ad], Á. Kadlecsik[57], C. Lee[57], K. Márton[57], A.J. Rádl[57,ae], F. Sikler[57], V. Veszpremi[57], D. Biro[58], M. Csanád[58], K. Farkas[58], A. Fehérkuti[58,af], M.M.A. Gadallah[58,ag], M. León Coello[58], G. Pásztor[58], G.I. Veres[58], B. Ujvari[59], G. Zilizi[59], G. Bencze[60], S. Czellar[60], J. Molnar[60], Z. Szillasi[60], T. Csorgo[61,af], F. Nemes[61,af], T. Novak[61], I. Szanyi[61,ah], S. Bahinipati[62], R. Raturi[62], S. Bansal[63], S.B. Beri[63], V. Bhatnagar[63], B. Chauhan[63], S. Chauhan[63], N. Dhingra[63,ai], A. Kaur[63], H. Kaur[63], M. Kaur[63], S. Kumar[63], T. Sheokand[63], J.B. Singh[63], A. Singla[63], K. Verma[63], A. Bhardwaj[64], A. Chhetri[64], B.C. Choudhary[64], A. Kumar[64], A. Kumar[64], M. Naimuddin[64], S. Phor[64], C. Prakash[64], K. Ranjan[64], M.K. Saini[64], P. Palni[65], S. Acharya[66,aj], B. Gomber[66], S. Ganguly[67], S. Mukherjee[67], S. Bhattacharya[68], S. Das Gupta[68], S. Dutta[68], S. Dutta[68], S. Sarkar[68], M.M. Ameen[69], P.K. Behera[69], S. Chatterjee[69], G. Dash[69], A. Dattamunsi[69], P. Jana[69], P. Kalbhor[69], S. Kamble[69], J.R. Komaragiri[69,ak], T. Mishra[69], P.R. Pujahari[69], A.K. Sikdar[69], R.K. Singh[69], P. Verma[69], S. Verma[69], A. Vijay[69], S. Nayak[70], H. Rajpoot[70], B.K. Sirasva[70], L. Bhatt[71], S. Dugad[71], G.B. Mohanty[71], M. Shelake[71], P. Suryadevara[71], A. Bala[72], S. Banerjee[72], S. Barman[72,al], R.M. Chatterjee[72], M. Guchait[72], Sh. Jain[72], A. Jaiswal[72], S. Kumar[72], M. Maity[72,al], G. Majumder[72], K. Mazumdar[72], S. Parolia[72], R. Pramanik[72], R. Saxena[72],

JHEP07(2026)248

A. Thachayath[72], D. Maity[73,am], P. Mal[73], K. Naskar[73,am], A. Nayak[73,am], K. Pal[73], P. Sadangi[73], S.K. Swain[73], S. Varghese[73,am], D. Vats[73,am], S. Dube[74], P. Hazarika[74], B. Kansal[74], A. Laha[74], R. Sharma[74], S. Sharma[74], K.Y. Vaish[74], S. Ghosh[75], H. Bakhshiansohi[76,an], A. Jafari[76,ao], V. Sedighzadeh Dalavi[76], M. Zeinali[76,ap], S. Bashiri[77], S. Chenarani[77,aq], S.M. Etesami[77], Y. Hosseini[77], M. Khakzad[77], E. Khazaie[77], M. Mohammadi Najafabadi[77], M. Nourbakhsh[77], S. Tizchang[77,ar], M. Felcini[78], M. Grunewald[78], M. Abbrescia[79a,79b], M. Barbieri[79a,79b], M. Buonsante[79a,79b], A. Colaleo[79a,79b], D. Creanza[79a,79c], N. De Filippis[79a,79c], M. De Palma[79a,79b], W. Elmetenawee[79a,79b,as], N. Ferrara[79a,79c], L. Fiore[79a], L. Generoso[79a,79b], L. Longo[79a], M. Louka[79a,79b], G. Maggi[79a,79c], M. Maggi[79a], I. Margjeka[79a], V. Mastrapasqua[79a,79b], S. My[79a,79b], F. Nenna[79a,79b], S. Nuzzo[79a,79b], A. Pellecchia[79a,79b], A. Pompili[79a,79b], F.M. Procacci[79a,79b], G. Pugliese[79a,79c], R. Radogna[79a,79b], D. Ramos[79a], A. Ranieri[79a], L. Silvestris[79a], F.M. Simone[79a,79c], Ü. Sözbilir[79a], A. Stamerra[79a,79b], D. Troiano[79a,79b], R. Venditti[79a,79b], P. Verwilligen[79a], A. Zaza[79a,79b], G. Abbiendi[80a], C. Battilana[80a,80b], D. Bonacorsi[80a,80b], P. Capiluppi[80a,80b], F.R. Cavallo[80a], M. Cruciani[80a,80b], G.M. Dallavalle[80a], T. Diotalevi[80a,80b], F. Fabbri[80a], A. Fanfani[80a,80b], R. Farinelli[80a], D. Fasanella[80a], L. Ferragina[80a,80b], P. Giacomelli[80a], C. Grandi[80a], L. Guiducci[80a,80b], S. Lo Meo[80a,at], M. Lorusso[80a,80b], L. Lunerti[80a], S. Marcellini[80a], G. Masetti[80a], F.L. Navarria[80a,80b], G. Paggi[80a,80b], A. Perrotta[80a], A.M. Rossi[80a,80b], S. Rossi Tisbeni[80a,80b], G.P. Siroli[80a,80b], S. Costa[81a,81b,au], A. Di Mattia[81a], A. Lapertosa[81a], R. Potenza[81a,81b], A. Tricomi[81a,81b,au], J. Altork[82a,82b], P. Assiouras[82a], G. Barbagli[82a], G. Bardelli[82a], M. Bartolini[82a,82b], A. Calandri[82a,82b], B. Camaiani[82a,82b], A. Cassese[82a], R. Ceccarelli[82a], V. Ciulli[82a,82b], C. Civinini[82a], R. D'Alessandro[82a,82b], L. Damenti[82a,82b], E. Focardi[82a,82b], T. Kello[82a], G. Latino[82a,82b], P. Lenzi[82a,82b], M. Lizzo[82a], M. Meschini[82a], S. Paoletti[82a], A. Papanastassiou[82a,82b], G. Sguazzoni[82a], L. Viliani[82a], L. Benussi[83], S. Colafranceschi[83,av], S. Meola[83,aw], D. Piccolo[83], M. Alves Gallo Pereira[84a], F. Ferro[84a], E. Robutti[84a], S. Tosi[84a,84b], A. Benaglia[85a], F. Brivio[85a], V. Camagni[85a,85b], F. Cetorelli[85a,85b], F. De Guio[85a,85b], M.E. Dinardo[85a,85b], P. Dini[85a], S. Gennai[85a], R. Gerosa[85a,85b], A. Ghezzi[85a,85b], P. Govoni[85a,85b], L. Guzzi[85a], M.R. Kim[85a], G. Lavizzari[85a,85b], M.T. Lucchini[85a,85b], M. Malberti[85a], S. Malvezzi[85a], A. Massironi[85a], D. Menasce[85a], L. Moroni[85a], M. Paganoni[85a,85b], S. Palluotto[85a,85b], D. Pedrini[85a], A. Perego[85a,85b], T. Tabarelli de Fatis[85a,85b], S. Buontempo[86a], F. Confortini[86a,86b], C. Di Fraia[86a,86b], F. Fabozzi[86a,86c], L. Favilla[86a,86d], A.O.M. Iorio[86a,86b], L. Lista[86a,86b,ax], P. Paolucci[86a,ab], B. Rossi[86a], P. Azzi[87a], N. Bacchetta[87a,ay], M. Bellato[87a], D. Bisello[87a,87b], L. Borella[87a], P. Bortignon[87a,87c], G. Bortolato[87a,87b], A.C.M. Bulla[87a,87c], R. Carlin[87a,87b], P. Checchia[87a], T. Dorigo[87a,az], F. Gasparini[87a,87b], S. Giorgetti[87a], N. Lai[87a], E. Lusiani[87a], M. Margoni[87a,87b], A.T. Meneguzzo[87a,87b], J. Pazzini[87a,87b], F. Primavera[87a,87b], P. Ronchese[87a,87b], R. Rossin[87a,87b], F. Simonetto[87a,87b], M. Tosi[87a,87b], A. Triossi[87a,87b], S. Ventura[87a], P. Zotto[87a,87b], A. Zucchetta[87a,87b], G. Zumerle[87a,87b], A. Braghieri[88a], M. Brunoldi[88a,88b], S. Calzaferri[88a,88b], P. Montagna[88a,88b], M. Pelliccioni[88a,88b], V. Re[88a], C. Riccardi[88a,88b], P. Salvini[88a], I. Vai[88a,88b], P. Vitulo[88a,88b], S. Ajmal[89a,89b], M.E. Ascioti[89a,89b], G.M. Bilei[89a,†],

C. Carrivale[89a,89b], D. Ciangottini[89a,89b], L. Della Penna[89a,89b], L. Fanò[89a,89b], V. Mariani[89a,89b], M. Menichelli[89a], F. Moscatelli[89a,ba], A. Rossi[89a,89b], A. Santocchia[89a,89b], D. Spiga[89a], T. Tedeschi[89a,89b], C. Aimè[90a,90b], C.A. Alexe[90a,90c], P. Asenov[90a,90b], P. Azzurri[90a], G. Bagliesi[90a], L. Bianchini[90a,90b], T. Boccali[90a], E. Bossini[90a], D. Bruschini[90a,90c], R. Castaldi[90a], F. Cattafesta[90a,90c], M.A. Ciocci[90a,90d], M. Cipriani[90a,90b], R. Dell'Orso[90a], S. Donato[90a,90b], R. Forti[90a,90b], A. Giassi[90a], F. Ligabue[90a,90c], A.C. Marini[90a,90b], A. Messineo[90a,90b], S. Mishra[90a], V.K. Muraleedharan Nair Bindhu[90a,90b], S. Nandan[90a], F. Palla[90a], M. Riggirello[90a,90c], A. Rizzi[90a,90b], G. Rolandi[90a,90c], S. Roy Chowdhury[90a,bb], T. Sarkar[90a], A. Scribano[90a], P. Solanki[90a,90b], P. Spagnolo[90a], F. Tenchini[90a,90b], R. Tenchini[90a], G. Tonelli[90a,90b], N. Turini[90a,90d], F. Vaselli[90a,90c], A. Venturi[90a], P.G. Verdini[90a], P. Akrap[91a,91b], C. Basile[91a,91b], S.C. Behera[91a], F. Cavallari[91a], L. Cunqueiro Mendez[91a,91b], F. De Riggi[91a,91b], D. Del Re[91a,91b], M. Del Vecchio[91a,91b], E. Di Marco[91a], M. Diemoz[91a], F. Errico[91a], L. Frosina[91a,91b], R. Gargiulo[91a,91b], B. Harikrishnan[91a,91b], F. Lombardi[91a,91b], E. Longo[91a,91b], L. Martikainen[91a,91b], G. Organtini[91a,91b], N. Palmeri[91a,91b], R. Paramatti[91a,91b], T. Pauletto[91a,91b], S. Rahatlou[91a,91b], C. Rovelli[91a], F. Santanastasio[91a,91b], L. Soffi[91a], V. Vladimirov[91a,91b], N. Amapane[92a,92b], R. Arcidiacono[92a,92c], S. Argiro[92a,92b], M. Arneodo[92a,92c,†], N. Bartosik[92a,92c], R. Bellan[92a,92b], A. Bellora[92a,92b], C. Biino[92a], C. Borca[92a,92b], N. Cartiglia[92a], M. Costa[92a,92b], R. Covarelli[92a,92b], N. Demaria[92a], E. Ferrando[92a,92b], L. Finco[92a], M. Grippo[92a,92b], B. Kiani[92a,92b], L. Lanteri[92a,92b], F. Legger[92a], F. Luongo[92a,92b], C. Mariotti[92a], S. Maselli[92a], A. Mecca[92a,92b], L. Menzio[92a,92b], P. Meridiani[92a], E. Migliore[92a,92b], M. Monteno[92a], M.M. Obertino[92a,92b], G. Ortona[92a], L. Pacher[92a,92b], N. Pastrone[92a], M. Ruspa[92a,92c], F. Siviero[92a,92b], V. Sola[92a,92b], A. Solano[92a,92b], A. Staiano[92a], C. Tarricone[92a,92b], D. Trocino[92a], G. Umoret[92a,92b], E. Vlasov[92a,92b], R. White[92a,92b], J. Babbar[93a,93b,bb], S. Belforte[93a], V. Candelise[93a,93b], M. Casarsa[93a], F. Cossutti[93a], K. De Leo[93a], G. Della Ricca[93a,93b], R. Delli Gatti[93a,93b], C. Giraldin[93a,93b], S. Dogra[94], J. Hong[94], J. Kim[94], T. Kim[94], D. Lee[94], H. Lee[94], J. Lee[94], S.W. Lee[94], C.S. Moon[94], Y.D. Oh[94], S. Sekmen[94], B. Tae[94], Y.C. Yang[94], M.S. Kim[95], G. Bak[96], P. Gwak[96], H. Kim[96], H. Lee[96], S. Lee[96], D.H. Moon[96], J. Seo[96], E. Asilar[97], F. Carnevali[97], J. Choi[97,bc], T.J. Kim[97], Y. Ryou[97], J. Song[97], S. Ha[98], S. Han[98], B. Hong[98], J. Kim[98], K. Lee[98], K.S. Lee[98], S. Lee[98], J. Padmanaban[98], J. Yoo[98], J. Goh[99], J. Shin[99], S. Yang[99], L. Kalipoliti[100], Y. Kang[100], H. S. Kim[100], Y. Kim[100], B. Ko[100], S. Lee[100], J. Almond[101], J.H. Bhyun[101], J. Choi[101], J. Choi[101], W. Jun[101], H. Kim[101], J. Kim[101], J. Kim[101], T. Kim[101], Y. Kim[101], Y.W. Kim[101], S. Ko[101], H. Lee[101], J. Lee[101], J. Lee[101], B.H. Oh[101], J. Shin[101], U.K. Yang[101], I. Yoon[101], W. Jang[102], D. Kim[102], S. Kim[102], J.S.H. Lee[102], Y. Lee[102], I.C. Park[102], Y. Roh[102], I.J. Watson[102], G. Cho[103], Y. Eo[103], K. Hwang[103], H. Jang[103], B. Kim[103], D. Kim[103], S. Kim[103], K. Lee[103], H.D. Yoo[103], Y. Lee[104], I. Yu[104], T. Beyrouthy[105], Y. Gharbia[105], F. Alazemi[106], K. Dreimanis[107], O.M. Eberlins[107], A. Gaile[107], M. Klevs[107], C. Munoz Diaz[107], D. Osite[107], G. Pikurs[107], R. Plese[107], A. Potrebko[107], M. Seidel[107], D. Sidiropoulos Kontos[107], N.R. Strautnieks[108], M. Ambrozas[109], A. Juodagalvis[109], S. Nargelas[109], S. Nayak[109], A. Rinkevicius[109], G. Tamulaitis[109], I. Yusuff[110,bd],

Z. Zolkapli[110], J.F. Benitez[111], A. Castaneda Hernandez[111], A. Cota Rodriguez[111], L.E. Cuevas Picos[111], H.A. Encinas Acosta[111], L.G. Gallegos Maríñez[111], J.A. Murillo Quijada[111], L. Valencia Palomo[111], G. Ayala[112], H. Castilla-Valdez[112], H. Crotte Ledesma[112], R. Lopez-Fernandez[112], J. Mejia Guisao[112], R. Reyes-Almanza[112], A. Sánchez Hernández[112], C. Oropeza Barrera[113], M. Ramírez García[113], D.L. Ramirez Guadarrama[113], I. Bautista[114], F.E. Neri Huerta[114], I. Pedraza[114], H.A. Salazar Ibarguen[114], C. Uribe Estrada[114], I. Bubanja[115], J. Mijuskovic[115], N. Raicevic[115], P.H. Butler[116], A. Ahmad[117], M.I. Asghar[117], A. Awais[117], M.I.M. Awan[117], W.A. Khan[117], V. Avati[118], L. Forthomme[118], L. Grzanka[118], M. Malawski[118], K. Piotrzkowski[118], H. Awedikian[119], M. Bluj[119], M. Ghimiray[119], M. Górski[119], M. Kazana[119], M. Szleper[119], P. Zalewski[119], K. Bunkowski[120], K. Doroba[120], A. Kalinowski[120], M. Konecki[120], J. Krolikowski[120], W. Matyszkiewicz[120], A. Muhammad[120], S. Slawinski[120], P. Fokow[121], K. Pozniak[121], W. Zabolotny[121], M. Araujo[122], C. Beirão Da Cruz E Silva[122], A. Boletti[122], M. Bozzo[122], T. Camporesi[122], G. Da Molin[122], M. Gallinaro[122], J. Hollar[122], N. Leonardo[122], G.B. Marozzo[122], A. Petrilli[122], M. Pisano[122], J. Seixas[122], J. Varela[122], J.W. Wulff[122], P. Adzic[123], L. Markovic[123], P. Milenovic[123], V. Milosevic[123], D. Devetak[124], M. Dordevic[124], J. Milosevic[124], L. Nadderd[124], V. Rekovic[124], M. Stojanovic[124], M. Alcalde Martinez[125], J. Alcaraz Maestre[125], Cristina F. Bedoya[125], J.A. Brochero Cifuentes[125], Oliver M. Carretero[125], M. Cepeda[125], M. Cerrada[125], N. Colino[125], B. De La Cruz[125], A. Delgado Peris[125], A. Escalante Del Valle[125], D. Fernández Del Val[125], J.P. Fernández Ramos[125], J. Flix[125], M.C. Fouz[125], M. Gonzalez Hernandez[125], O. Gonzalez Lopez[125], S. Goy Lopez[125], J.M. Hernandez[125], M.I. Josa[125], J. Llorente Merino[125], C. Martin Perez[125], E. Martin Viscasillas[125], D. Moran[125], C. M. Morcillo Perez[125], Á. Navarro Tobar[125], R. Paz Herrera[125], A. Pérez-Calero Yzquierdo[125], J. Puerta Pelayo[125], I. Redondo[125], J. Vazquez Escobar[125], J.F. de Trocóniz[126], E. Aller Gutierrez[127], B. Alvarez Gonzalez[127], J. Ayllon Torresano[127], A. Cardini[127], J. Cuevas[127], J. Del Riego Badas[127], D. Estrada Acevedo[127], J. Fernandez Menendez[127], S. Folgueras[127], I. Gonzalez Caballero[127], P. Leguina[127], M. Obeso Menendez[127], E. Palencia Cortezon[127], J. Prado Pico[127], A. Soto Rodríguez[127], P. Vischia[127], S. Blanco Fernández[128], I.J. Cabrillo[128], A. Calderon[128], M. Caserta[128], J. Duarte Campderros[128], M. Fernandez[128], G. Gomez[128], C. Lasaosa García[128], R. Lopez Ruiz[128], C. Martinez Rivero[128], P. Martinez Ruiz del Arbol[128], F. Matorras[128], P. Matorras Cuevas[128], E. Navarrete Ramos[128], J. Piedra Gomez[128], C. Quintana San Emeterio[128], V. Rodriguez[128], L. Scodellaro[128], I. Vila[128], R. Vilar Cortabitarte[128], J.M. Vizan Garcia[128], B. Kailasapathy[129,be], D.D.C. Wickramarathna[129], W.G.D. Dharmaratna[130,bf], K. Liyanage[130], N. Perera[130], D. Abbaneo[131], C. Amendola[131], R. Ardino[131], E. Auffray[131], J. Baechler[131], D. Barney[131], J. Bendavid[131], I. Bestintzanos[131], M. Bianco[131], A. Bocci[131], L. Borgonovi[131], C. Botta[131], A. Bragagnolo[131], C.E. Brown[131], C. Caillol[131], G. Cerminara[131], P. Connor[131], K. Cormier[131], D. d'Enterria[131], A. Dabrowski[131], P. Das[131], A. David[131], A. De Roeck[131], M.M. Defranchis[131], M. Deile[131], M. Dobson[131], P.J. Fernández Manteca[131], B.A. Fontana Santos Alves[131], E. Fontanesi[131], W. Funk[131], A. Gaddi[131], S. Giani[131], D. Gigi[131], K. Gill[131], F. Glege[131], M. Glowacki[131],

A. Gruber[131], J. Hegeman[131], J.K. Heikkilä[131], R. Hofsaess[131], B. Huber[131], T. James[131], P. Janot[131], L. Jeppe[131], O. Kaluzinska[131], O. Karacheban[131,y], G. Karathanasis[131], S. Laurila[131], P. Lecoq[131], E. Leutgeb[131], C. Lourenço[131], A.-M. Lyon[131], M. Magherini[131], L. Malgeri[131], M. Mannelli[131], A. Mehta[131], F. Meijers[131], J.A. Merlin[131], S. Mersi[131], E. Meschi[131], M. Migliorini[131], F. Monti[131], F. Moortgat[131], M. Mulders[131], M. Musich[131], I. Neutelings[131], S. Orfanelli[131], F. Pantaleo[131], M. Pari[131], G. Petrucciani[131], A. Pfeiffer[131], M. Pierini[131], M. Pitt[131], H. Qu[131], D. Rabady[131], A. Reimers[131], B. Ribeiro Lopes[131], F. Riti[131], P. Rosado[131], M. Rovere[131], H. Sakulin[131], R. Salvatico[131], S. Sanchez Cruz[131], S. Scarfi[131], M. Selvaggi[131], K. Shchelina[131], P. Silva[131], P. Sphicas[131,bg], A.G. Stahl Leiton[131], A. Steen[131], S. Summers[131], G. Terragni[131], D. Treille[131], P. Tropea[131], E. Vernazza[131], J. Wanczyk[131,bh], S. Wuchterl[131], M. Zarucki[131], P. Zehetner[131], P. Zejdl[131], G. Zevi Della Porta[131], L. Caminada[132,bi], W. Erdmann[132], R. Horisberger[132], Q. Ingram[132], H.C. Kaestli[132], D. Kotlinski[132], C. Lange[132], U. Langenegger[132], A. Nigamova[132], L. Noehte[132,bi], L. Redard-Jacot[132], T. Rohe[132], A. Samalan[132], T.K. Aarrestad[133], M. Backhaus[133], T. Bevilacqua[133,bi], G. Bonomelli[133], C. Cazzaniga[133], K. Datta[133], P. De Bryas Dexmiers D'Archiacchiac[133,bh], A. De Cosa[133], G. Dissertori[133], M. Dittmar[133], M. Donegà[133], F. Glessgen[133], C. Grab[133], N. Härringer[133], T.G. Harte[133], W. Lustermann[133], M.Köppel[133], M. Malucchi[133], R.A. Manzoni[133], L. Marchese[133], A. Mascellani[133,bh], F. Nessi-Tedaldi[133], F. Pauss[133], A.A. Petre[133], J. Prendi[133], B. Ristic[133], S. Rohletter[133], P.M. Sander[133], R. Seidita[133], J. Steggemann[133,bh], A. Tarabini[133], C.Z. Tee[133], D. Valsecchi[133], P.H. Wagner[133], R. Wallny[133], C. Amsler[134,bj], P. Bärtschi[134], F. Bilandzija[134], M.F. Canelli[134], G. Celotto[134], T.A. Goldschmidt[134], V. Guglielmi[134], A. Jofrehei[134], B. Kilminster[134], T.H. Kwok[134], S. Leontsinis[134], V. Lukashenko[134], A. Macchiolo[134], F. Meng[134], M. Missiroli[134], J. Motta[134], P. Robmann[134], E. Shokr[134], F. Stäger[134], R. Tramontano[134], P. Viscone[134], D. Bhowmik[135], C.M. Kuo[135], P.K. Rout[135], S. Taj[135], P.C. Tiwari[135,ak], L. Ceard[136], K.F. Chen[136], Z.g. Chen[136], A. De Iorio[136], W.-S. Hou[136], T.h. Hsu[136], Y.w. Kao[136], S. Karmakar[136], F. Khuzaimah[136], G. Kole[136], Y.y. Li[136], R.-S. Lu[136], E. Paganis[136], X.f. Su[136], J. Thomas-Wilsker[136], L.s. Tsai[136], D. Tsionou[136], H.y. Wu[136], E. Yazgan[136], C. Asawatangtrakuldee[137], N. Srimanobhas[137], Y. Maghrbi[138], D. Agyel[139], F. Dolek[139], I. Dumanoglu[139,bk], Y. Guler[139,bl], E. Gurpinar Guler[139,bl], C. Isik[139], O. Kara[139,bm], A. Kayis Topaksu[139], Y. Komurcu[139], G. Onengut[139], K. Ozdemir[139,bn], B. Tali[139,bo], U.G. Tok[139], E. Uslan[139], I.S. Zorbakir[139], S. Sen[140], M. Yalvac[141,bp], B. Akgun[142], I.O. Atakisi[142,bq], E. Gülmez[142], M. Kaya[142,br], O. Kaya[142,bs], M.A. Sarkisla[142,bt], S. Tekten[142,bu], D. Boncukcu[143], A. Cakir[143], K. Cankocak[143,bk,bv], B. Hacisahinoglu[144], I. Hos[144,bw], B. Kaynak[144], S. Ozkorucuklu[144], O. Potok[144], H. Sert[144], C. Simsek[144], C. Zorbilmez[144], S. Cerci[145], C. Dozen[145,bx], B. Isildak[145], E. Simsek[145], D. Sunar Cerci[145], T. Yetkin[145,bx], A. Boyaryntsev[146], O. Dadazhanova[146], B. Grynyov[146], L. Levchuk[147], J.J. Brooke[148], A. Bundock[148], F. Bury[148], E. Clement[148], D. Cussans[148], D. Dharmender[148], H. Flacher[148], J. Goldstein[148], H.F. Heath[148], M.-L. Holmberg[148], A. Karakoulaki[148], L. Kreczko[148], S. Paramesvaran[148], L. Robertshaw[148], M.S. Sanjrani[148,an], J. Segal[148], V.J. Smith[148], A.H. Ball[149], K.W. Bell[149],

A. Belyaev[149,by], C. Brew[149], R.M. Brown[149], D.J.A. Cockerill[149], A. Elliot[149], K.V. Ellis[149], J. Gajownik[149], K. Harder[149], S. Harper[149], J. Linacre[149], K. Manolopoulos[149], M. Moallemi[149], D.M. Newbold[149], E. Olaiya[149], D. Petyt[149], T. Reis[149], A.R. Sahasransu[149], G. Salvi[149], T. Schuh[149], C.H. Shepherd-Themistocleous[149], I.R. Tomalin[149], K.C. Whalen[149], T. Williams[149], I. Andreou[150], R. Bainbridge[150], P. Bloch[150], O. Buchmuller[150], C.A. Carrillo Montoya[150], D. Colling[150], I. Das[150], P. Dauncey[150], G. Davies[150], M. Della Negra[150], S. Fayer[150], G. Fedi[150], G. Hall[150], H.R. Hoorani[150], A. Howard[150], G. Iles[150], C.R. Knight[150], P. Krueper[150], J. Langford[150], K.H. Law[150], J. León Holgado[150], L. Lyons[150], A.-M. Magnan[150], B. Maier[150], S. Mallios[150], A. Mastronikolis[150], M. Mieskolainen[150], J. Nash[150,bz], M. Pesaresi[150], P.B. Pradeep[150], B.C. Radburn-Smith[150], A. Richards[150], A. Rose[150], T.B. Runting[150], L. Russell[150], K. Savva[150], R. Schmitz[150], C. Seez[150], R. Shukla[150], A. Tapper[150], K. Uchida[150], G.P. Uttley[150], T. Virdee[150,ab], M. Vojinovic[150], N. Wardle[150], D. Winterbottom[150], J. Xiao[150], J.E. Cole[151], A. Khan[151], P. Kyberd[151], I.D. Reid[151], S. Abdullin[152], A. Brinkerhoff[152], E. Collins[152], M.R. Darwish[152], J. Dittmann[152], K. Hatakeyama[152], V. Hegde[152], J. Hiltbrand[152], B. McMaster[152], J. Samudio[152], S. Sawant[152], C. Sutantawibul[152], J. Wilson[152], J.M. Hogan[153], R. Bartek[154], A. Dominguez[154], S. Raj[154], B. Sahu[154], A.E. Simsek[154], S.S. Yu[154], B. Bam[155], A. Buchot Perraguin[155], S. Campbell[155], R. Chudasama[155], S.I. Cooper[155], C. Crovella[155], G. Fidalgo[155], S.V. Gleyzer[155], A. Khukhunaishvili[155], K. Matchev[155], E. Pearson[155], P. Rumerio[155,ca], E. Usai[155], R. Yi[155], S. Cholak[156], G. De Castro[156], Z. Demiragli[156], C. Erice[156], C. Fangmeier[156], C. Fernandez Madrazo[156], J. Fulcher[156], J. Garcia De Castro[156], F. Golf[156], S. Jeon[156], J. O'Cain[156], I. Reed[156], J. Rohlf[156], K. Salyer[156], D. Sperka[156], I. Suarez[156], A. Tsatsos[156], E. Wurtz[156], A.G. Zecchinelli[156], G. Barone[157], G. Benelli[157], D. Cutts[157], S. Ellis[157], L. Gouskos[157], M. Hadley[157], U. Heintz[157], K.W. Ho[157], T. Kwon[157], L. Lambrecht[157], G. Landsberg[157], K.T. Lau[157], M. LeBlanc[157], J. Luo[157], S. Mondal[157], J. Roloff[157], T. Russell[157], S. Sagir[157,cb], X. Shen[157], M. Stamenkovic[157], S. Sunnarborg[157], J. Tang[157], N. Venkatasubramanian[157], S. Abbott[158], S. Baradia[158], B. Barton[158], R. Breedon[158], H. Cai[158], M. Calderon De La Barca Sanchez[158], E. Cannaert[158], M. Chertok[158], M. Citron[158], J. Conway[158], P.T. Cox[158], F. Eble[158], R. Erbacher[158], C. Fairchild[158], O. Kukral[158], G. Mocellin[158], S. Ostrom[158], I. Salazar Segovia[158], J.H. Steenis[158], J.S. Tafoya Vargas[158], W. Wei[158], S. Yoo[158], K. Adamidis[159], H. Ancelin[159], M. Bachtis[159], D. Campos[159], R. Cousins[159], S. Crossley[159], G. Flores Avila[159], J. Hauser[159], M. Ignatenko[159], M.A. Iqbal[159], T. Lam[159], Y.f. Lo[159], E. Manca[159], A. Nunez Del Prado[159], D. Saltzberg[159], V. Valuev[159], R. Clare[160], J.W. Gary[160], G. Hanson[160], A. Aportela[161], A. Arora[161], J.G. Branson[161], S. Cittolin[161], B. D'Anzi[161], D. Diaz[161], J. Duarte[161], L. Giannini[161], Y. Gu[161], J. Guiang[161], V. Krutelyov[161], R. Lee[161], J. Letts[161], H. Li[161], R. Marroquin Solares[161], M. Masciovecchio[161], F. Mokhtar[161], S. Mukherjee[161], M. Pieri[161], D. Primosch[161], M. Quinnan[161], V. Sharma[161], M. Tadel[161], E. Vourliotis[161], F. Würthwein[161], A. Yagil[161], Z. Zhao[161], A. Barzdukas[162], L. Brennan[162], C. Campagnari[162], S. Carron Montero[162,cc], K. Downham[162], C. Grieco[162], M.M. Hussain[162], J. Incandela[162], M.W.K. Lai[162], A.J. Li[162], P. Masterson[162], J. Richman[162], S.N. Santpur[162], D. Stuart[162], T.Á. Vámi[162], X. Yan[162], D. Zhang[162], A. Albert[163], S. Bhattacharya[163], A. Bornheim[163], O. Cerri[163], Z. Hao[163], R. Kansal[163], L. Mori[163], H.B. Newman[163], G. Reales Gutiérrez[163], T. Sievert[163], P. Simmerling[163], M. Spiropulu[163], C. Sun[163], J.R. Vlimant[163], R.A. Wynne[163], S. Xie[163], J. Alison[164], S. An[164], M. Cremonesi[164], V. Dutta[164], E.Y. Ertorer[164], T. Ferguson[164], T.A. Gómez Espinosa[164], A. Harilal[164], A. Kallil Tharayil[164], M. Kanemura[164], C. Liu[164], M. Marchegiani[164], P. Meiring[164], S. Murthy[164], P. Palit[164], K. Park[164], M. Paulini[164], A. Roberts[164], A. Sanchez[164], Y. Zhou[164], J.P. Cumalat[165], W.T. Ford[165], J. Fraticelli[165], A. Hart[165], M. Herrmann[165], S. Kwan[165], J. Pearkes[165], C. Savard[165], N. Schonbeck[165], K. Stenson[165], K.A. Ulmer[165], S.R. Wagner[165], N. Zipper[165], D. Zuolo[165], J. Alexander[166], X. Chen[166], J. Dickinson[166], A. Duquette[166], J. Fan[166], X. Fan[166], J. Grassi[166], P. Kotamnives[166], J. Monroy[166], G. Niendorf[166], M. Oshiro[166], J.R. Patterson[166], A. Ryd[166], J. Thom[166], H.A. Weber[166], B. Weiss[166], P. Wittich[166], R. Zou[166], L. Zygala[166], M. Albrow[167], M. Alyari[167], O. Amram[167], G. Apollinari[167], A. Apresyan[167], L.A.T. Bauerdick[167], D. Berry[167], J. Berryhill[167], P.C. Bhat[167], K. Burkett[167], J.N. Butler[167], A. Canepa[167], G.B. Cerati[167], H.W.K. Cheung[167], F. Chlebana[167], C. Cosby[167], G. Cummings[167], I. Dutta[167], V.D. Elvira[167], J. Freeman[167], A. Gandrakota[167], Z. Gecse[167], L. Gray[167], D. Green[167], A. Grummer[167], S. Grünendahl[167], D. Guerrero[167], O. Gutsche[167], R.M. Harris[167], J. Hirschauer[167], V. Innocente[167], B. Jayatilaka[167], S. Jindariani[167], M. Johnson[167], U. Joshi[167], R.S. Kim[167], B. Klima[167], S. Lammel[167], D. Lincoln[167], R. Lipton[167], T. Liu[167], K. Maeshima[167], D. Mason[167], P. McBride[167], P. Merkel[167], S. Mrenna[167], S. Nahn[167], J. Ngadiuba[167], D. Noonan[167], S. Norberg[167], V. Papadimitriou[167], N. Pastika[167], K. Pedro[167], C. Pena[167,cd], C.E. Perez Lara[167], V. Perovic[167], F. Ravera[167], A. Reinsvold Hall[167,ce], L. Ristori[167], M. Safdari[167], E. Sexton-Kennedy[167], E. Smith[167], N. Smith[167], A. Soha[167], L. Spiegel[167], S. Stoynev[167], J. Strait[167], L. Taylor[167], S. Tkaczyk[167], N.V. Tran[167], L. Uplegger[167], E.W. Vaandering[167], C. Wang[167], I. Zoi[167], C. Aruta[168], P. Avery[168], D. Bourilkov[168], P. Chang[168], V. Cherepanov[168], R.D. Field[168], C. Huh[168], E. Koenig[168], M. Kolosova[168], J. Konigsberg[168], A. Korytov[168], G. Mitselmakher[168], K. Mohrman[168], A. Muthirakalayil Madhu[168], N. Rawal[168], S. Rosenzweig[168], V. Sulimov[168], Y. Takahashi[168], J. Wang[168], T. Adams[169], A. Al Kadhim[169], A. Askew[169], S. Bower[169], R. Goff[169], R. Hashmi[169], A. Hassani[169], T. Kolberg[169], G. Martinez[169], M. Mazza[169], H. Prosper[169], P.R. Prova[169], R. Yohay[169], B. Alsufyani[170], S. Das[170], S. Demarest[170], L. Hasa[170], M. Hohlmann[170], M. Lavinsky[170], E. Yanes[170], M.R. Adams[171], N. Barnett[171], A. Baty[171], C. Bennett[171], N. Brandman-hughes[171], R. Cavanaugh[171], R. Escobar Franco[171], O. Evdokimov[171], C.E. Gerber[171], H. Gupta[171], M. Hawksworth[171], A. Hingrajiya[171], D.J. Hofman[171], Z. Huang[171], J.h. Lee[171], C. Mills[171], S. Nanda[171], G. Nigmatkulov[171], B. Ozek[171], T. Phan[171], D. Pilipovic[171], R. Pradhan[171], E. Prifti[171], P. Roy[171], T. Roy[171], D. Shekar[171], N. Singh[171], F. Strug[171], A. Thielen[171], M.B. Tonjes[171], N. Varelas[171], M.A. Wadud[171], A. Wang[171], J. Yoo[171], M. Alhusseini[172], D. Blend[172], K. Dilsiz[172,cf], O.K. Köseyan[172], A. Mestvirishvili[172,cg], O. Neogi[172], H. Ogul[172,ch], Y. Onel[172], A. Penzo[172], C. Snyder[172], E. Tiras[172,ci], B. Blumenfeld[173], J. Davis[173], A.V. Gritsan[173], L. Kang[173], S. Kyriacou[173], P. Maksimovic[173], N. Pinto[173], M. Roguljic[173], S. Sekhar[173], M.V. Srivastav[173], M. Swartz[173], A. Abreu[174], L.F. Alcerro Alcerro[174], J. Anguiano[174], S. Arteaga Escatel[174], P. Baringer[174], A. Bean[174], R. Bhattacharya[174], Z. Flowers[174], D. Grove[174], J. King[174], G. Krintiras[174], M. Lazarovits[174], C. Le Mahieu[174], J. Marquez[174], M. Murray[174], M. Nickel[174], S. Popescu[174,cj], C. Rogan[174], C. Royon[174], S. Rudrabhatla[174], S. Sanders[174], C. Smith[174], G. Wilson[174], A. Ahmad[175], B. Allmond[175], N. Islam[175], A. Ivanov[175], K. Kaadze[175], Y. Maravin[175], J. Natoli[175], G.G. Reddy[175], D. Roy[175], G. Sorrentino[175], A. Baden[176], A. Belloni[176], J. Bistany-riebman[176], S.C. Eno[176], N.J. Hadley[176], S. Jabeen[176], R.G. Kellogg[176], T. Koeth[176], B. Kronheim[176], S. Lascio[176], P. Major[176], A.C. Mignerey[176], C. Palmer[176], C. Papageorgakis[176], M.M. Paranjpe[176], E. Popova[176,ck], A. Shevelev[176], L. Zhang[176], C. Baldenegro Barrera[177], H. Bossi[177], S. Bright-Thonney[177], I.A. Cali[177], Y.c. Chen[177], P.c. Chou[177], M. D'Alfonso[177], J. Eysermans[177], C. Freer[177], G. Gomez-Ceballos[177], M. Goncharov[177], G. Grosso[177], P. Harris[177], D. Hoang[177], G.M. Innocenti[177], K. Ivanov[177], G. Kopp[177], D. Kovalskyi[177], L. Lavezzo[177], Y.-J. Lee[177], K. Long[177], P. Lugato[177], C. Mcginn[177], E. Moreno[177], A. Novak[177], M.I. Park[177], C. Paus[177], C. Reissel[177], C. Roland[177], G. Roland[177], S. Rothman[177], T.a. Sheng[177], G.S.F. Stephans[177], D. Walter[177], J. Wang[177], Z. Wang[177], B. Wyslouch[177], T. J. Yang[177], A. Alpana[178], B. Crossman[178], W.J. Jackson[178], C. Kapsiak[178], M. Krohn[178], D. Mahon[178], J. Mans[178], B. Marzocchi[178], R. Rusack[178], O. Sancar[178], R. Saradhy[178], N. Strobbe[178], K. Bloom[179], D.R. Claes[179], S.V. Dixit[179], G. Haza[179], J. Hossain[179], C. Joo[179], I. Kravchenko[179], K.H.M. Kwok[179], Y. Mehra[179], J. Morris[179], A. Rohilla[179], J.E. Siado[179], A. Vagnerini[179], A. Wightman[179], H. Bandyopadhyay[180], L. Hay[180], H.w. Hsia[180], I. Iashvili[180], A. Kalogeropoulos[180], A. Kharchilava[180], A. Mandal[180], M. Morris[180], D. Nguyen[180], O. Poncet[180], S. Rappoccio[180], H. Rejeb Sfar[180], W. Terrill[180], A. Williams[180], D. Yu[180], A. Aarif[181], G. Alverson[181], E. Barberis[181], J. Bonilla[181], B. Bylsma[181], M. Campana[181], J. Dervan[181], Y. Haddad[181], Y. Han[181], I. Israr[181], A. Krishna[181], M. Lu[181], N. Manganelli[181], R. Mccarthy[181], D.M. Morse[181], T. Orimoto[181], L. Skinnari[181], C.S. Thoreson[181], E. Tsai[181], D. Wood[181], S. Dittmer[182], K.A. Hahn[182], S. King[182], M. Mcginnis[182], Y. Miao[182], D.G. Monk[182], M.H. Schmitt[182], A. Taliercio[182], M. Velasco[182], J. Wang[182], G. Agarwal[183], R. Band[183], R. Bucci[183], S. Castells[183], A. Das[183], A. Datta[183], A. Ehnis[183], R. Goldouzian[183], M. Hildreth[183], K. Hurtado Anampa[183], T. Ivanov[183], C. Jessop[183], A. Karneyeu[183], K. Lannon[183], J. Lawrence[183], N. Loukas[183], L. Lutton[183], J. Mariano[183], N. Marinelli[183], P. Mastrapasqua[183], A. Masud[183], T. McCauley[183], C. Mcgrady[183], C. Moore[183], Y. Musienko[183,cl], H. Nelson[183], M. Osherson[183], A. Piccinelli[183], R. Ruchti[183], A. Townsend[183], Y. Wan[183], M. Wayne[183], H. Yockey[183], M. Carrigan[184], R. De Los Santos[184], L.S. Durkin[184], C. Hill[184], M. Joyce[184], D.A. Wenzl[184], B.L. Winer[184], B. R. Yates[184], H. Bouchamaoui[185], G. Dezoort[185], P. Elmer[185], A. Frankenthal[185], M. Galli[185], B. Greenberg[185], K. Kennedy[185], Y. Lai[185], D. Lange[185], A. Loeliger[185], D. Marlow[185], I. Ojalvo[185], J. Olsen[185], F. Simpson[185], D. Stickland[185], C. Tully[185], S. Yoon[185], S. Malik[186], R. Sharma[186], S. Chandra[187], A. Gu[187], L. Gutay[187], M. Huwiler[187], M. Jones[187], A.W. Jung[187], I.G. Karslioglu[187], D. Kondratyev[187], J. Li[187], M. Liu[187], M. Macedo[187], G. Negro[187], N. Neumeister[187], G. Paspalaki[187], S. Piperov[187], N.R. Saha[187], J.F. Schulte[187], F. Wang[187], A.L. Wesolek[187], A. Wildridge[187], W. Xie[187], Y. Yao[187], Y. Zhong[187], N. Parashar[188], A. Pathak[188], E. Shumka[188], D. Acosta[189], A. Agrawal[189], C. Arbour[189], T. Carnahan[189], K.M. Ecklund[189], F.J.M. Geurts[189], T. Huang[189], I. Krommydas[189], N. Lewis[189], W. Li[189], J. Lin[189], O. Miguel Colin[189], B.P. Padley[189], R. Redjimi[189], J. Rotter[189], C. Vico Villalba[189], M. Wulansatiti[189], E. Yigitbasi[189], Y. Zhang[189], O. Bessidskaia Bylund[190], A. Bodek[190], P. de Barbaro[190,†], R. Demina[190], A. Garcia-Bellido[190], H.S. Hare[190], O. Hindrichs[190], N. Parmar[190], P. Parygin[190,ck], H. Seo[190], R. Taus[190], Y.h. Yu[190], B. Chiarito[191], J.P. Chou[191], S.V. Clark[191], S. Donnelly[191], D. Gadkari[191], Y. Gershtein[191], E. Halkiadakis[191], C. Houghton[191], D. Jaroslawski[191], A. Kobert[191], I. Laflotte[191], A. Lath[191], J. Martins[191], P. Meltzer[191], M. Perez Prada[191], B. Rand[191], J. Reichert[191], P. Saha[191], S. Salur[191], S. Somalwar[191], R. Stone[191], S.A. Thayil[191], S. Thomas[191], J. Vora[191], D. Ally[192], A.G. Delannoy[192], S. Fiorendi[192], J. Harris[192], T. Holmes[192], A.R. Kanuganti[192], N. Karunarathna[192], J. Lawless[192], L. Lee[192], E. Nibigira[192], B. Skipworth[192], S. Spanier[192], D. Aebi[193], M. Ahmad[193], T. Akhter[193], K. Androsov[193], A. Basnet[193], A. Bolshov[193], O. Bouhali[193,cm], A. Cagnotta[193], S. Cooperstein[193], V. D'Amante[193], R. Eusebi[193], P. Flanagan[193], J. Gilmore[193], Y. Guo[193], T. Kamon[193], S. Luo[193], R. Mueller[193], G. Pizzati[193], A. Safonov[193], N. Akchurin[194], J. Damgov[194], Y. Feng[194], N. Gogate[194], W. Jin[194], S.W. Lee[194], C. Madrid[194], A. Mankel[194], T. Peltola[194], I. Volobouev[194], E. Appelt[195], Y. Chen[195], S. Greene[195], A. Gurrola[195], W. Johns[195], R. Kunnawalkam Elayavalli[195], A. Melo[195], D. Rathjens[195], F. Romeo[195], P. Sheldon[195], S. Tuo[195], J. Velkovska[195], J. Viinikainen[195], J. Zhang[195], B. Cardwell[196], H. Chung[196], B. Cox[196], J. Hakala[196], G. Hamilton Ilha Machado[196], R. Hirosky[196], M. Jose[196], A. Ledovskoy[196], C. Mantilla[196], C. Neu[196], C. Ramón Álvarez[196], Z. Wu[196], S. Bhattacharya[197], P.E. Karchin[197], A. Aravind[198], S. Banerjee[198], K. Black[198], T. Bose[198], E. Chavez[198], R. Cruz[198], S. Dasu[198], P. Everaerts[198], C. Galloni[198], H. He[198], M. Herndon[198], A. Herve[198], C.K. Koraka[198], S. Lomte[198], R. Loveless[198], A. Mallampalli[198], J. Marquez[198], A. Mohammadi[198], S. Mondal[198], T. Nelson[198], G. Parida[198], L. Pétré[198], D. Pinna[198], A. Savin[198], V. Shang[198], V. Sharma[198], R. Simeon[198], W.H. Smith[198], D. Teague[198], A. Thete[198], A. Warden[198], S. Afanasiev[199], V. Alexakhin[199], Yu. Andreev[199], T. Aushev[199], D. Budkouski[199], R. Chistov[199], M. Danilov[199], T. Dimova[199], A. Ershov[199], S. Gninenko[199], I. Gorbunov[199], A. Kamenev[199], V. Karjavine[199], M. Kirsanov[199], V. Klyukhin[199], O. Kodolova[199,cn], V. Korenkov[199], I. Korsakov[199], A. Kozyrev[199], N. Krasnikov[199], A. Lanev[199], A. Malakhov[199], V. Matveev[199], A. Nikitenko[199,co,cp], V. Palichik[199], V. Perelygin[199], S. Petrushanko[199], O. Radchenko[199], M. Savina[199], V. Shalaev[199], S. Shmatov[199], S. Shulha[199], Y. Skovpen[199], K. Slizhevskiy[199], V. Smirnov[199], O. Teryaev[199], I. Tlisova[199], A. Toropin[199], N. Voytishin[199], A. Zarubin[199], I. Zhizhin[199], E. Boos[200], V. Bunichev[200], M. Dubinin[200,cd], L. Dudko[200], A. Gribushin[200], V. Kim[200,cl], V. Murzin[200], V. Oreshkin[200], V. Savrin[200], A. Snigirev[200], D. Sosnov[200]

[1] *Yerevan Physics Institute, Yerevan, Armenia*
[2] *Institut für Hochenergiephysik, Vienna, Austria*
[3] *Universiteit Antwerpen, Antwerpen, Belgium*

[4] *Vrije Universiteit Brussel, Brussel, Belgium*
[5] *Université Libre de Bruxelles, Bruxelles, Belgium*
[6] *Ghent University, Ghent, Belgium*
[7] *Université Catholique de Louvain, Louvain-la-Neuve, Belgium*
[8] *Centro Brasileiro de Pesquisas Fisicas, Rio de Janeiro, Brazil*
[9] *Universidade do Estado do Rio de Janeiro, Rio de Janeiro, Brazil*
[10] *Universidade Estadual Paulista, Universidade Federal do ABC, São Paulo, Brazil*
[11] *Institute for Nuclear Research and Nuclear Energy, Bulgarian Academy of Sciences, Sofia, Bulgaria*
[12] *University of Sofia, Sofia, Bulgaria*
[13] *Instituto De Alta Investigación, Universidad de Tarapacá, Casilla 7 D, Arica, Chile*
[14] *Universidad Tecnica Federico Santa Maria, Valparaiso, Chile*
[15] *Beihang University, Beijing, China*
[16] *Department of Physics, Tsinghua University, Beijing, China*
[17] *Institute of High Energy Physics, Beijing, China*
[18] *State Key Laboratory of Nuclear Physics and Technology, Peking University, Beijing, China*
[19] *State Key Laboratory of Nuclear Physics and Technology, Institute of Quantum Matter, South China Normal University, Guangzhou, China*
[20] *Sun Yat-Sen University, Guangzhou, China*
[21] *University of Science and Technology of China, Hefei, China*
[22] *Nanjing Normal University, Nanjing, China*
[23] *Institute of Frontier and Interdisciplinary Science, Shandong University, Qingdao, China*
[24] *Institute of Modern Physics and Key Laboratory of Nuclear Physics and Ion-beam Application (MOE) — Fudan University, Shanghai, China*
[25] *Zhejiang University, Hangzhou, Zhejiang, China*
[26] *Universidad de Los Andes, Bogota, Colombia*
[27] *Universidad de Antioquia, Medellin, Colombia*
[28] *University of Split, Faculty of Electrical Engineering, Mechanical Engineering and Naval Architecture, Split, Croatia*
[29] *University of Split, Faculty of Science, Split, Croatia*
[30] *Institute Rudjer Boskovic, Zagreb, Croatia*
[31] *University of Cyprus, Nicosia, Cyprus*
[32] *Charles University, Prague, Czech Republic*
[33] *Escuela Politecnica Nacional, Quito, Ecuador*
[34] *Universidad San Francisco de Quito, Quito, Ecuador*
[35] *Academy of Scientific Research and Technology of the Arab Republic of Egypt, Egyptian Network of High Energy Physics, Cairo, Egypt*
[36] *Center for High Energy Physics (CHEP-FU), Fayoum University, El-Fayoum, Egypt*
[37] *National Institute of Chemical Physics and Biophysics, Tallinn, Estonia*
[38] *Department of Physics, University of Helsinki, Helsinki, Finland*
[39] *Helsinki Institute of Physics, Helsinki, Finland*
[40] *Lappeenranta-Lahti University of Technology, Lappeenranta, Finland*
[41] *IRFU, CEA, Université Paris-Saclay, Gif-sur-Yvette, France*
[42] *Laboratoire Leprince-Ringuet, CNRS/IN2P3, Ecole Polytechnique, Institut Polytechnique de Paris, Palaiseau, France*
[43] *Université de Strasbourg, CNRS, IPHC UMR 7178, Strasbourg, France*
[44] *Centre de Calcul de l'Institut National de Physique Nucleaire et de Physique des Particules, CNRS/IN2P3, Villeurbanne, France*
[45] *Institut de Physique des 2 Infinis de Lyon (IP2I), Villeurbanne, France*
[46] *Georgian Technical University, Tbilisi, Georgia*
[47] *RWTH Aachen University, I. Physikalisches Institut, Aachen, Germany*
[48] *RWTH Aachen University, III. Physikalisches Institut A, Aachen, Germany*
[49] *RWTH Aachen University, III. Physikalisches Institut B, Aachen, Germany*
[50] *Deutsches Elektronen-Synchrotron, Hamburg, Germany*

JHEP07(2026)248

[51] *University of Hamburg, Hamburg, Germany*
[52] *Karlsruher Institut fuer Technologie, Karlsruhe, Germany*
[53] *Institute of Nuclear and Particle Physics (INPP), NCSR Demokritos, Aghia Paraskevi, Greece*
[54] *National and Kapodistrian University of Athens, Athens, Greece*
[55] *National Technical University of Athens, Athens, Greece*
[56] *University of Ioánnina, Ioánnina, Greece*
[57] *HUN-REN Wigner Research Centre for Physics, Budapest, Hungary*
[58] *MTA-ELTE Lendület CMS Particle and Nuclear Physics Group, Eötvös Loránd University, Budapest, Hungary*
[59] *Faculty of Informatics, University of Debrecen, Debrecen, Hungary*
[60] *HUN-REN ATOMKI — Institute of Nuclear Research, Debrecen, Hungary*
[61] *Karoly Robert Campus, MATE Institute of Technology, Gyongyos, Hungary*
[62] *IIT Bhubaneswar, Bhubaneswar, India*
[63] *Panjab University, Chandigarh, India*
[64] *University of Delhi, Delhi, India*
[65] *Indian Institute of Technology Mandi (IIT-Mandi), Himachal Pradesh, India*
[66] *University of Hyderabad, Hyderabad, India*
[67] *Indian Institute of Technology Kanpur, Kanpur, India*
[68] *Saha Institute of Nuclear Physics, HBNI, Kolkata, India*
[69] *Indian Institute of Technology Madras, Madras, India*
[70] *IISER Mohali, India, Mohali, India*
[71] *Tata Institute of Fundamental Research-A, Mumbai, India*
[72] *Tata Institute of Fundamental Research-B, Mumbai, India*
[73] *National Institute of Science Education and Research, An OCC of Homi Bhabha National Institute, Bhubaneswar, Odisha, India*
[74] *Indian Institute of Science Education and Research (IISER), Pune, India*
[75] *Indian Institute of Technology Hyderabad, Telangana, India*
[76] *Isfahan University of Technology, Isfahan, Iran*
[77] *Institute for Research in Fundamental Sciences (IPM), Tehran, Iran*
[78] *University College Dublin, Dublin, Ireland*
[79a] *INFN Sezione di Bari, Bari, Italy*
[79b] *Università di Bari, Bari, Italy*
[79c] *Politecnico di Bari, Bari, Italy*
[80a] *INFN Sezione di Bologna, Bologna, Italy*
[80b] *Università di Bologna, Bologna, Italy*
[81a] *INFN Sezione di Catania, Catania, Italy*
[81b] *Università di Catania, Catania, Italy*
[82a] *INFN Sezione di Firenze, Firenze, Italy*
[82b] *Università di Firenze, Firenze, Italy*
[83] *INFN Laboratori Nazionali di Frascati, Frascati, Italy*
[84a] *INFN Sezione di Genova, Genova, Italy*
[84b] *Università di Genova, Genova, Italy*
[85a] *INFN Sezione di Milano-Bicocca, Milano, Italy*
[85b] *Università di Milano-Bicocca, Milano, Italy*
[86a] *INFN Sezione di Napoli, Napoli, Italy*
[86b] *Università di Napoli 'Federico II', Napoli, Italy*
[86c] *Università della Basilicata, Potenza, Italy*
[86d] *Scuola Superiore Meridionale (SSM), Napoli, Italy*
[87a] *INFN Sezione di Padova, Padova, Italy*
[87b] *Università di Padova, Padova, Italy*
[87c] *Universita degli Studi di Cagliari, Cagliari, Italy*
[88a] *INFN Sezione di Pavia, Pavia, Italy*
[88b] *Università di Pavia, Pavia, Italy*

JHEP07(2026)248

[89a] *INFN Sezione di Perugia, Perugia, Italy*
[89b] *Università di Perugia, Perugia, Italy*
[90a] *INFN Sezione di Pisa, Pisa, Italy*
[90b] *Università di Pisa, Pisa, Italy*
[90c] *Scuola Normale Superiore di Pisa, Pisa, Italy*
[90d] *Università di Siena, Siena, Italy*
[91a] *INFN Sezione di Roma, Roma, Italy*
[91b] *Sapienza Università di Roma, Roma, Italy*
[92a] *INFN Sezione di Torino, Torino, Italy*
[92b] *Università di Torino, Torino, Italy*
[92c] *Università del Piemonte Orientale, Novara, Italy*
[93a] *INFN Sezione di Trieste, Trieste, Italy*
[93b] *Università di Trieste, Trieste, Italy*
[94] *Kyungpook National University, Daegu, Korea*
[95] *Department of Mathematics and Physics — GWNU, Gangneung, Korea*
[96] *Chonnam National University, Institute for Universe and Elementary Particles, Kwangju, Korea*
[97] *Hanyang University, Seoul, Korea*
[98] *Korea University, Seoul, Korea*
[99] *Kyung Hee University, Department of Physics, Seoul, Korea*
[100] *Sejong University, Seoul, Korea*
[101] *Seoul National University, Seoul, Korea*
[102] *University of Seoul, Seoul, Korea*
[103] *Yonsei University, Department of Physics, Seoul, Korea*
[104] *Sungkyunkwan University, Suwon, Korea*
[105] *College of Engineering and Technology, American University of the Middle East (AUM), Dasman, Kuwait*
[106] *Kuwait University — College of Science — Department of Physics, Safat, Kuwait*
[107] *Riga Technical University, Riga, Latvia*
[108] *University of Latvia (LU), Riga, Latvia*
[109] *Vilnius University, Vilnius, Lithuania*
[110] *National Centre for Particle Physics, Universiti Malaya, Kuala Lumpur, Malaysia*
[111] *Universidad de Sonora (UNISON), Hermosillo, Mexico*
[112] *Centro de Investigacion y de Estudios Avanzados del IPN, Mexico City, Mexico*
[113] *Universidad Iberoamericana, Mexico City, Mexico*
[114] *Benemerita Universidad Autonoma de Puebla, Puebla, Mexico*
[115] *University of Montenegro, Podgorica, Montenegro*
[116] *University of Canterbury, Christchurch, New Zealand*
[117] *National Centre for Physics, Quaid-I-Azam University, Islamabad, Pakistan*
[118] *AGH University of Krakow, Krakow, Poland*
[119] *National Centre for Nuclear Research, Swierk, Poland*
[120] *Institute of Experimental Physics, Faculty of Physics, University of Warsaw, Warsaw, Poland*
[121] *Warsaw University of Technology, Warsaw, Poland*
[122] *Laboratório de Instrumentação e Física Experimental de Partículas, Lisboa, Portugal*
[123] *Faculty of Physics, University of Belgrade, Belgrade, Serbia*
[124] *VINCA Institute of Nuclear Sciences, University of Belgrade, Belgrade, Serbia*
[125] *Centro de Investigaciones Energéticas Medioambientales y Tecnológicas (CIEMAT), Madrid, Spain*
[126] *Universidad Autónoma de Madrid, Madrid, Spain*
[127] *Universidad de Oviedo, Instituto Universitario de Ciencias y Tecnologías Espaciales de Asturias (ICTEA), Oviedo, Spain*
[128] *Instituto de Física de Cantabria (IFCA), CSIC-Universidad de Cantabria, Santander, Spain*
[129] *University of Colombo, Colombo, Sri Lanka*
[130] *University of Ruhuna, Department of Physics, Matara, Sri Lanka*
[131] *CERN, European Organization for Nuclear Research, Geneva, Switzerland*
[132] *PSI Center for Neutron and Muon Sciences, Villigen, Switzerland*

[133] ETH Zurich — Institute for Particle Physics and Astrophysics (IPA), Zurich, Switzerland
[134] Universität Zürich, Zurich, Switzerland
[135] National Central University, Chung-Li, Taiwan
[136] National Taiwan University (NTU), Taipei, Taiwan
[137] High Energy Physics Research Unit, Department of Physics, Faculty of Science, Chulalongkorn University, Bangkok, Thailand
[138] Tunis El Manar University, Tunis, Tunisia
[139] Çukurova University, Physics Department, Science and Art Faculty, Adana, Turkey
[140] Hacettepe University, Ankara, Turkey
[141] Middle East Technical University, Physics Department, Ankara, Turkey
[142] Bogazici University, Istanbul, Turkey
[143] Istanbul Technical University, Istanbul, Turkey
[144] Istanbul University, Istanbul, Turkey
[145] Yildiz Technical University, Istanbul, Turkey
[146] Institute for Scintillation Materials of National Academy of Science of Ukraine, Kharkiv, Ukraine
[147] National Science Centre, Kharkiv Institute of Physics and Technology, Kharkiv, Ukraine
[148] University of Bristol, Bristol, U.K.
[149] Rutherford Appleton Laboratory, Didcot, U.K.
[150] Imperial College, London, U.K.
[151] Brunel University, Uxbridge, U.K.
[152] Baylor University, Waco, Texas, U.S.A.
[153] Bethel University, St. Paul, Minnesota, U.S.A.
[154] Catholic University of America, Washington, DC, U.S.A.
[155] The University of Alabama, Tuscaloosa, Alabama, U.S.A.
[156] Boston University, Boston, Massachusetts, U.S.A.
[157] Brown University, Providence, Rhode Island, U.S.A.
[158] University of California, Davis, Davis, California, U.S.A.
[159] University of California, Los Angeles, California, U.S.A.
[160] University of California, Riverside, Riverside, California, U.S.A.
[161] University of California, San Diego, La Jolla, California, U.S.A.
[162] University of California, Santa Barbara — Department of Physics, Santa Barbara, California, U.S.A.
[163] California Institute of Technology, Pasadena, California, U.S.A.
[164] Carnegie Mellon University, Pittsburgh, Pennsylvania, U.S.A.
[165] University of Colorado Boulder, Boulder, Colorado, U.S.A.
[166] Cornell University, Ithaca, New York, U.S.A.
[167] Fermi National Accelerator Laboratory, Batavia, Illinois, U.S.A.
[168] University of Florida, Gainesville, Florida, U.S.A.
[169] Florida State University, Tallahassee, Florida, U.S.A.
[170] Florida Institute of Technology, Melbourne, Florida, U.S.A.
[171] University of Illinois Chicago, Chicago, Illinois, U.S.A.
[172] The University of Iowa, Iowa City, Iowa, U.S.A.
[173] Johns Hopkins University, Baltimore, Maryland, U.S.A.
[174] The University of Kansas, Lawrence, Kansas, U.S.A.
[175] Kansas State University, Manhattan, Kansas, U.S.A.
[176] University of Maryland, College Park, Maryland, U.S.A.
[177] Massachusetts Institute of Technology, Cambridge, Massachusetts, U.S.A.
[178] University of Minnesota, Minneapolis, Minnesota, U.S.A.
[179] University of Nebraska-Lincoln, Lincoln, Nebraska, U.S.A.
[180] State University of New York at Buffalo, Buffalo, New York, U.S.A.
[181] Northeastern University, Boston, Massachusetts, U.S.A.
[182] Northwestern University, Evanston, Illinois, U.S.A.
[183] University of Notre Dame, Notre Dame, Indiana, U.S.A.
[184] The Ohio State University, Columbus, Ohio, U.S.A.

[185] Princeton University, Princeton, New Jersey, U.S.A.
[186] University of Puerto Rico, Mayaguez, Puerto Rico, U.S.A.
[187] Purdue University, West Lafayette, Indiana, U.S.A.
[188] Purdue University Northwest, Hammond, Indiana, U.S.A.
[189] Rice University, Houston, Texas, U.S.A.
[190] University of Rochester, Rochester, New York, U.S.A.
[191] Rutgers, The State University of New Jersey, Piscataway, New Jersey, U.S.A.
[192] University of Tennessee, Knoxville, Tennessee, U.S.A.
[193] Texas A&M University, College Station, Texas, U.S.A.
[194] Texas Tech University, Lubbock, Texas, U.S.A.
[195] Vanderbilt University, Nashville, Tennessee, U.S.A.
[196] University of Virginia, Charlottesville, Virginia, U.S.A.
[197] Wayne State University, Detroit, Michigan, U.S.A.
[198] University of Wisconsin — Madison, Madison, Wisconsin, U.S.A.
[199] An institute or international laboratory covered by a cooperation agreement with CERN
[200] An institute formerly covered by a cooperation agreement with CERN

[a] Also at Yerevan State University, Yerevan, Armenia
[b] Also at TU Wien, Vienna, Austria
[c] Also at Ghent University, Ghent, Belgium
[d] Also at FACAMP — Faculdades de Campinas, Sao Paulo, Brazil
[e] Also at Universidade Estadual de Campinas, Campinas, Brazil
[f] Also at Federal University of Rio Grande do Sul, Porto Alegre, Brazil
[g] Also at The University of the State of Amazonas, Manaus, Brazil
[h] Also at University of Chinese Academy of Sciences, Beijing, China
[i] Also at University of Chinese Academy of Sciences, Beijing, China
[j] Also at School of Physics, Zhengzhou University, Zhengzhou, China
[k] Now at Henan Normal University, Xinxiang, China
[l] Also at University of Shanghai for Science and Technology, Shanghai, China
[m] Also at The University of Iowa, Iowa City, Iowa, U.S.A.
[n] Also at Nanjing Normal University, Nanjing, China
[o] Also at Center for High Energy Physics, Peking University, Beijing, China
[p] Also at Cairo University, Cairo, Egypt
[q] Also at Suez University, Suez, Egypt
[r] Now at British University in Egypt, Cairo, Egypt
[s] Also at Université de Haute Alsace, Mulhouse, France
[t] Also at Purdue University, West Lafayette, Indiana, U.S.A.
[u] Also at Another institute or international laboratory covered by a cooperation agreement with CERN
[v] Also at University of Hamburg, Hamburg, Germany
[w] Also at RWTH Aachen University, III. Physikalisches Institut A, Aachen, Germany
[x] Also at Bergische University Wuppertal (BUW), Wuppertal, Germany
[y] Also at Brandenburg University of Technology, Cottbus, Germany
[z] Also at Forschungszentrum Jülich, Juelich, Germany
[aa] Now at RWTH Aachen University, III. Physikalisches Institut A, Aachen, Germany
[ab] Also at CERN, European Organization for Nuclear Research, Geneva, Switzerland
[ac] Also at HUN-REN ATOMKI — Institute of Nuclear Research, Debrecen, Hungary
[ad] Now at Universitatea Babes-Bolyai — Facultatea de Fizica, Cluj-Napoca, Romania
[ae] Also at MTA-ELTE Lendület CMS Particle and Nuclear Physics Group, Eötvös Loránd University, Budapest, Hungary
[af] Also at HUN-REN Wigner Research Centre for Physics, Budapest, Hungary
[ag] Also at Physics Department, Faculty of Science, Assiut University, Assiut, Egypt
[ah] Also at The University of Kansas, Lawrence, Kansas, U.S.A.
[ai] Also at Punjab Agricultural University, Ludhiana, India

JHEP07(2026)248

[aj] Also at University of Hyderabad, Hyderabad, India
[ak] Also at Indian Institute of Science (IISc), Bangalore, India
[al] Also at University of Visva-Bharati, Santiniketan, India
[am] Also at Institute of Physics, Bhubaneswar, India
[an] Also at Deutsches Elektronen-Synchrotron, Hamburg, Germany
[ao] Also at Isfahan University of Technology, Isfahan, Iran
[ap] Also at Sharif University of Technology, Tehran, Iran
[aq] Also at Department of Physics, University of Science and Technology of Mazandaran, Behshahr, Iran
[ar] Also at Department of Physics, Faculty of Science, Arak University, ARAK, Iran
[as] Also at Helwan University, Cairo, Egypt
[at] Also at Italian National Agency for New Technologies, Energy and Sustainable Economic Development, Bologna, Italy
[au] Also at Centro Siciliano di Fisica Nucleare e di Struttura Della Materia, Catania, Italy
[av] Also at James Madison University, Harrisonburg, N/A, U.S.A.
[aw] Also at Università degli Studi Guglielmo Marconi, Roma, Italy
[ax] Also at Scuola Superiore Meridionale, Università di Napoli 'Federico II', Napoli, Italy
[ay] Also at Fermi National Accelerator Laboratory, Batavia, Illinois, U.S.A.
[az] Also at Lulea University of Technology, Lulea, Sweden
[ba] Also at Consiglio Nazionale delle Ricerche — Istituto Officina dei Materiali, Perugia, Italy
[bb] Also at UPES — University of Petroleum and Energy Studies, Dehradun, India
[bc] Also at Institut de Physique des 2 Infinis de Lyon (IP2I), Villeurbanne, France
[bd] Also at Department of Applied Physics, Faculty of Science and Technology, Universiti Kebangsaan Malaysia, Bangi, Malaysia
[be] Also at Trincomalee Campus, Eastern University, Sri Lanka, Nilaveli, Sri Lanka
[bf] Also at Saegis Campus, Nugegoda, Sri Lanka
[bg] Also at National and Kapodistrian University of Athens, Athens, Greece
[bh] Also at Ecole Polytechnique Fédérale Lausanne, Lausanne, Switzerland
[bi] Also at Universität Zürich, Zurich, Switzerland
[bj] Also at Stefan Meyer Institute for Subatomic Physics, Vienna, Austria
[bk] Also at Near East University, Research Center of Experimental Health Science, Mersin, Turkey
[bl] Also at Konya Technical University, Konya, Turkey
[bm] Also at Istanbul Topkapi University, Istanbul, Turkey
[bn] Also at Izmir Bakircay University, Izmir, Turkey
[bo] Also at Adiyaman University, Adiyaman, Turkey
[bp] Also at Bozok Universitetesi Rektörlügü, Yozgat, Turkey
[bq] Also at Istanbul Sabahattin Zaim University, Istanbul, Turkey
[br] Also at Marmara University, Istanbul, Turkey
[bs] Also at Milli Savunma University, Istanbul, Turkey
[bt] Also at Informatics and Information Security Research Center, Gebze/Kocaeli, Turkey
[bu] Also at Kafkas University, Kars, Turkey
[bv] Now at Istanbul Okan University, Istanbul, Turkey
[bw] Also at Istanbul University — Cerrahpasa, Faculty of Engineering, Istanbul, Turkey
[bx] Also at Istinye University, Istanbul, Turkey
[by] Also at School of Physics and Astronomy, University of Southampton, Southampton, U.K.
[bz] Also at Monash University, Faculty of Science, Clayton, Australia
[ca] Also at Università di Torino, Torino, Italy
[cb] Also at Karamanoğlu Mehmetbey University, Karaman, Turkey
[cc] Also at California Lutheran University, Thousand Oaks, California, U.S.A.
[cd] Also at California Institute of Technology, Pasadena, California, U.S.A.
[ce] Also at United States Naval Academy, Annapolis, Maryland, U.S.A.
[cf] Also at Bingol University, Bingol, Turkey
[cg] Also at Georgian Technical University, Tbilisi, Georgia
[ch] Also at Sinop University, Sinop, Turkey

JHEP07(2026)248

[ci] *Also at Erciyes University, Kayseri, Turkey*
[cj] *Also at Horia Hulubei National Institute of Physics and Nuclear Engineering (IFIN-HH), Bucharest, Romania*
[ck] *Now at Another institute formerly covered by a cooperation agreement with CERN*
[cl] *Also at Another institute formerly covered by a cooperation agreement with CERN*
[cm] *Also at Hamad Bin Khalifa University (HBKU), Doha, Qatar*
[cn] *Also at Yerevan Physics Institute, Yerevan, Armenia*
[co] *Also at Imperial College, London, U.K.*
[cp] *Now at Yerevan Physics Institute, Yerevan, Armenia*
[†] *Deceased*

JHEP07(2026)248